AD-A130 070 PRESSURE MODELING OF CHAR-FORMING AND LAMINATED MATERIALS(U) FACTORY MUTUAL RESEARCH CORP NORWOOD MASS R L ALPERT JUN 83 OGON3-BU DOT/FAA/CT-83/24 1/2

UNCLASSIFIED DTFA03-81-C-00043 F/G 11/4 NL

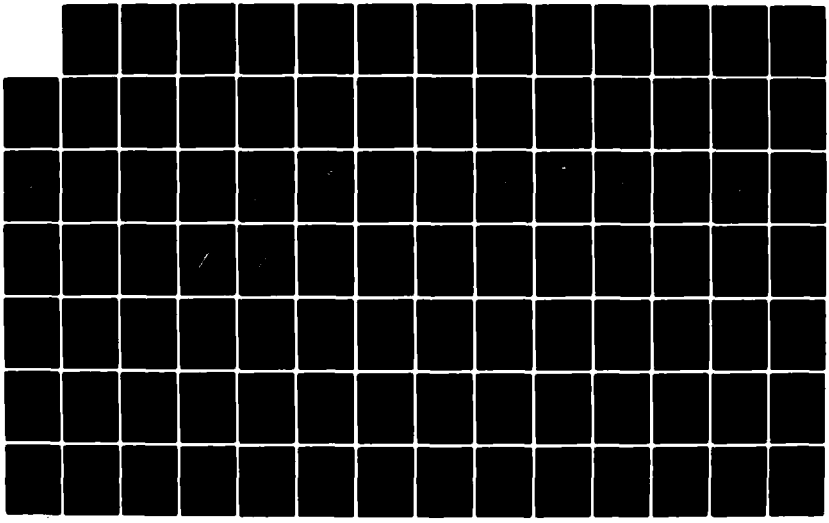

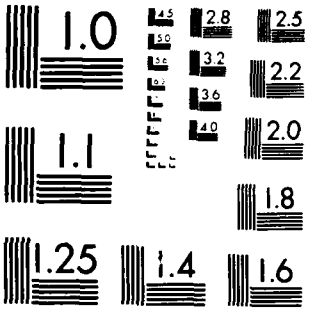

MICROCOPY RESOLUTION TEST CHART
NATIONAL BUREAU OF STANDARDS-1963-A

AD A130070

(11)

DOT/FAA/CT-83/24

Pressure Modeling of Char-Forming and Laminated Materials

R. L. Alpert

Factory Mutual Research Corp.
1151 Boston-Providence Turnpike
Norwood, Massachusetts 02062

June 1983

Final Report

This document is available to the U.S. public through the National Technical Information Service, Springfield, Virginia 22161.

DTIC
ELECTE
JUL 6 1983
A

US Department of Transportation
Federal Aviation Administration
Technical Center
Atlantic City Airport, N.J. 08405

DTIC FILE COPY

83 07 6 003

NOTICE

This document is disseminated under the sponsorship of the Department of Transportation in the interest of information exchange. The United States Government assumes no liability for the contents or use thereof.

The United States Government does not endorse products or manufacturers. Trade or manufacturer's names appear herein solely because they are considered essential to the object of this report.

Technical Report Documentation Page

1. Report No.	2. Government Accession No.	3. Recipient's Catalog No.
DOT/FAA/CT-83/24	AD-A130 070	

4. Title and Subtitle	5. Report Date
PRESSURE MODELING OF CHAR-FORMING AND LAMINATED MATERIALS	June 1983
	6. Performing Organization Code
7. Author(s) R. L. Alpert	8. Performing Organization Report No. ØGON3-BU; RC82-BR-6
9. Performing Organization Name and Address Factory Mutual Research Corporation 1151 Boston-Providence Turnpike Norwood, Massachusetts 02062	10. Work Unit No. (TRAIS)
	11. Contract or Grant No. DTFA03-81-C-00043
12. Sponsoring Agency Name and Address U.S. Department of Transportation Federal Aviation Administration Technical Center Atlantic City Airport, New Jersey 08405	13. Type of Report and Period Covered Final April 1981 - Nov. 1982
	14. Sponsoring Agency Code

15. Supplementary Notes

16. Abstract

The pressure modeling technique is used to study upward fire spread on fuel wall composed of char-forming or laminated materials. Time-resolved measurements are obtained at one-atmosphere (full-scale) and at elevated air pressure (model scales) to characterize fire growth in terms of rate of total mass loss, flame height, upward flame spread rate, and maximum lateral flame dimensions during the spread process. The char-forming materials (pine-wood, particle-board and a rigid, polyurethane foam) are tested in a 90° wall-corner configuration while the laminated materials (PMMA in combination with PMMA or ceramic backings) are tested in a wall configuration. Thermally-thick PMMA is tested in both configurations for purposes of comparison. Results are generally consistent with the pressure modeling scheme and a series of one-dimensional, transient thermal conduction and pyrolysis calculations. The behavior of the rigid polyurethane foam, however, is an exception. This material does not support self-sustained upward flame spread at one-atmosphere when exposed to flames from a 0.1 m high PMMA ignition source but does support rapid fire growth at elevated pressures. A possible reason for the anomalous polyurethane behavior is the intumescent structure of the hot char at one-atmosphere, but a better understanding of the mechanism of upward or wind-aided flame spread on charring materials is needed to resolve the issue. It is concluded that additional measurements of upward flame spread rates on a variety of simplified, laminated materials will be necessary. It is also concluded that the pressure modeling technique may be valid for predicting fire growth on most charring fuels in corner configurations (with or without a ceiling) as long as a sufficiently large heat flux initiates self-sustained fire spread.

17. Key Words	18. Distribution Statement
Pressure Modeling Laminated Materials Char-Forming Materials Flammability	Document is available to the U.S. public through the National Technical Information Service, Springfield, Virginia 22161

19. Security Classif. (of this report)	20. Security Classif. (of this page)	21. No. of Pages	22. Price
Unclassified	Unclassified		

Form DOT F 1700.7 (8-72) Reproduction of completed page authorized

METRIC CONVERSION FACTORS

Approximate Conversions to Metric Measures

Symbol	When You Know	Multiply by	To Find	Symbol
		LENGTH		
in	inches	*2.5	centimeters	cm
ft	feet	30	centimeters	cm
yd	yards	0.9	meters	m
mi	miles	1.6	kilometers	km
		AREA		
in^2	square inches	6.5	square centimeters	cm^2
ft^2	square feet	0.09	square meters	m^2
yd^2	square yards	0.8	square meters	m^2
mi^2	square miles	2.6	square kilometers	km^2
	acres	0.4	hectares	ha
		MASS (weight)		
oz	ounces	28	grams	g
lb	pounds	0.45	kilograms	kg
	short tons (2000 lb)	0.9	tonnes	t
		VOLUME		
tsp	teaspoons	5	milliliters	ml
Tbsp	tablespoons	15	milliliters	ml
fl oz	fluid ounces	30	milliliters	ml
c	cups	0.24	liters	l
pt	pints	0.47	liters	l
qt	quarts	0.95	liters	l
gal	gallons	3.8	liters	l
ft^3	cubic feet	0.03	cubic meters	m^3
yd^3	cubic yards	0.76	cubic meters	m^3
		TEMPERATURE (exact)		
°F	Fahrenheit temperature	5/9 (after subtracting 32)	Celsius temperature	°C

*1 in = 2.54 (exactly). For other exact conversions and more detailed tables, see NBS Misc. Publ. 286, Units of Weights and Measures, Price $2.25, SD Catalog No. C13.10:286.

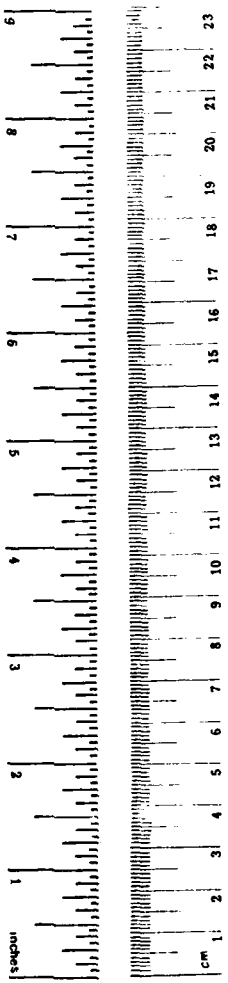

Approximate Conversions from Metric Measures

Symbol	When You Know	Multiply by	To Find	Symbol
		LENGTH		
mm	millimeters	0.04	inches	in
cm	centimeters	0.4	inches	in
m	meters	3.3	feet	ft
m	meters	1.1	yards	yd
km	kilometers	0.6	miles	mi
		AREA		
cm^2	square centimeters	0.16	square inches	in^2
m^2	square meters	1.2	square yards	yd^2
km^2	square kilometers	0.4	square miles	mi^2
ha	hectares (10,000 m^2)	2.5	acres	
		MASS (weight)		
g	grams	0.035	ounces	oz
kg	kilograms	2.2	pounds	lb
t	tonnes (1000 kg)	1.1	short tons	
		VOLUME		
ml	milliliters	0.03	fluid ounces	fl oz
l	liters	2.1	pints	pt
l	liters	1.06	quarts	qt
l	liters	0.26	gallons	gal
m^3	cubic meters	35	cubic feet	ft^3
m^3	cubic meters	1.3	cubic yards	yd^3
		TEMPERATURE (exact)		
°C	Celsius temperature	9/5 (then add 32)	Fahrenheit temperature	°F

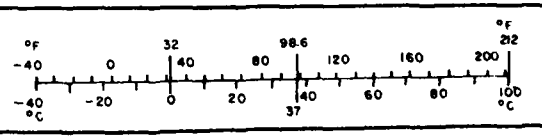

PREFACE

This work was sponsored by the Federal Aviation Administration, through a contract from the FAA Technical Center, Atlantic City, New Jersey. The FAA Technical Officer for this contract was Dr. Thor Eklund, whose valuable advice and encouragement during the project are gratefully acknowledged.

Ms. Mary K. Mathews modified the computer code for the pyrolysis calculations, allowing the code to be used on the Factory Mutual Research Corporation HP1000 minicomputer. This work, as well as the support of Dr. John de Ris, Manager of FMRC Basic Research, is sincerely appreciated.

Accession For
NTIS
DTIC
COPY INSPECTED 2
A

TABLE OF CONTENTS

Section	Title	Page
I	INTRODUCTION	1
	1.1 Purpose	1
	1.2 Background	1
II	PRESSURE MODELING EXPERIMENTS	2
	2.1 Experimental Arrangement	2
	2.1.1 Configuration of Laminated Fuels	2
	2.1.2 Configuration of Char-Forming Fuels	5
	2.1.3 Experimental Measurements and Procedures	6
	2.2 Fire Growth Behavior	7
	2.2.1 Ignition Source	7
	2.2.2 Wall Fires	7
	2.2.3 Wall-Corner Fires	8
	2.3 Experimental Results	9
	2.3.1 Flame Height	9
	2.3.2 Upward Flame Spread Rate	18
	2.3.3 Flame Width	23
	2.3.4 Mass Loss Rates	31
III	ANALYSIS	37
	3.1 Laminated Fuels	37
	3.1.1 Background	37
	3.1.2 Behavior of Thermal Wave During Fire Spread	42
	3.1.3 Pressure Modeling Laminated Fuels	45
	3.2 Charring Fuels	46
	3.2.1 Fuel Mass Flux	48
	3.2.2 Fuel Surface Temperature	53
	3.2.3 Char Production	58
IV	SUMMARY OF RESULTS	58
V	CONCLUSIONS	59
VI	REFERENCES	61
	APPENDIX A	63

LIST OF FIGURES

Number	Title	Page
1	Correlation of Flame Height on PMMA Walls	12
2	Correlation of Pyrolysis Height on PMMA Walls	13
3	Correlation of Flame Height on PMMA-PMMA Laminate Walls	14
4	Correlation of Flame Height on PMMA-Inert Laminate Walls	15
5	Correlation of Flame Height on PMMA Wall Corners	16
6	Correlation of Flame Height on Particle-Board Wall Corners	17
7	Correlation of Flame Height on Pine-Wood Wall Corners	19
7a	Correlation of Flame Height on GM-37 Wall Corners	20
8	Correlation of Vertical Flame Spread Rate Up PMMA Walls	21
9	Correlation of Vertical Pyrolysis Spread Rate Up PMMA Walls	22
10	Correlation of Vertical Flame Spread Rate Up PMMA-Inert Laminate Walls	24
11	Correlation of Vertical Flame Spread Rate Up PMMA Wall Corners	25
12	Correlation of Vertical Flame Spread Rate Up Particle-Board Wall Corners	26
13	Correlation of Vertical Flame Spread Rate Up Pine-Wood Wall Corners	27
14	Correlation of Maximum Pyrolysis Zone Width on PMMA Walls	28
15	Correlation of Maximum Flame Width on PMMA-PMMA Laminate Walls	29
16	Correlation of Maximum Flame Width on PMMA-Inert Laminate Walls	30
17	Correlation of Maximum Projected Flame Width on PMMA Wall Corners	32
18	Correlation of Maximum Projected Flame Width on Particle-Board Wall Corners	33
19	Correlation of Maximum Projected Flame Width on Pine-Wood Corners	34

20	Correlation of Mass Loss Rate for PMMA Walls	35
21	Correlation of Mass Loss Rate for PMMA-PMMA Laminate Walls	36
22	Correlation of Mass Loss Rate for PMMA-Inert Laminate Walls	38
23	Correlation of Mass Loss Rate for PMMA Wall Corners	39
24	Correlation of Mass Loss Rate for Particle-Board Wall Corners	40
25	Correlation of Mass Loss Rate for Pine-Wood Wall Corners	41
26	Calculation of One-Dimensional Pine-Wood Pyrolysis: Scaled Vapor Mass Flux Due to 20 kW/m^2 Scaled Heat Flux With Standard Thermal and Kinetics Properties	49
27	Calculation of One-Dimensional Pine-Wood Pyrolysis: Scaled Mass Flux Due to 20 kW/m^2 Scaled Heat Flux With Low Activation Energy in Pyrolysis Kinetics	50
28	Calculation of One-Dimensional Pine-Wood Pyrolysis: Scaled Vapor Mass Flux Due to 40 kW/m^2 Scaled Heat Flux With Standard Thermal and Kinetics Properties	51
29	Calculation of One-Dimensional Particle-Board Pyrolysis: Scaled Vapor Mass Flux Due to 20 kW/m^2 Scaled Heat Flux	52
30	Calculation of One-Dimensional Pine-Wood Pyrolysis: Fuel Surface Temperature Due to 20 kW/m^2 Scaled Heat Flux With Standard Thermal and Kinetics Properties	54
31	Calculation of One-Dimensional Pine-Wood Pyrolysis: Fuel Surface Temperature Due to 20 kW/m^2 Scaled Heat Flux With Low Activation Energy in Pyrolysis Kinetics	55
32	Calculation of One-Dimensional Pine-Wood Pyrolysis: Fuel Surface Temperature Due to 40 kW/m^2 Scaled Heat Flux With Standard Thermal and Kinetics Properties	56
33	Calculation of One-Dimensional Particle-Board Pyrolysis: Fuel Surface Temperature Due to 20 kW/m^2 Scaled Heat Flux	57

LIST OF SYMBOLS

c	specific heat of wall material
d	thickness of face layer
kL_m	optical depth (product of absorption coefficient, k, and mean beam length, L_m)
$\dot{m}$	mass loss rate of fuel
$\dot{m}''$	fuel mass flux
p	absolute gas pressure
$\dot{Q}$	heat release rate of fire
$\dot{Q}'$	heat release rate per unit width of wall fire
$\dot{q}''$	net heat flux to fuel
$\dot{q}''_r$	radiant exposure flux from flame
t	time
T	solid phase temperature
T^*	temperature of backing layer at face layer boundary
V	fuel regression rate (no subscript); rate of upward spread (with subscript)
W	width of flame or pyrolysis zone
x	height of flame or pyrolysis zone
α	thermal diffusivity, $\lambda/\rho c$
δ	thickness of thermal wave
λ	thermal conductivity of wall material
ρ	density of wall material
σ	Stefan-Boltzmann constant

Subscripts

f	flame condition
o	condition at one-atmosphere
p	pyrolysis condition
∞	ambient condition

EXECUTIVE SUMMARY

The pressure modeling technique is used to study upward fire spread on fuel walls composed of char-forming or laminated materials. Time-resolved measurements are obtained at one-atmosphere (full-scale) and at elevated pressure (model scales) to characterize fire growth in terms of rate of total mass loss, flame height and maximum lateral flame extent during the spread process. The char-forming materials (pine-wood, particle-board and a rigid, polyurethane foam) are tested in a 90° wall corner configuration while the laminated materials (polymethylmethacrylate (PMMA) or ceramic backings) are tested in a wall configuration. Thermally-thick PMMA is tested in both configurations for purposes of comparison.

The following results are obtained from the modeling study:

1. Pressure modeling is sufficiently accurate for the prediction of fire growth from a point ignition on a uniform PMMA wall when both upward and lateral flame spread processes occur.

2. The behavior of the flame spread process at elevated air pressures, for walls composed of a face layer of PMMA with a thick nonburning backing layer, is not completely consistent with a simplified analysis of thermal conduction processes.

3. Pressure modeling of fire growth in a wall corner configuration is quite accurate for cellulosic, char-forming materials and for PMMA. The cellulosics at one atmosphere exhibit a flame extinction phenomenon due to char buildup after significant lateral flame spread that is not observed at elevated pressures.

4. Thermally thick, rigid, high density polyurethane foam in a corner configuration will not support significant flame spread at one-atmosphere but will at elevated pressures with a properly scaled, small PMMA ignition source. This behavior is perhaps due to excessive radiant heat loss from the char and the intumescent character of the char at one-atmosphere. Gas phase chemical kinetics, which may be the most important factor in the initiation of flame spread on the full-scale foam, is clearly not modeled.

5. A simplified analysis of thermal conduction in a laminated material is used to show how flame spread rates are affected by the thermal properties of the face layer and backing at both one-atmosphere and at elevated pressures.

6. A numerical technique is used to predict one-dimensional, transient fuel mass flux, fuel surface temperature and char thickness during material exposure to a prescribed radiant (and convective) heat flux. Calculated results show that reasonable pressure modeling of flame spread rates should be expected for the cellulosic fuels due to increases in surface temperature and char production for conditions simulating elevated air pressure.

These results lead to two main conclusions:

1. Pressure modeling of three-dimensional fire spread on uniform wal and wall corners has now been validated for PMMA and for wood fuels. has not yet been established that the modeling technique is valid for predicting fire growth on other charring fuels in corner configurations. Results from this and previous studies have shown that in general, the complex process by which self-sustained fire spread is initiated is not pressure modeled. Such fire spread initiation occurs readily at elevated pressures because surface radiant heat loss and the action of gas phase chemical retardents cannot be modeled. With the wood and PMMA fuels, fire spread rates on wall-ceiling corners should also be predictable by pressure modeling, based on previous work[20] with ceiling channel configurations.

2. It appears that much more experimental information is needed before pressure modeling can be used to predict fire growth on practical composite materials. At present the thickness of all components (including adhesives) within the thermal wave developed during fire spread must be modified according to the pressure modeling scheme. However, radiant exposure in real enclosure fires may well be sufficiently high (2-4 W/cm^2) to confine thermal wave penetration to a surface layer of fuel during fire spread. Pressure modeling of such a fire spread process would then be accurate without any modification of the laminated material.

I
INTRODUCTION

1.1 PURPOSE

The purpose of this project is: 1) to study, by experiment, the behavior of upward fire spread and growth at both atmospheric and elevated air pressures; and 2) to perform an analysis of transient, one-dimensional heat conduction and pyrolysis, in order to determine the applicability of the pressure modeling technique to char-forming and laminated materials.

1.2 BACKGROUND

Materials within an aircraft cabin can be exposed to flame heat transfer from external fuel-spill fires after an aircraft accident. It is desirable to have cabin materials which will limit any compartment fire growth initiated by the external fire. Methods for characterizing the fire growth potential of a variety of aircraft cabin materials in various configurations are therefore needed. One method for studying the effect of fuel configuration and geometry on transient fire growth is the pressure modeling technique, whereby experiments with small-scale fuels are conducted at elevated air pressures to simulate full-scale, controlling fluid mechanic and thermal parameters. It is important to determine how effects due to changes in fuel composition will alter such a modeling process.

Fire growth within an aircraft cabin can occur by several different modes. One such mode is by upward and lateral fire spread on vertical cabin surfaces. In a previous study[1], the feasibility of modeling fire spread on vertical walls through the use of small-scale experiments at elevated air pressure (pressure modeling technique) was proven for a homogeneous fuel with simple vaporization characteristics, polymethylmethacrylate (PMMA). The present study deals with fuels which undergo pyrolysis reactions leading to char formation and fuels that are composites of two different materials laminated together. While such materials are more like real fuels than homogeneous PMMA, an effort has been made to use the simplest possible charring and laminated materials so that the pressure modeling behavior can be understood.

Relatively simple fuel configurations are also used for this study in order to facilitate subsequent analysis. Laminated materials are burned in an unbounded wall configuration ignited at a single point to take advantage of the flame spread characteristics of the surface layer of PMMA fuel. Char-forming materials will ordinarily not sustain extensive flame spread unless exposed to a minimum heat flux level. In the present study, the exposure is provided, in part, by a small, PMMA initiator built into the charring fuel. The remainder of the exposure flux results from the use of a 90° corner configuration, which allows some thermal radiation lost from one wall of the corner to be captured by the opposite wall.

II

PRESSURE MODELING EXPERIMENTS

2.1 EXPERIMENTAL ARRANGEMENT SKETCHED IN FIGURES 1 AND 5

2.1.1 CONFIGURATION OF LAMINATED FUELS. An unbounded vertical wall ignited at a point near the wall base is used to test pressure modeling concepts for laminated fuels and for uniform PMMA. Tables 1 and 2 list the fuel compositions and dimensions, respectively, used in the assembly of the full-scale and model wall configurations. Those dimensions in Table 2 denoted as "scaled" (fuel height and width, etc.) are reduced from the full-scale values listed when used in the model configurations. As explained in References 1 and 2, the pressure modeling scheme requires that such a reduction of length scales be made proportional to the minus 2/3 power of absolute air pressure. At air pressures of 11.2, 20.5 and 31.6 atmospheres, this tranlates into respective length scale reductions by factors of 1/5, 1/7.5 and 1/10. Fuel thickness, except for that of the uniform PMMA wall, is not scaled in this manner due to practical limitations. Instead, a thermally thick backing layer is used while the PMMA face layer is maintained at a constant thickness for all pressures. A fixed fuel thickness would be used in practice if complex composite fuels were to be subjected to any flammability test. For the case of uniform PMMA, cast slabs 1/5 and 1/10 the full-scale, 31.75 mm thickness happen to be commercially available. Another exception to the modeling scheme is the case of the PMMA-PMMA laminate wall. The model fuels correspond to the PMMA-Inert prototype dimensions, instead of those for the PMMA-PMMA laminate.

TABLE I

DESCRIPTION OF WALL MATERIALS AT AMBIENT TEMPERATURE

Wall Material	Composition	Density [kg/m^3]	Thermal Diffusivity [m^2/s]	$\rho C\lambda$ [J^2/m^{4}K^{2}s]
Inert	"Cotronics" type 360 Ceramic Board	256	2.425×10^{-7}	1.742×10^{4}
PMMA (Melting)	Polymethylmethacrylate ("Plexiglas, cast, type G)	1200	7.95×10^{-8}	5.54×10^{5}
Pine-Wood (Char-Forming)	Cellulose "1 x 10" pine board	434	1.92×10^{-7}	5.21×10^{4}
Particle-Board (Char-Forming)	Cellulose particleboard ("Versaboard" Douglas Fir)	694	9.07×10^{-8}	1.75×10^{5}
GM-37 (Char-Forming)	Rigid Polyurethane Foam (from NBS office of Standard Reference Materials) Polymeric Isocyanate	320	1.76×10^{-7}	1.98×10^{4}

TABLE II

DIMENSIONS OF FUEL CONFIGURATIONS
SKETCHED IN FIGURES 1 AND 5

Fuel Type	Material Thickness [mm]	Scaled Height [m]	Scaled Width of Wall (each leg of corner) [m]	PMMA Initiator Scaled Height [mm]
PMMA Wall	31.75, scaled	0.8985	0.2286	-
PMMA-PMMA laminate wall	3.18 - front face 31.75 - backing at 1 atm 12.7 - backing at > 1 atm	0.8985	0.2286	-
PMMA-Inert laminate wall	3.18 - front face 25.4 - inert backing	1.22	0.305	-
PMMA wall corner	31.75 at 1 atm 12.7 at > 1 atm	0.8985	0.137	-
Particle-board wall corner	19.05	1.22	0.2 and 0.15	102
Pine-wood wall corner	19.05	1.21	0.22	51
Inert wall corner	12.7	0.61	0.2	102
GM-37 wall corner	51 at 1 atm 25 at > 1 atm	1.22	0.2	102

Both laminated fuel walls are assembled with a ceramic adhesive ("Cotronics" type 901) to bond the face layer to the backing layer. This bonding is aided by mechanical fasteners (machine screws at 1 atm and small diameter bolts at 11.2 atm) or clamps. For the PMMA-PMMA laminate, the ceramic adhesive also acts as an inerting agent, preventing the involvement of the PMMA backing in fuel vaporization while allowing heat transmission to the backing.

Two difficulties were encountered during use of the ceramic paste in the full-scale laminate; a nonuniform paste thickness and an overly long drying time, both due to the large area of PMMA involved. The thickness of the ceramic paste varied from 0.8 mm up to 3 mm, with the average thickness being 1.6 mm at full-scale but perhaps an order of magnitude less in the model fuels. Complete drying of the ceramic paste was prevented by the impermeable PMMA surface at full-scale but reasonable drying times of several hours were possible with the model fuels.

2.1.2 CONFIGURATION OF CHAR-FORMING FUELS. An unbounded, 90° degree corner arrangement is used to test pressure modeling predictions for char-forming fuels and for uniform PMMA. Fire spread is initiated for the char-forming fuels by a small PMMA corner insert which is flush with the front surface and bottom edges of the larger, charring material. Dimensions and compositions of all these components are listed in Tables 1 and 2. The width of each leg of the PMMA corner initiator is one-half the scaled height listed in Table 2 while the initiator thickness is a constant 12.7 mm for both the full-scale and model tests. This constant PMMA thickness, which results in the initiator approaching a thermally thin condition in the latter stages of the full-scale experiments, is probably not important in the modeling of fire spread. To characterize the flame height from the PMMA initiator alone, an inert wall corner was fabricated with the initiator insert.

For the laminated fuels, the thickness dimensions listed in Table 2 are not scaled down with increased pressure since a thermally thick condition is maintained. The larger-than-required thickness of the models enables the cellulosic corners to be fabricated conveniently with finishing nails. A solvent-type cement is used to fabricate both the PMMA fuel corners and PMMA

initiators. The ceramic adhesive noted above is used to bond the two legs of the inert corner. This same adhesive is applied to the outer, top and bottom edges of all the fuel samples, (wall as well as corners) thereby confining flame spread to the front face.

Because cellulosic fuels absorb moisture, both the pine-wood and particle-board configurations are dried thoroughly before each experiment in an oven set for 90-100°C. Values of density for the char-forming fuels listed in Table 1 are measured from oven-dried samples. The model cellulosic fuels, after being cut from the same board as the full-scale sample, are dried and then stored (no more than 2 days) in plastic bags until being placed in the pressure vessel. To insure a dry atmosphere in the vessel, room air is purged from the chamber before pressurization with air having a dew point below 194 K (-79°C).

2.1.3 EXPERIMENTAL MEASUREMENTS AND PROCEDURES. The flame spread experiments commence with the ignition of a 25.4 mm long, 6.35 mm diameter PMMA rod at one atmosphere or a small wooden toothpick at elevated pressures. For the wall configurations, this ignition source protrudes from the vertical centerline a scaled distance of 25.4 mm from the wall base, normal to the fuel surface. The same ignition source is used for the wall-corner configurations. Instead of being in contact with the fuel, however, the rod or toothpick is inserted horizontally into the apex of an inert, corner-shaped slab of "Cotronics" board upon which the fuel corner rests. The ignition source is then directly below the bottom edge of the apex of the PMMA initiator, separated from the PMMA by 12.7 mm at one-atmosphere and by 3 mm at elevated pressures. At all scales, the energy provided by the burning rod or toothpick is probably close to the minimum amount needed for initiation of upward fire spread.

Once flame spread up the wall or corner begins, flame position and total fuel mass are measured as functions of time. The mass-loss measurement, obtained from a strain gauge type of load transducer, contains random fluctuations of up to $\pm$ 0.5 and $\pm$ 0.1 grams at one atmosphere and elevated pressures, respectively. These fluctuations are 0.2% and 2% of the respective total average mass-loss during the experiment. The relatively high noise level of the mass loss signal at elevated pressures is due to the fast scan rates required

during a maximum of 30 seconds of digital data acquisition, with a consequent decrease in filtering efficiency. Most of this noise is eliminated during data reduction by obtaining mass loss rates from a least squares regression fit to the raw measurements.

Flame position on or above the fuel is obtained by motorized, 35 mm still photography at rates up to 4 frames per second. Projection of the 35 mm transparencies onto a ground glass screen alows flame height and width to be measured conveniently. A vertical length scale, graduated in alternately colored 1 centimeter bands, appears next to the fuel in the photographs to permit resolution of flame position to within 0.3% of total fuel height. Flame spread time is obtained from a photographed digital clock. At one-atmosphere, the time measurement can be resolved to within 1 second about 0.2% of the total fire spread duration. Time is resolvable to 0.1 second at elevated pressures, which represents about 0.5% of total spread time in most cases.

2.2 FIRE GROWTH BEHAVIOR

2.2.1 IGNITION SOURCE. The flame height above the PMMA rod ignition source at one atmosphere is about 0.1 m. For the corner configuration, this means that the ignition flame nearly reaches the top edge of the PMMA corner initiator. Flame height from the burning toothpick at 11.2 atmospheres is 0.0175 to 0.02 m high, or about the required factor of five smaller than the one-atmosphere flame. At higher pressures, the toothpick flame height is roughly the same 20 mm value and thus is somewhat larger than required for modeling.

2.2.2 WALL FIRES. The flame spreads upward on the wall from the PMMA ignition rod or wooden toothpick at a much higher rate than that of lateral or downward flame spread. A tear-shaped flame on the surface of the PMMA fuel results, with the maximum flame width occurring near the ignition level during most of the spread process (as the total spread width approaches .14 - .16 m, lateral spread rates near the top of the fuel become more important). The uniform PMMA wall is transparent, allowing both the flame and pyrolysis fronts to be seen by photography from the (nonburning) back side.

For the PMMA-PMMA laminate, the ceramic paste between the thin face layer and backing prevents the thick backing layer from burning. At one-atmosphere, a region without flame is visible at the base of the wall where the face layer has been consumed. This burnout region grows from .03 m to 0.3 m above the wall base as flame spread proceeds from half-way up the wall to the top of the fuel. For the PMMA-Inert laminate, upward flame spread on the face layer is much more rapid due to the low density backing. The face layer is consumed near the base of this laminate only after flame spread to the top of the wall has occurred. However, about 600 seconds after ignition, burnout of the face layer is observed to a height of 0.7 m above the wall base.

2.2.3 WALL-CORNER FIRES. To characterize the 0.1 m high PMMA initiator of fire spread in the corner configuration, flame height is measured with inert walls supporting the PMMA insert. At one-atmosphere, peak flame height of about 0.41 m occurs roughly 540 seconds after ignition. Similar values of flame height, about 0.45 m if scaled to one-atmosphere conditions, are measured during model tests at 11.2 and 20.5 atmospheres for corresponding scaled times after ignition. Generally, flame spread on fuel walls of the corner configuration occurs within 200-300 seconds, when flames are just slightly above the 0.1 m high PMMA initiator.

Experiments with cellulosic char-forming fuels in the corner configuration demonstrate self-sustained upward flame spread from a PMMA initiator if the fuels have low moisture content. A 51 mm high PMMA initiator is found to be adequate for pine-wood ignition but not for the particle-board fuel, which requires the 102 mm high PMMA. In both cases, flame spreads to the top of the corner while generally confined to the apex region. Lateral spread then follows most rapidly near the top of the fuel as a "V" shaped pattern is formed. In contrast to PMMA fuel, flame spread does not continue laterally to the outer edge of the walls at one-atmosphere. The one-atmosphere process of lateral spread halts rather suddenly with pine-wood and particle-board when the char build-up in the apex region extinguishes flaming combustion there. In two tests with particle-board at one-atmosphere, complete extinction occurs reproducibly after about 720 seconds and a maximum lateral propagation on each leg of 0.127 m from the corner (0.18 m total flame width projected onto a plane normal to the apex angle bisector). Complete extinction occurs with

full-scale pine-wood after about 360 seconds and maximum lateral propagation of 0.165 m from the corner (0.23 m total projected flame width). This extinction phenomenon is not observed with cellulosic fuels at elevated pressures until well after flame spread across the entire fuel surface is complete.

Experiments with GM-37, a rigid polyurethane foam[3], as the wall corner material show that self-sustained upward flame spread is not possible at one-atmosphere during exposure to 0.05, 0.1 or 0.2 m high PMMA initiators. With the 0.1 m high initiator discussed before, flame spreads upward to a maximum height of only 0.61 m. Further upward spread is retarded by bubbling of the GM-37 surface (intumescent effect) and dripping of urethane fuel down over the PMMA initiator. By 600 seconds after ignition, this dripping partially extinguishes the PMMA fire. The result for GM-37 is very different at elevated pressures since rapid upward and lateral flame spread occurs.

2.3 EXPERIMENTAL RESULTS

Time resolved measurements of total flame height, upward flame spread rate, maximum flame width and fuel mass loss rate are shown in Figures 1-25. For the transparent PMMA fuel wall, measurements of pyrolysis zone height, upward pyrolysis spread rate and maximum pyrolysis width are shown in addition to the flame height time-history. Data from full-scale and model experiments has been correlated in Figures 1-25 by utilizing the pressure modeling scheme. Since the time scale of model experiments is reduced as the -4/3 power of ambient air pressure, all time measurements are multiplied by the 4/3 power of the ratio of actual air pressure, p, to standard atmospheric pressure, p_o. Beyond this pressure correction, the time origin for many elevated pressure experiments has been shifted to yield the best correlation of data during the initial stages of upward fire spread. The time origin for the full-scale experiments corresponds roughly to ignition of the PMMA fuel or corner initiator.

2.3.1 FLAME HEIGHT. It can easily be shown that successful modeling of transient heat release rates, $\dot{Q}$, by elevated pressure experiments also implies successful modeling of flame heights. Consider the burning of fuel vapor in a free plume above a burning solid. Empirical correlations from

Steward[4] and from You and Faeth[5] give the flame height, x_f, above such a fuel source as follows:

$$x_f = C_1 \left(\frac{\dot{Q}}{\rho_\infty}\right)^{2/5}$$

where ρ_∞ is ambient air density and C_1 is a constant for a given fuel heat of combustion, stoichiometry and ambient temperature. In the pressure modeling scheme, heat flux, $\dot{Q}''$, increases as $p^{2/3}$ but since fuel area is decreasing as $p^{-4/3}$, total heat release rate decreases as $p^{-2/3}$. Ambient air density at constant ambient temperature is simply proportional to ambient pressure, p. As a result, the flame height correlation yields a decrease in x_f as $p^{-2/3}$, which is just the dependence required by the pressure modeling technique.

If combustion occurs in a wall plume (or wall fire, as in the present experiments) instead of a free plume, the following expression can be derived from the analysis of Steward[6] by assuming one-half the entrainment of the free plume:

$$x_f = C_2 \left(\frac{\dot{Q}'}{\rho_\infty}\right)^{2/3}$$

where C_2 is a constant for a given fuel and $\dot{Q}'$ is the total heat release rate per unit width of the wall configuration. Since heat flux, $\dot{Q}''$, should increase a $p^{2/3}$ while pyrolysis height x_p, decreases as $p^{-2/3}$,

$\dot{Q}' = \int_0^{x_p} \dot{Q}''\, dx$ should be independent of pressure. The wall fire flame height therefore decreases as $p^{-2/3}$, in accord with the modeling scheme.

Because all characteristic lengths are reduced as $(p/p_o)^{-2/3}$, the correction of flame height, x_f, (and pyrolysis height, x_p) for pressure by the factor shown in Figures 1-7A should result in a correlation of data for each material. To the extent that fuel thickness is important during the flame spread process, a high degree of correlation, and hence modeling success, would not be expected in those cases where the sample thickness is the same at both atmospheric and ambient pressures.

Modeling of flame height and pyrolysis height on the PMMA wall (Figures 1 and 2) is quite good. It appears that the maximum scaled flame height for the models is somewhat greater than that for the full-scale fuel even though the fuel is thermally thick and fuel thickness is scaled properly. Flame heights greater than 0.9 m, it should be noted, are above the top edge of the PMMA wall.

Figure 3 shows the expected similarity between flame spread on the laminate and that on uniform PMMA walls at one atmosphere. This flame spread similarity is probably due to the small disturbance of PMMA thermal characteristics by the ceramic cement and the small amount of PMMA surface layer consumed during most of the one-atmosphere flame spread process. At extinguishment of the full-scale PMMA-PMMA laminate fire, the 3.18 mm face layer is indeed consumed in a triangular region only 0.46 m high and 0.11 m wide at the base of the wall. The amount of face layer consumed was apparently not enough to reduce the wall burning rate and hence the flame height.

It is not clear why the scaled flame heights for the model PMMA-PMMA laminates are much greater than the values at one-atmosphere. In fact, these model flame heights are very similar to those for the PMMA-Inert laminate in Figure 4. The inert backing in the latter case reduces the heat loss sufficiently to cause an observable increase in flame spread rate compared to uniform PMMA, data for which is also shown in Figure 4. Another unexpected result is the good agreement between model and full-scale flame heights for the PMMA-Inert laminate. At elevated pressures, the PMMA face layer should begin to simulate a thermally thick PMMA slab rather than the thermally thin condition that roughly exists at one-atmosphere. It can be seen in Figure 4 that flame heights tend progressively toward those for the uniform PMMA wall as ambient pressure increases but this shift is much less than expected.

Pressure modeling accuracy for flame height on the PMMA wall-corner is exceptionally good, as shown by the data in Figure 5. This excellent flame height correlation even extends to the region above the fuel surface at $x_f = 0.9$ m. For the particle-board corner (see Figure 6), modeling of flame height is also fairly good at 11.2 and 20.5 atmospheres. Flame heights are clearly less than expected (below the correlation) at the 31.6 atmosphere pressure. Note that

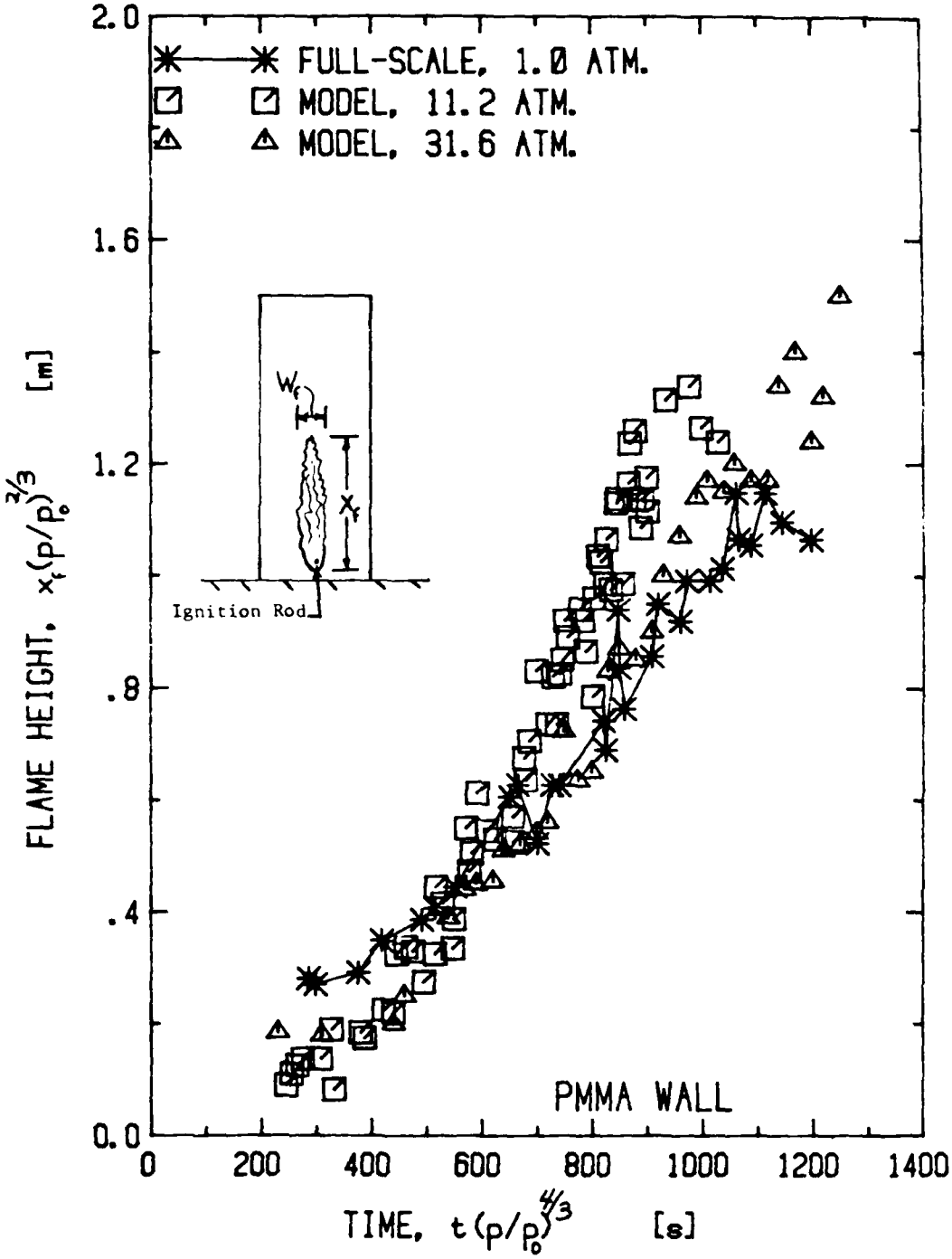

FIGURE 1 CORRELATION OF FLAME HEIGHT ON PMMA WALLS

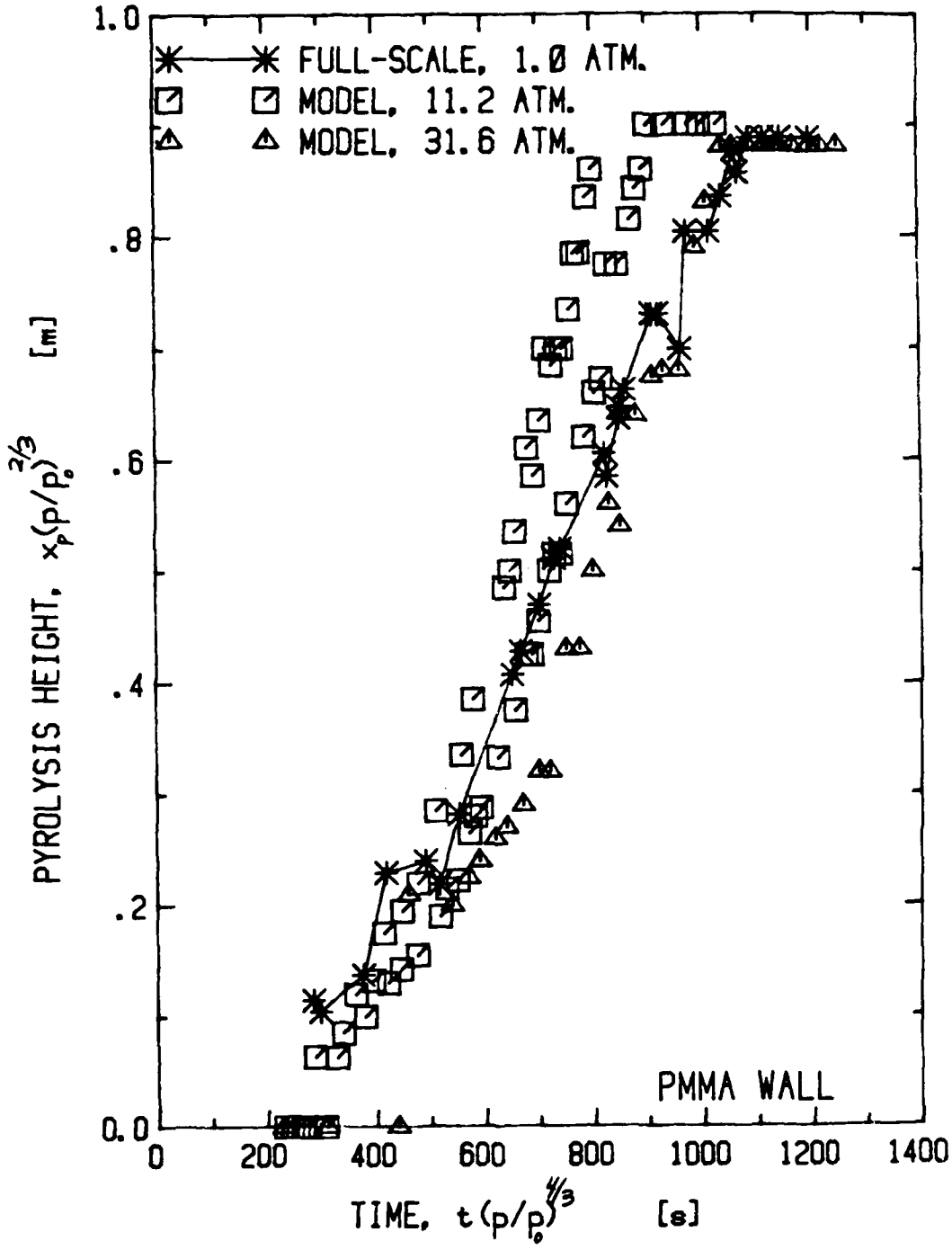

FIGURE 2 CORRELATION OF PYROLYSIS HEIGHT ON PMMA WALLS

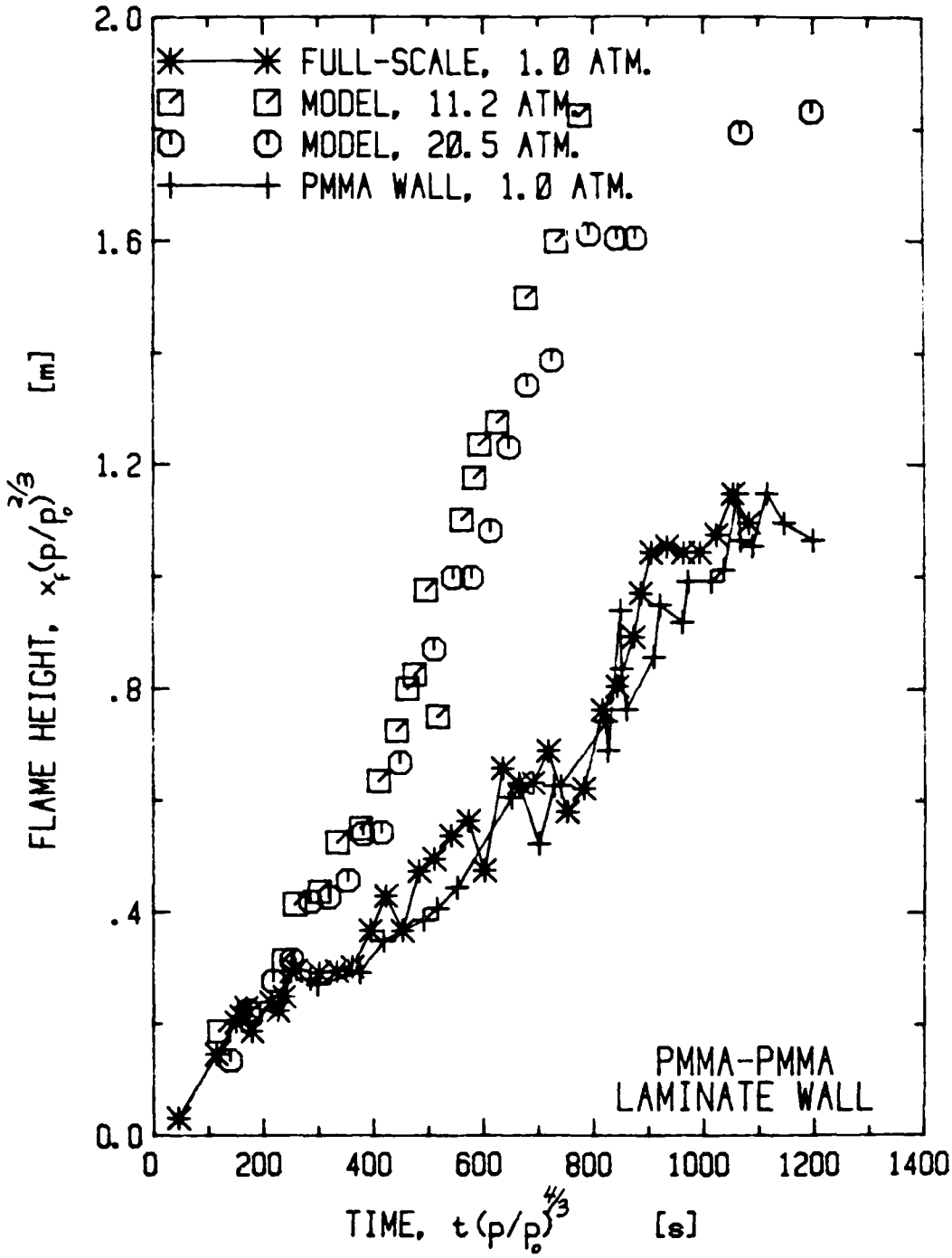

FIGURE 3 CORRELATION OF FLAME HEIGHT ON PMMA-PMMA LAMINATE WALLS

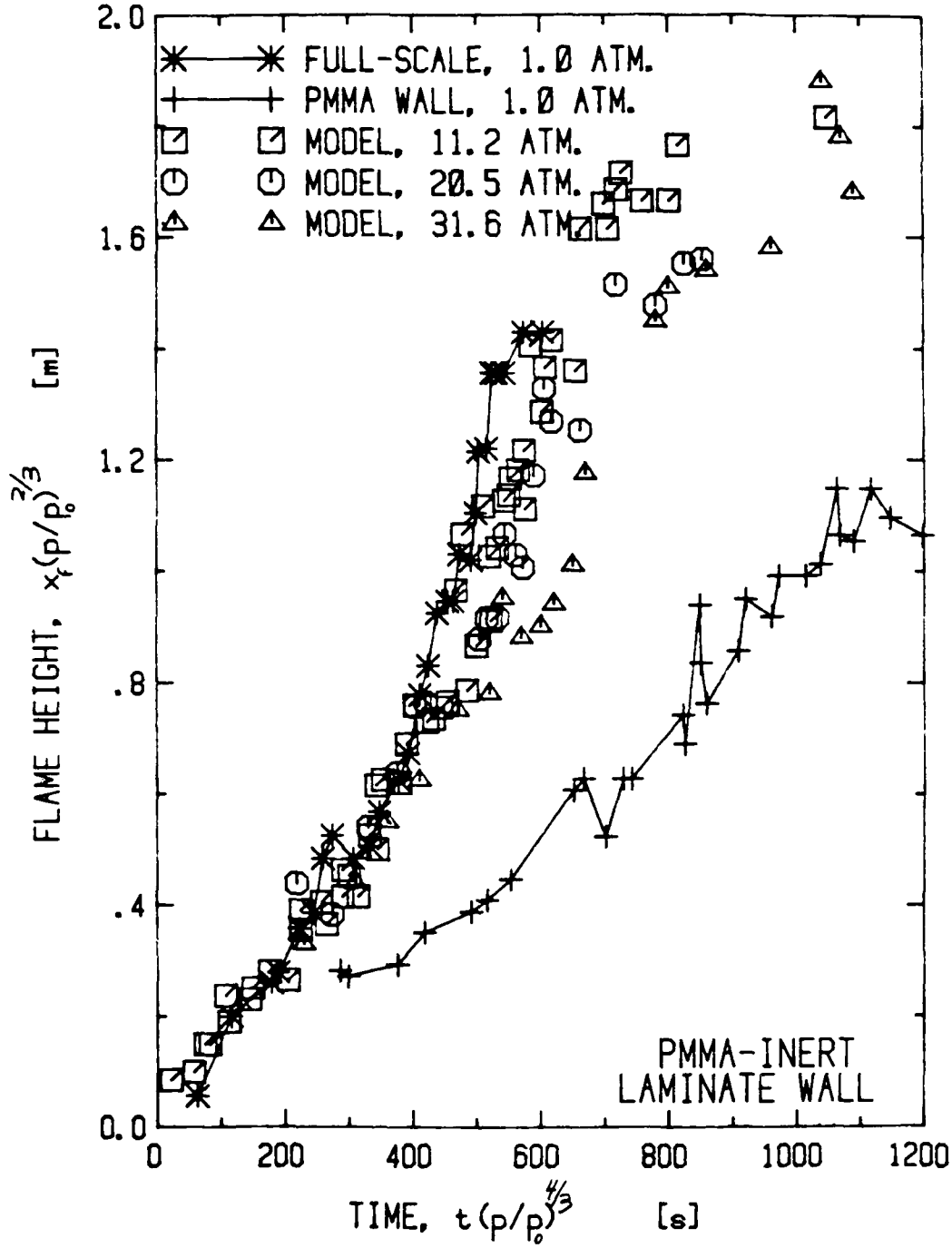

FIGURE 4 CORRELATION OF FLAME HEIGHT ON PMMA-INERT LAMINATE WALLS

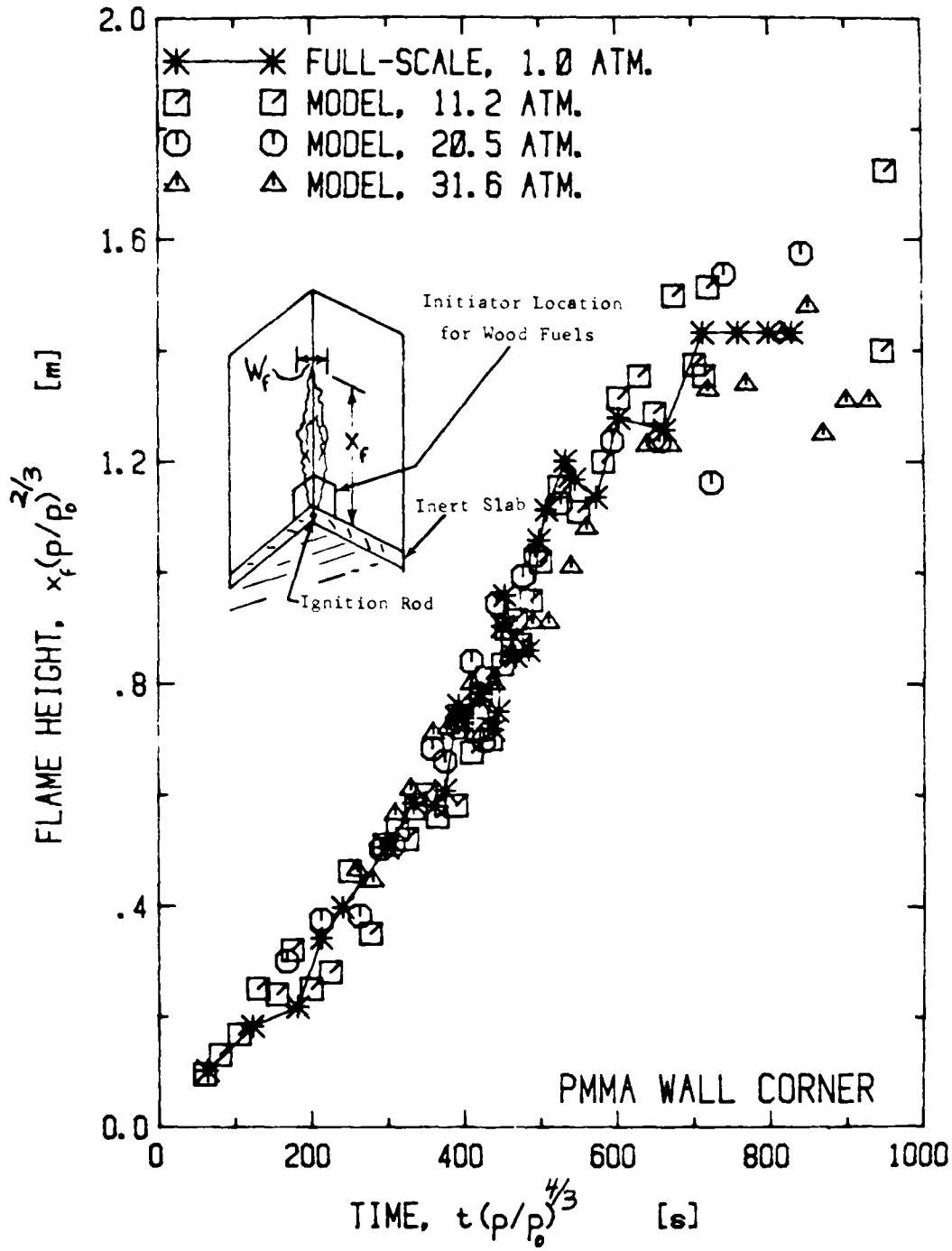

FIGURE 5 CORRELATION OF FLAME HEIGHT ON PMMA WALL CORNERS

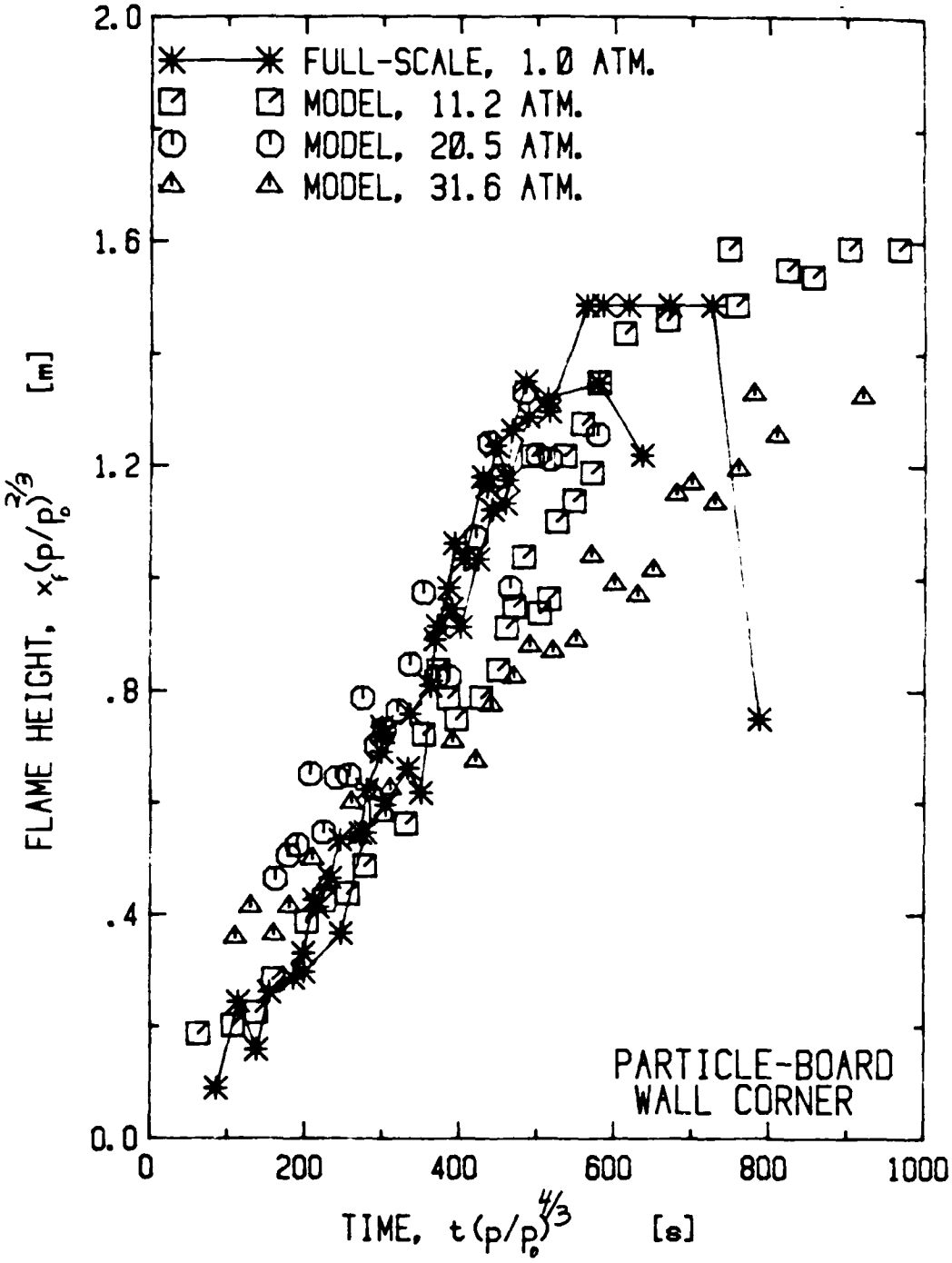

FIGURE 6 CORRELATION OF FLAME HEIGHT ON PARTICLE-BOARD WALL CORNERS

the 1 atmosphere extinction phenomenon discussed earlier leads to a sharp decrease in full-scale flame height at about 700 seconds. A similar flame height behavior is seen in Figure 7, where results for pine-wood are correlated. In this case, the modeling scheme is quite accurate at all three elevated pressures. The extinction of lateral fire spread at one atmoshpere leads to a peak, full-scale flame height somewhat below that predicted by the model tests.

Flame height measurements for the GM-37 rigid foam material are correlated in Figure 7A. The lack of sustained upward flame spread at one atmosphere is evident from the nearly constant, 0.6 m flame height on the 1.22 m high fuel from 350 to 550 seconds after ignition. Flame heights associated with the PMMA initiator alone set into an inert corner are also shown in Figure 7A. There appears to be only a small contribution from the GM-37 fuel at one atmosphere, leading to a peak flame height about 0.2 m greater than that due to the PMMA alone. On the other hand, upward flame spread is seen to proceed rapidly up the total fuel height of the models at 11.2 and 20.5 atmospheres. Flame heights for the two model scales are well-correlated by the variables in Figure 7A. It is possible that the full-scale flame heights would also follow the model correlation if a sufficiently large initiator of flame spread were used.

2.3.2 UPWARD FLAME SPREAD RATE. For each of the fuel configurations, the transient flame height data in Figures 1-7 are fit with a cubic polynomial least squares regression. This polynomial fit is then differentiated to give vertical flame spread rates. Since the ratio of length to solid phase time (velocity) should increase as $p^{2/3}$ in the modeling scheme, flame spread rates are corrected for pressure by the $p^{2/3}$ factor shown in Figures 8-13. As expected, correlation of rates of change of flame heights are far less satisfactory than the original flame height correlations. Only the PMMA corner configuration still yields favorable modeling success when upward spread rates are examined.

Figures 8 and 9 show clearly that modeling of upward flame spread rate on a PMMA wall improves as air pressure increases from 11.2 to 31.6 atmosphere. This phenomenon, which has been discussed previously, is due to the competing

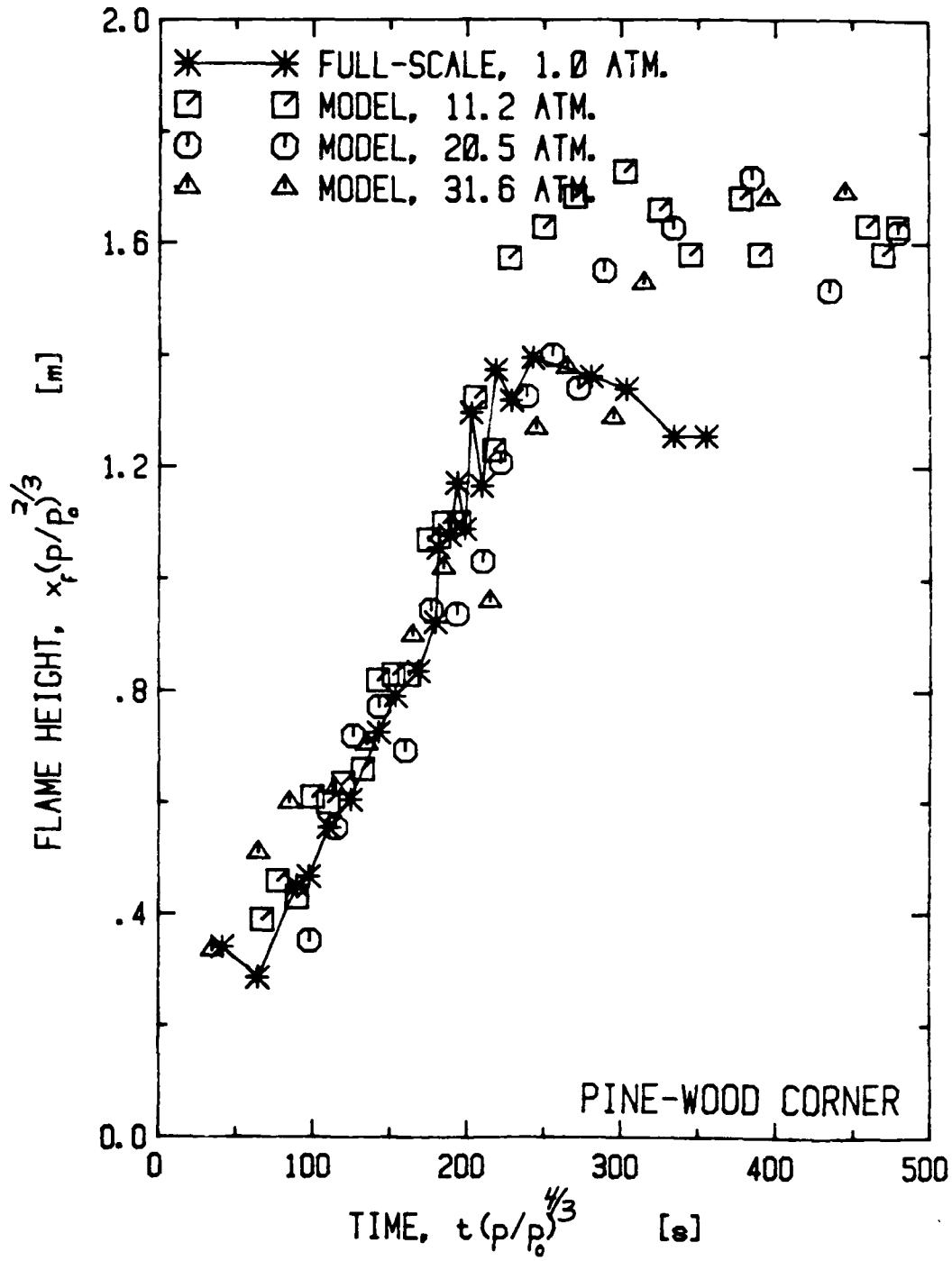

FIGURE 7 CORRELATION OF FLAME HEIGHT ON PINE-WOOD WALL CORNERS

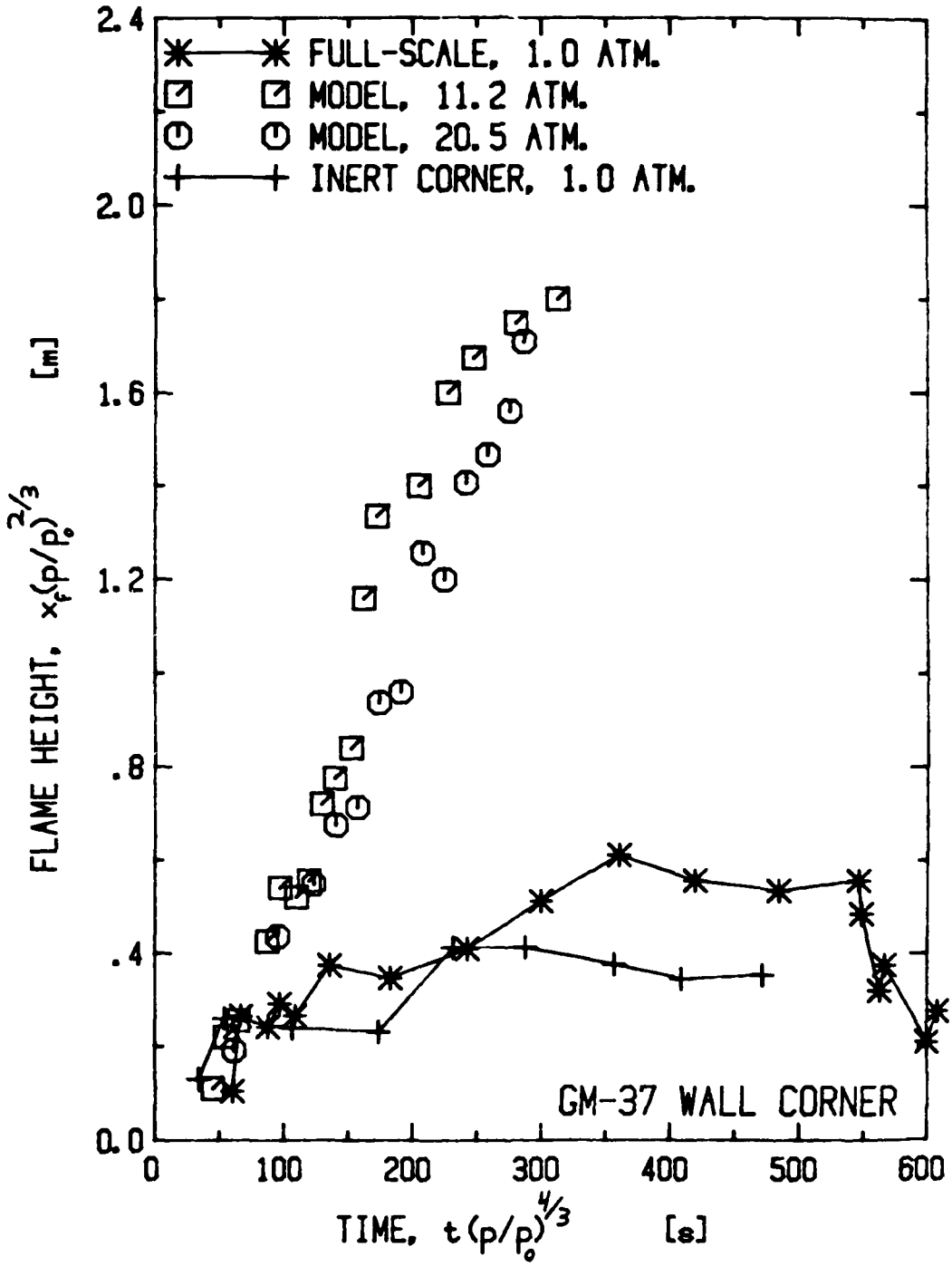

FIGURE 7a CORRELATION OF FLAME HEIGHT ON GM-37 WALL CORNERS

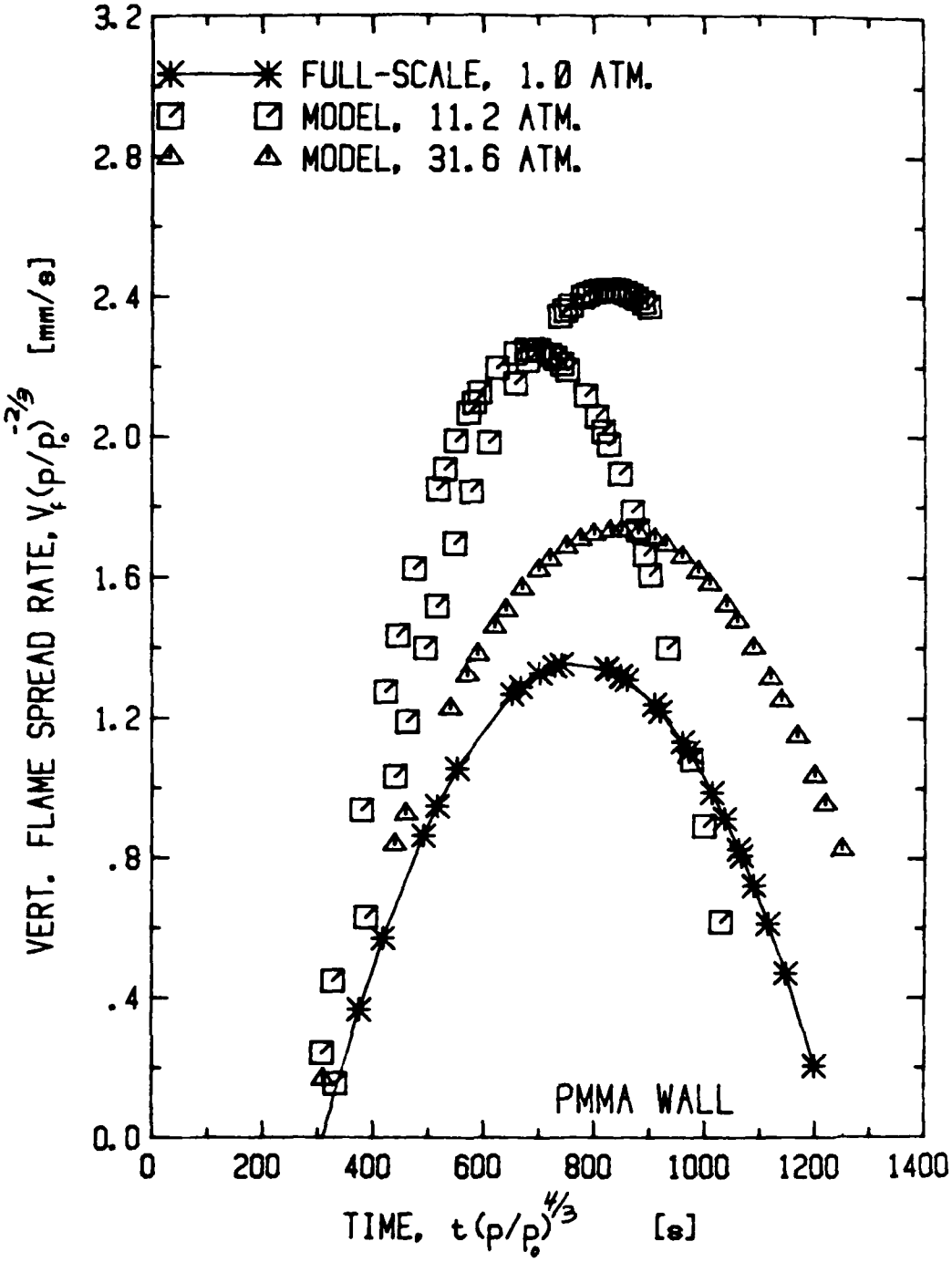

FIGURE 8 CORRELATION OF VERTICAL FLAME SPREAD RATE UP PMMA WALLS

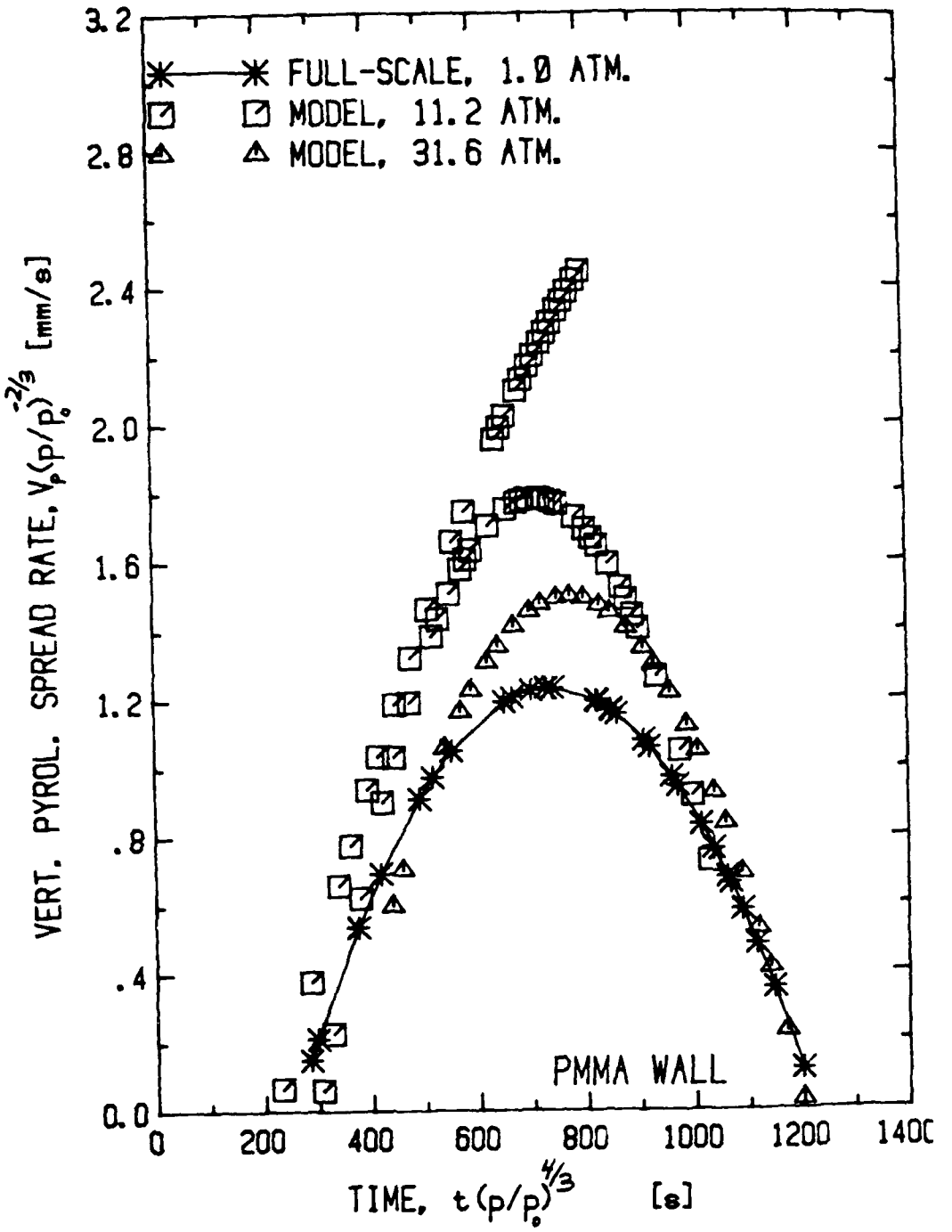

FIGURE 9 CORRELATION OF VERTICAL PYROLYSIS SPREAD RATE UP PMMA WALLS

effects of low solid surface radiative heat loss and flame radiative saturation. The former effect is more important at 11.2 atmoshperes, leading to spread rates higher than expected from the modeling scheme while flame saturation leads to reduced spread rates, closer to the expected values at 31.6 atmospheres.

Upward flame spread rates on the PMMA-inert laminate wall are correlated in Figure 10. Here, the approach to thermally thick behavior as elevated pressure increases can be seen more clearly than was the case for the flame height data in Figure 4.

For the wall-corner configurations, modeling of upward flame spread rate is only accurate for the PMMA fuel, as is evident in Figures 11-13. Spread rates for particle-board are less than expected at 11.2 and 20.5 atmospheres but modeling for pine-wood is reasonably good at these pressures (see Figures 12 and 13). At 31.6 atmospheres, scaled spread rates for both particle-board and pine-wood are much less than corresponding one-atmosphere values.

2.3.3 FLAME WIDTH. Data on the maximum width of the flame zone (or pyrolysis zone for the case of the PMMA wall) as a function of time are correlated in Figures 14-19. For the PMMA wall (see Figure 14), the data correlation is quite good until the flame extends above the top edge of the model and full-scale fuel walls at t = 600 and 800 seconds, respectively. This degree of modeling success is somewhat better than previous pressure modeling results[1], perhaps because of the lack of side-walls in the present fuel configuration. There still seems to be a strong tendency for the scaled, lateral fire growth on the model walls to be more rapid than that at one-atmosphere.

This same tendency is evident for the PMMA-PMMA laminate, data for which are correlated in Figure 15. The lateral spread rate for both the model and full-scale laminates are seen to be somewhat greater than that for a uniform PMMA wall. With the PMMA-inert laminate, the flame widths shown in Figure 16 clearly approach those characteristics of a uniform PMMA wall as ambient pressure increases and the face layer becomes thermally thick. As a result, scaled lateral spread rates for the model laminates are less than the values measured for the full-scale PMMA-inert laminate.

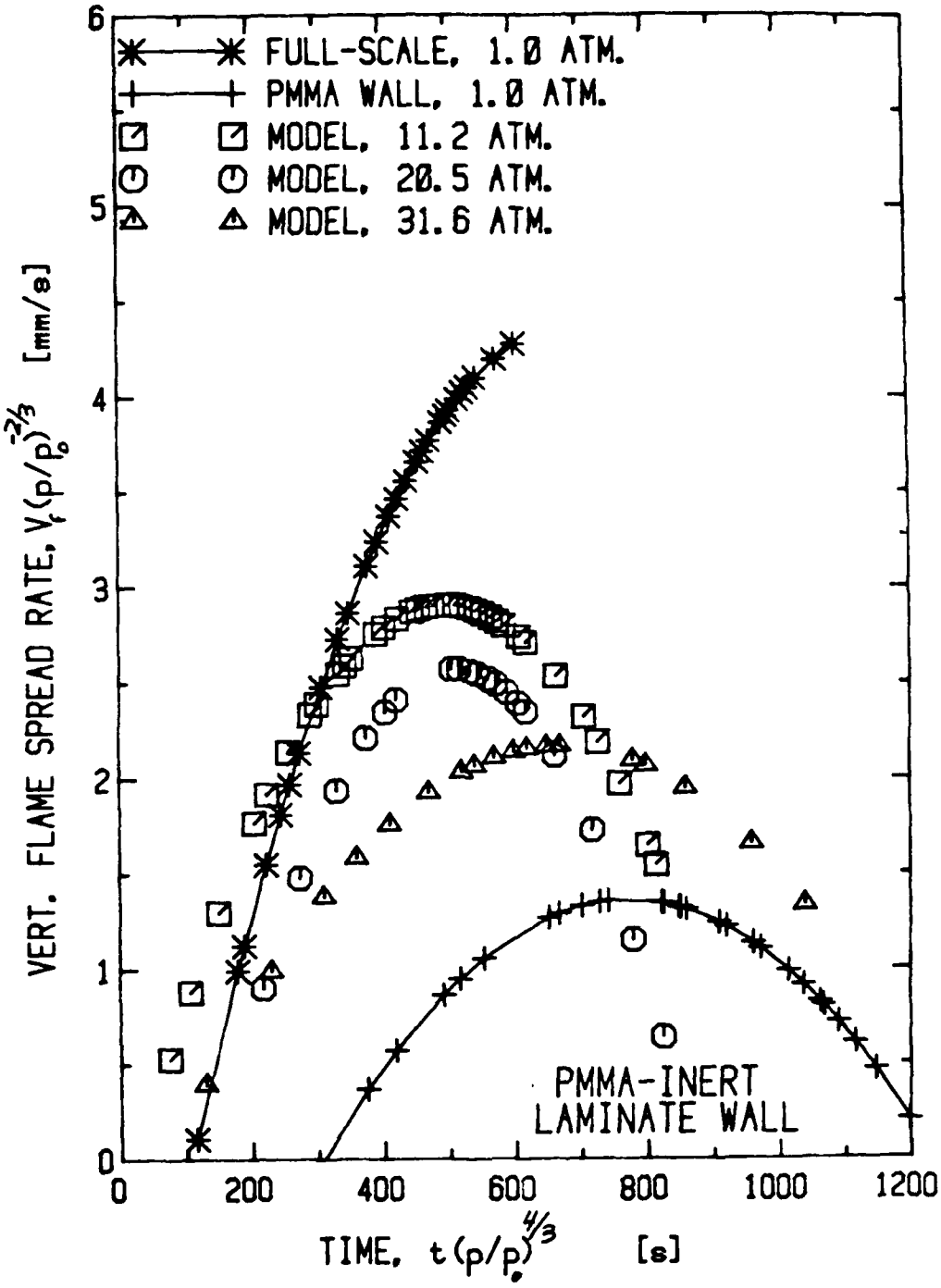

FIGURE 10 CORRELATION OF VERTICAL FLAME SPREAD RATE UP PMMA-INERT LAMINATE WALLS

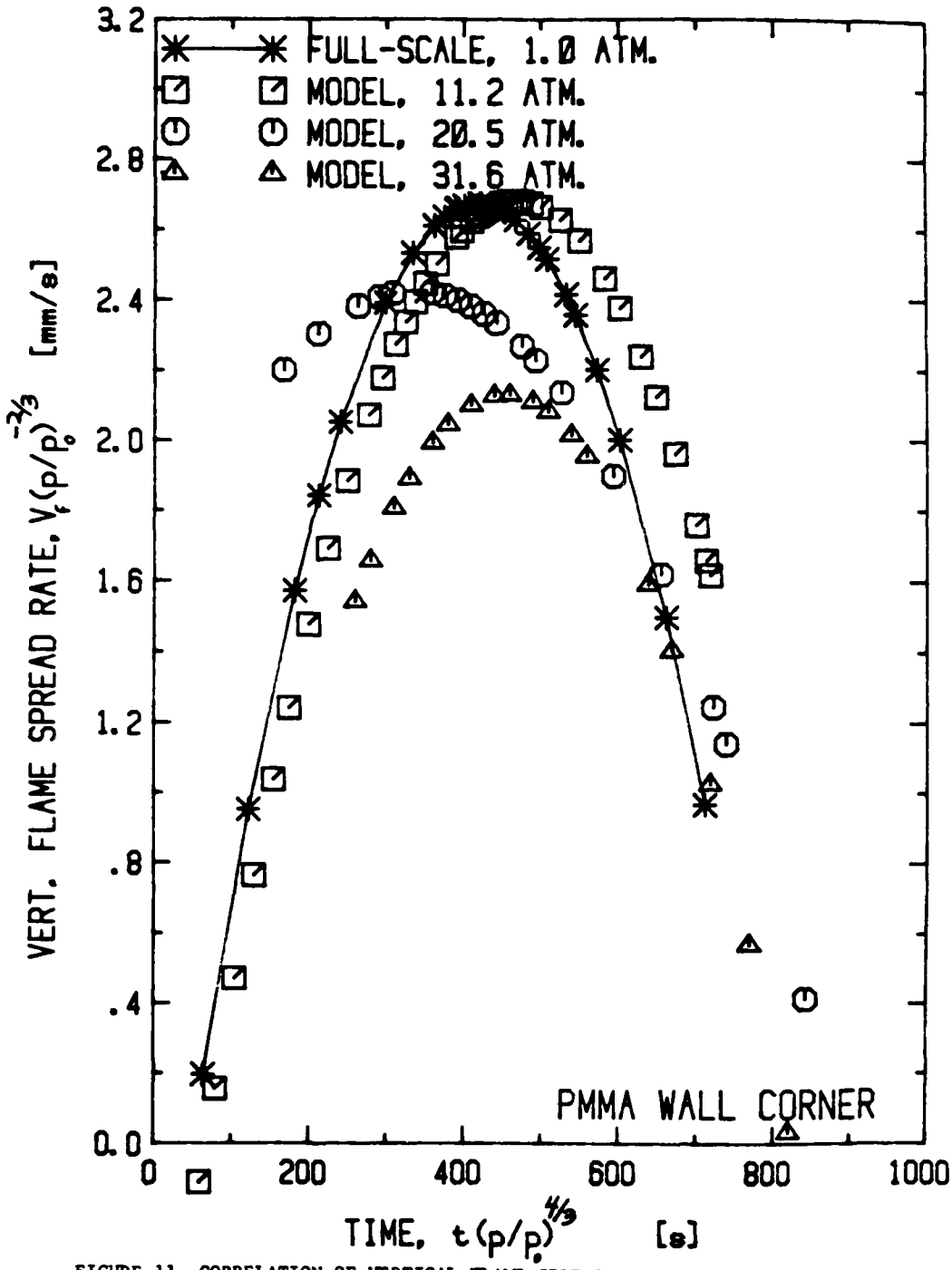

FIGURE 11 CORRELATION OF VERTICAL FLAME SPREAD RATE UP PMMA WALL CORNERS

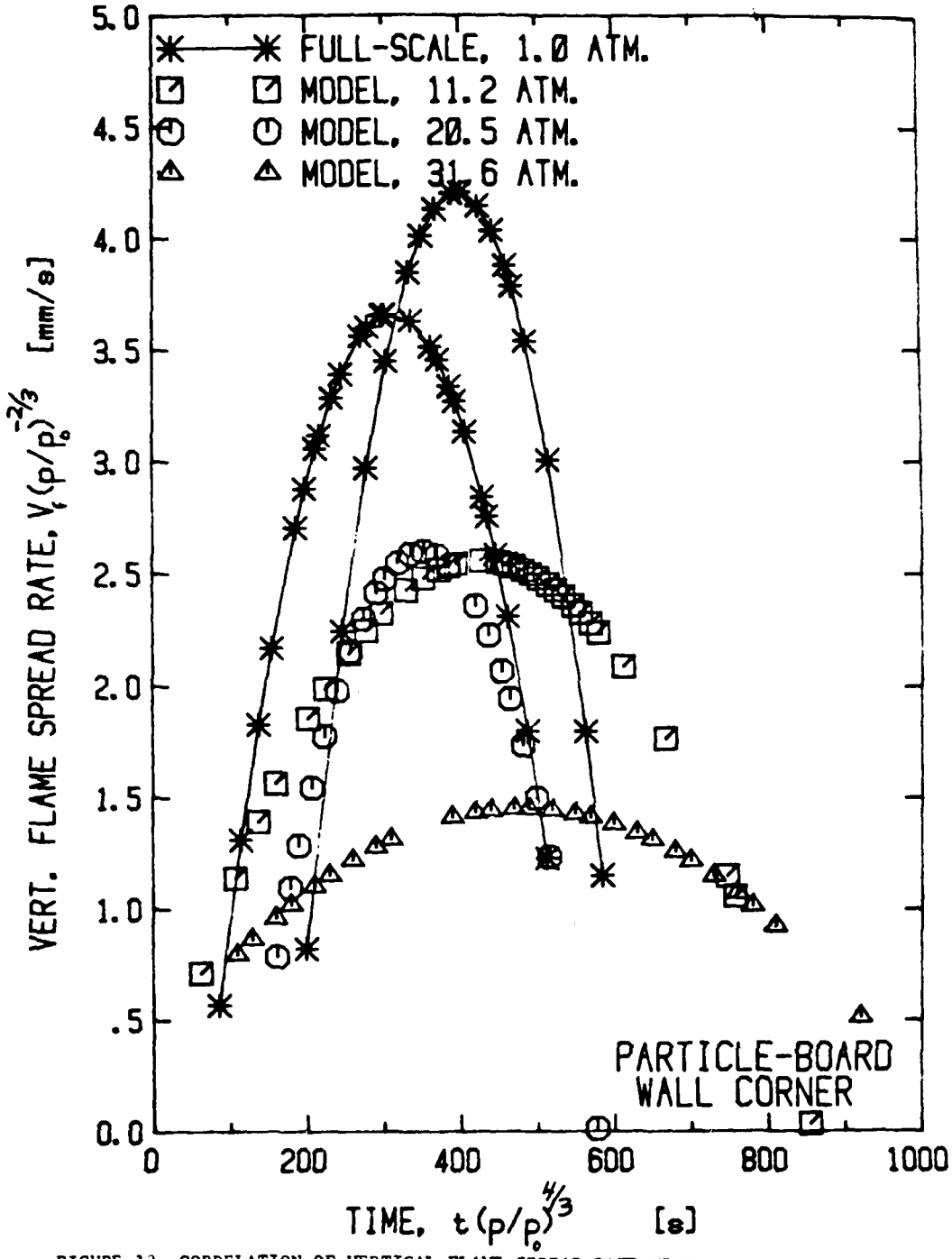

FIGURE 12 CORRELATION OF VERTICAL FLAME SPREAD RATE UP PARTICLE-BOARD WALL CORNERS

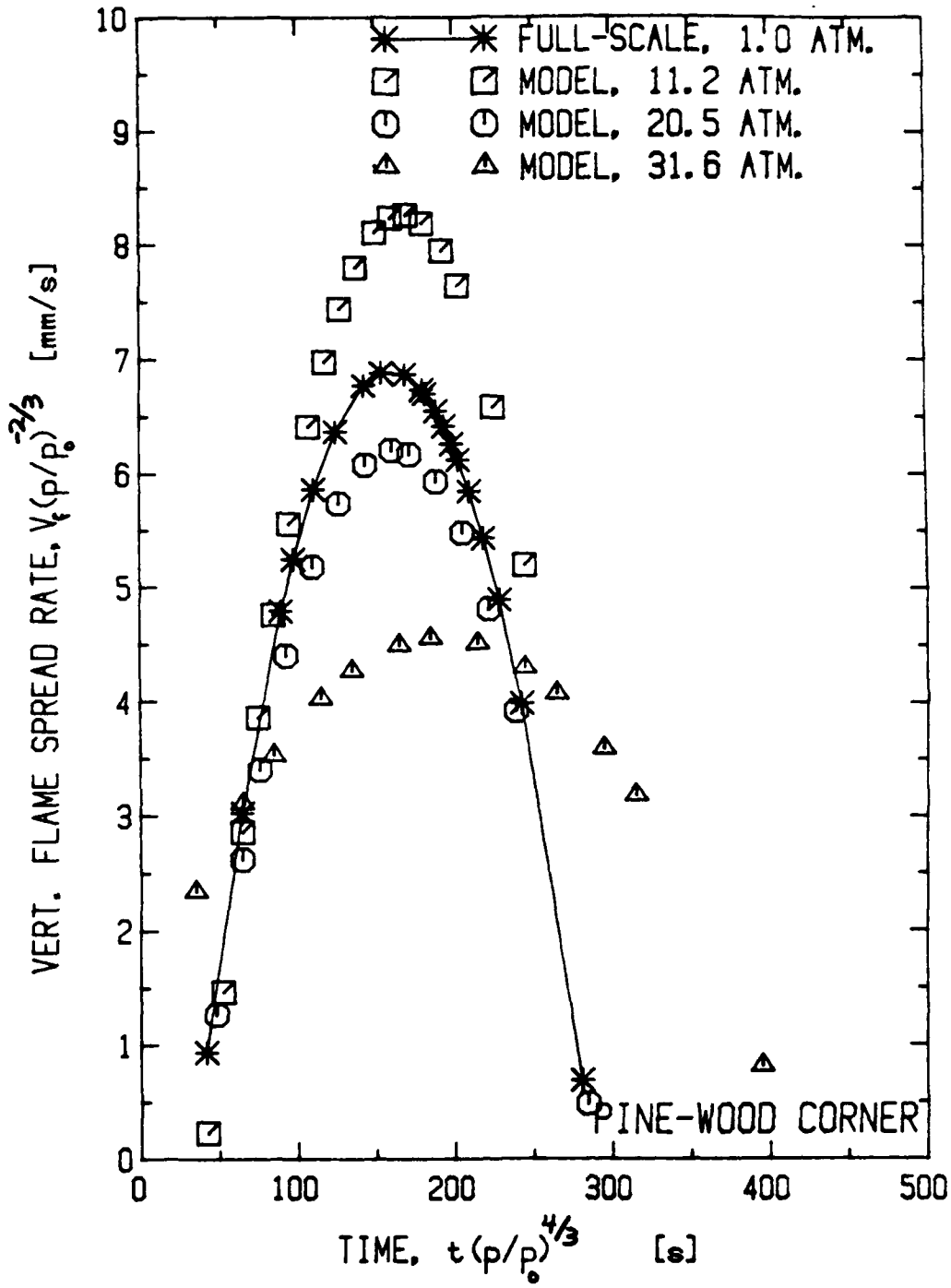

FIGURE 13 CORRELATION OF VERTICAL FLAME SPREAD RATE UP PINE-WOOD WALL CORNERS

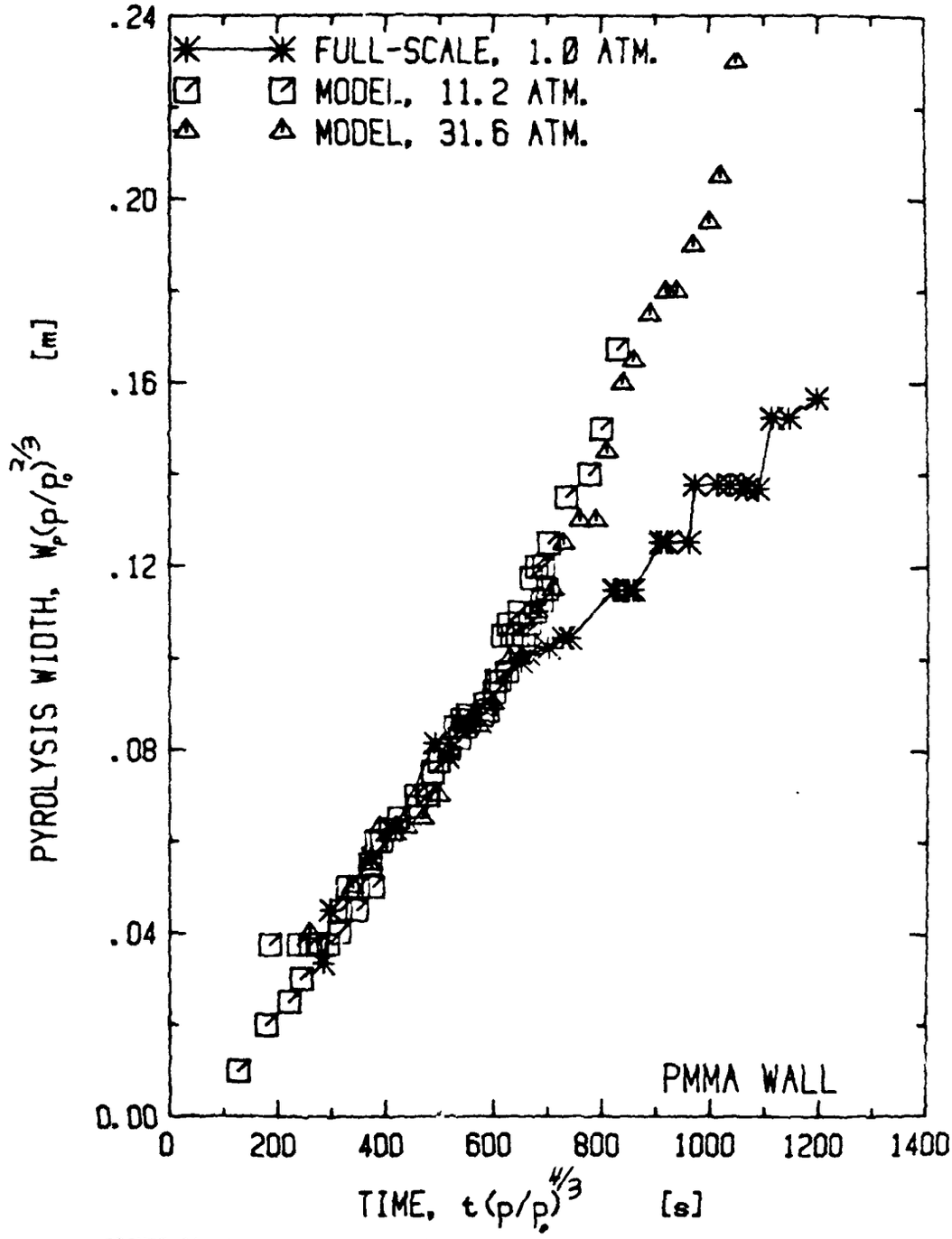

FIGURE 14 CORRELATION OF MAXIMUM PYROLYSIS ZONE WIDTH ON PMMA WALLS

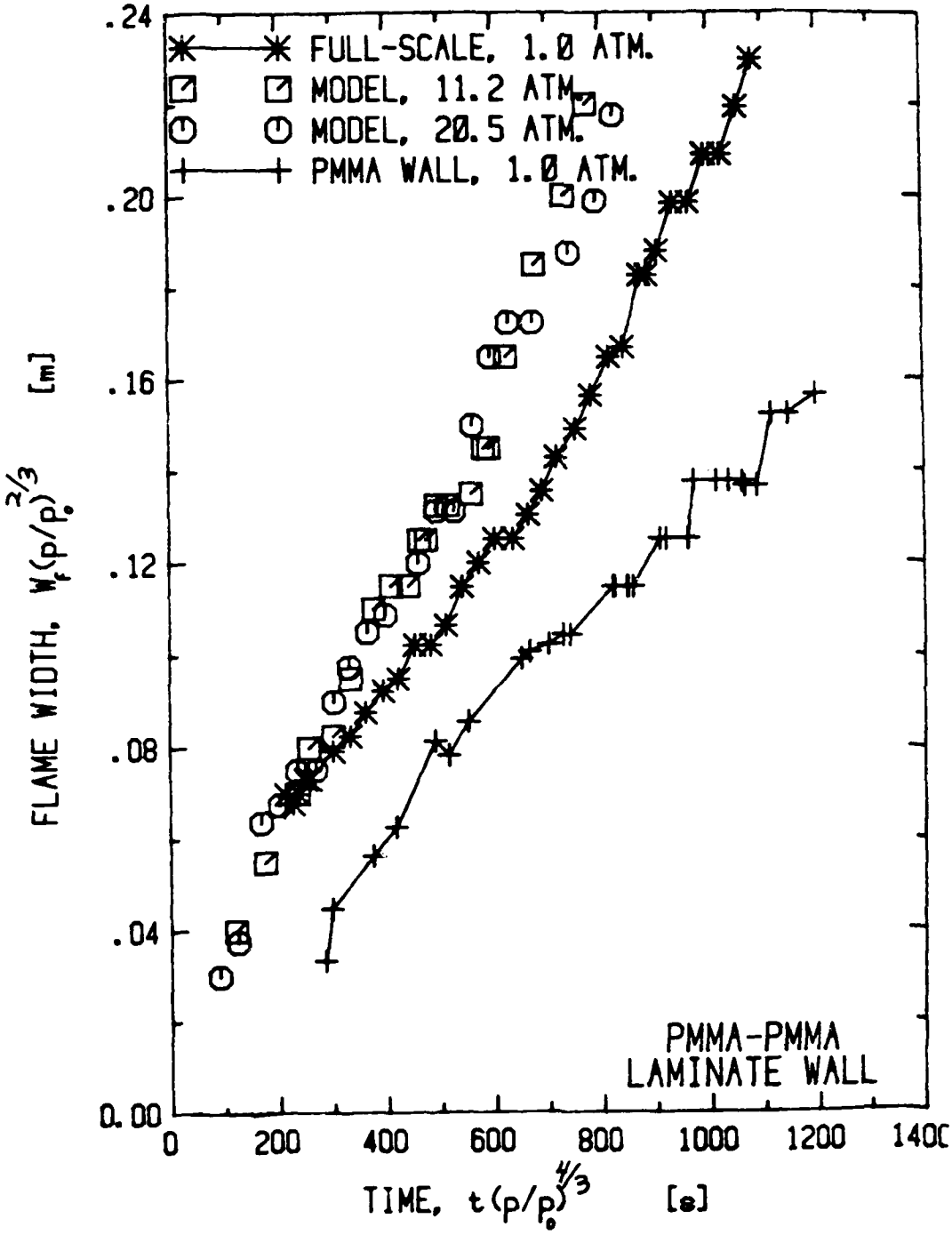

FIGURE 15 CORRELATION OF MAXIMUM FLAME WIDTH ON PMMA-PMMA LAMINATE WALLS

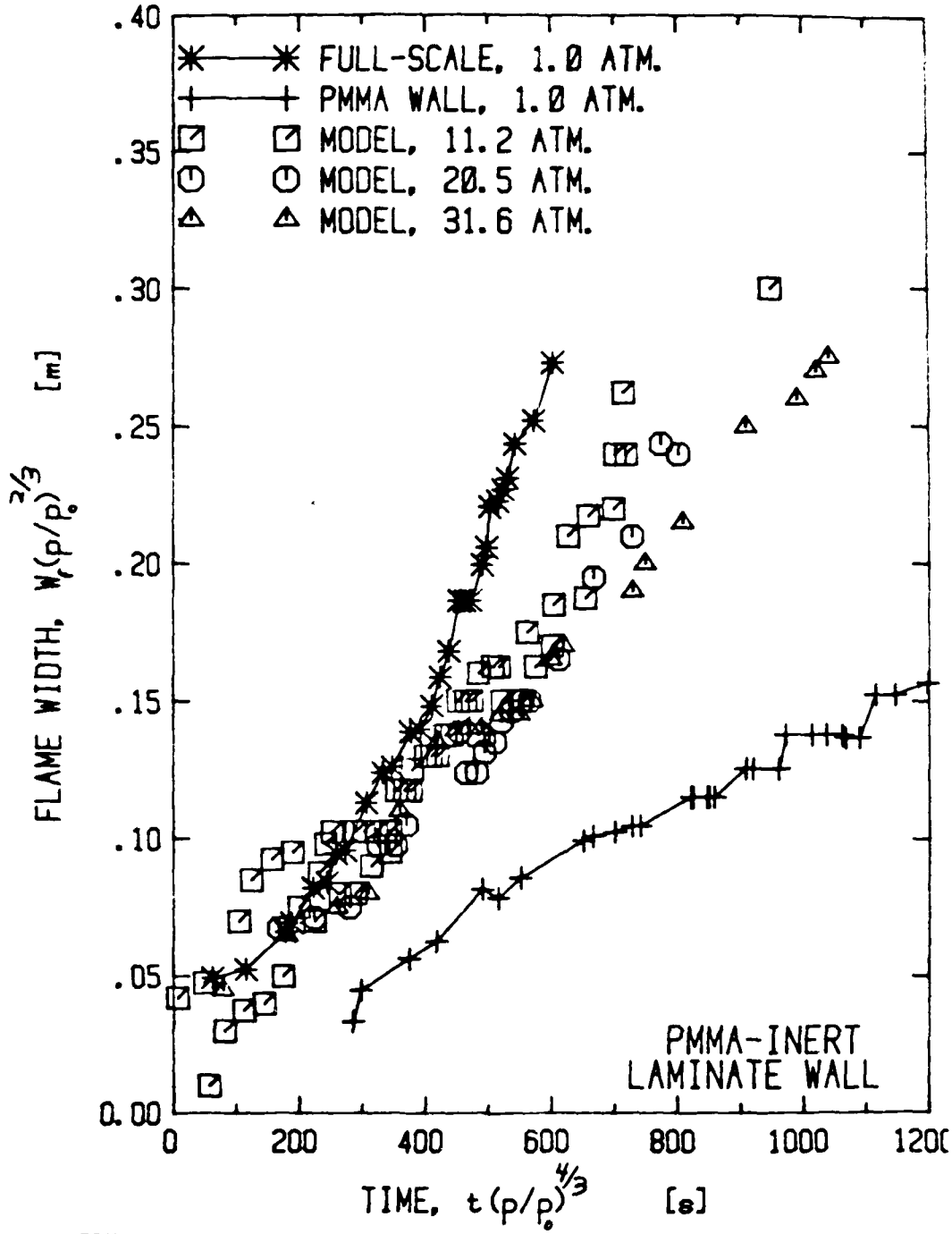

FIGURE 16 CORRELATION OF MAXIMUM FLAME WIDTH ON PMMA-INERT LAMINATE WALLS

Figures 17-19 contain flame width data for the corner fire as seen by an observer on the bisector of the 90° corner angle. Flame width, W, is therefore the value projected onto a plane normal to this angle bisector, or $\sqrt{2}$ times the horizontal distance on the fuel surface between the corner apex and each side of a symmetric flame front.

Modeling of lateral flame spread with the corner configurations is seen in Figures 17-19 to be reasonably good. In fact, the correlation of data is excellent for PMMA fuel (see Figure 17). Lateral flame spread for particleboard is modeled well, with the exception of the 31.6 atmosphere test. The smaller lateral flame widths in this case (see Figure 18), while consistent with the mass loss data shown in Figure 24, may simply represent data scatter. There appears to be a similar type of behavior for the pine-wood data shown in Figure 19.

2.3.4 MASS LOSS RATE. Transient measurements of fuel mass loss during upward and lateral fire spread are fit with a cubic polynomial least-squares regression. Differentiation of this polynomial fit yields the fuel mass loss rate, $\dot{m}$, which equals the rates of soot production plus fuel gasification. Since mass flux ($kg/m^2.s$) at homologous locations should increase as $p^{2/3}$ and burning areas decrease as $p^{-4/3}$ in the pressure modeling scheme, total mass loss rate should decrease as $p^{-2/3}$. Mass loss rates are therefore corrected for pressure by use of a $p^{2/3}$ factor in Figures 20-25 in order to correlate the data.

Results for the PMMA wall fire are shown in Figure 20. Measurements with the smallest model fuel at 31.6 atm pressure are not available because too high a load system sensitivity is required. Up to the time of extinguishment of the full-scale wall, modeling of mass loss rate is reasonable. Much of the discrepancy in the correlation is probably due to the lack of modeling ofthe lateral spread process after a test time of 800-900 seconds (see Figure 14).

In Figure 21, the mass loss rate of the full-scale PMMA-PMMA laminate is seen to be somewhat higher than that of a uniform PMMA wall of the same size, probably because of a slightly greater lateral flame spread (see Figure 15) in the former case. The greater scaled flame heights and widths on the model

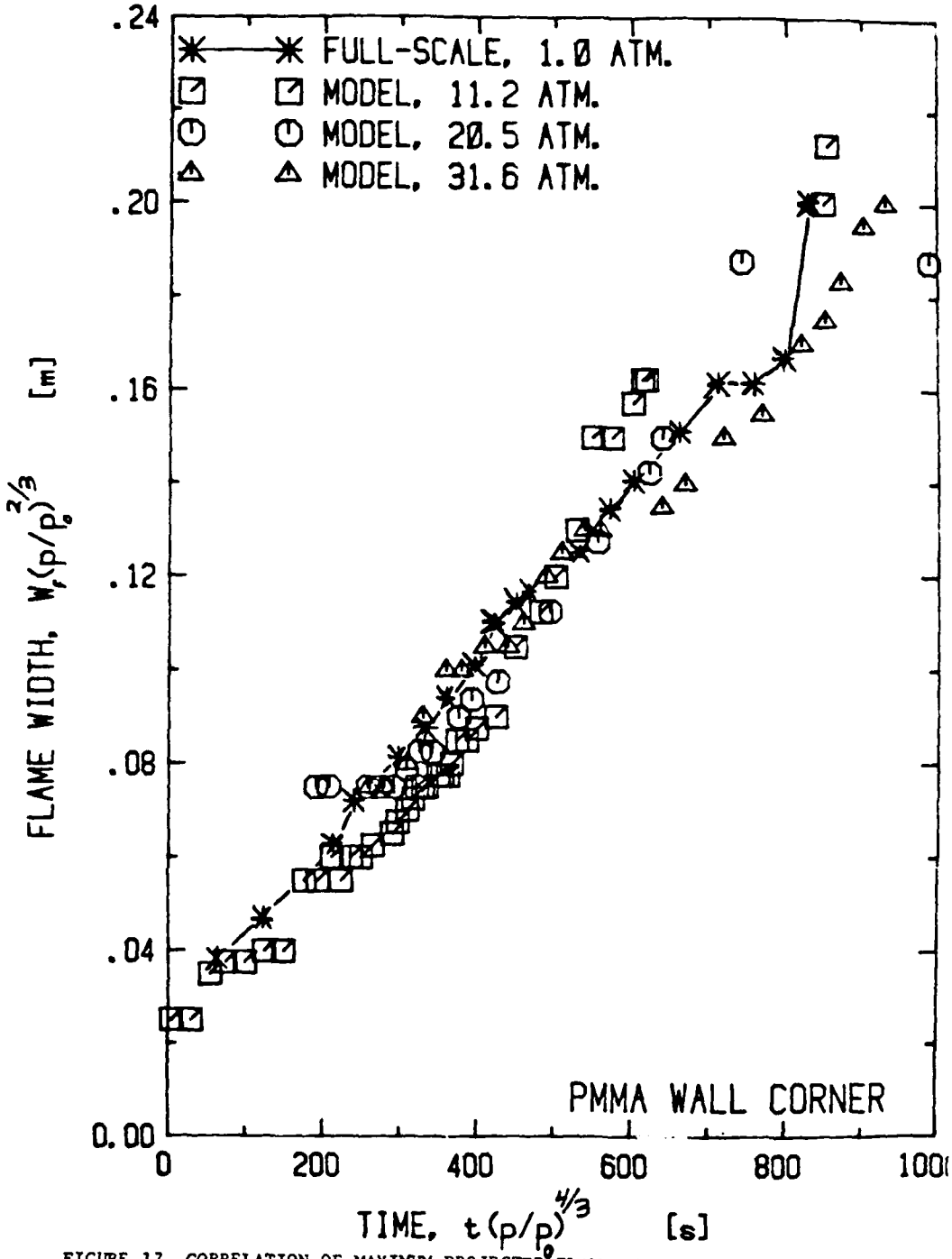

FIGURE 17 CORRELATION OF MAXIMUM PROJECTED FLAME WIDTH ON PMMA WALL CORNERS

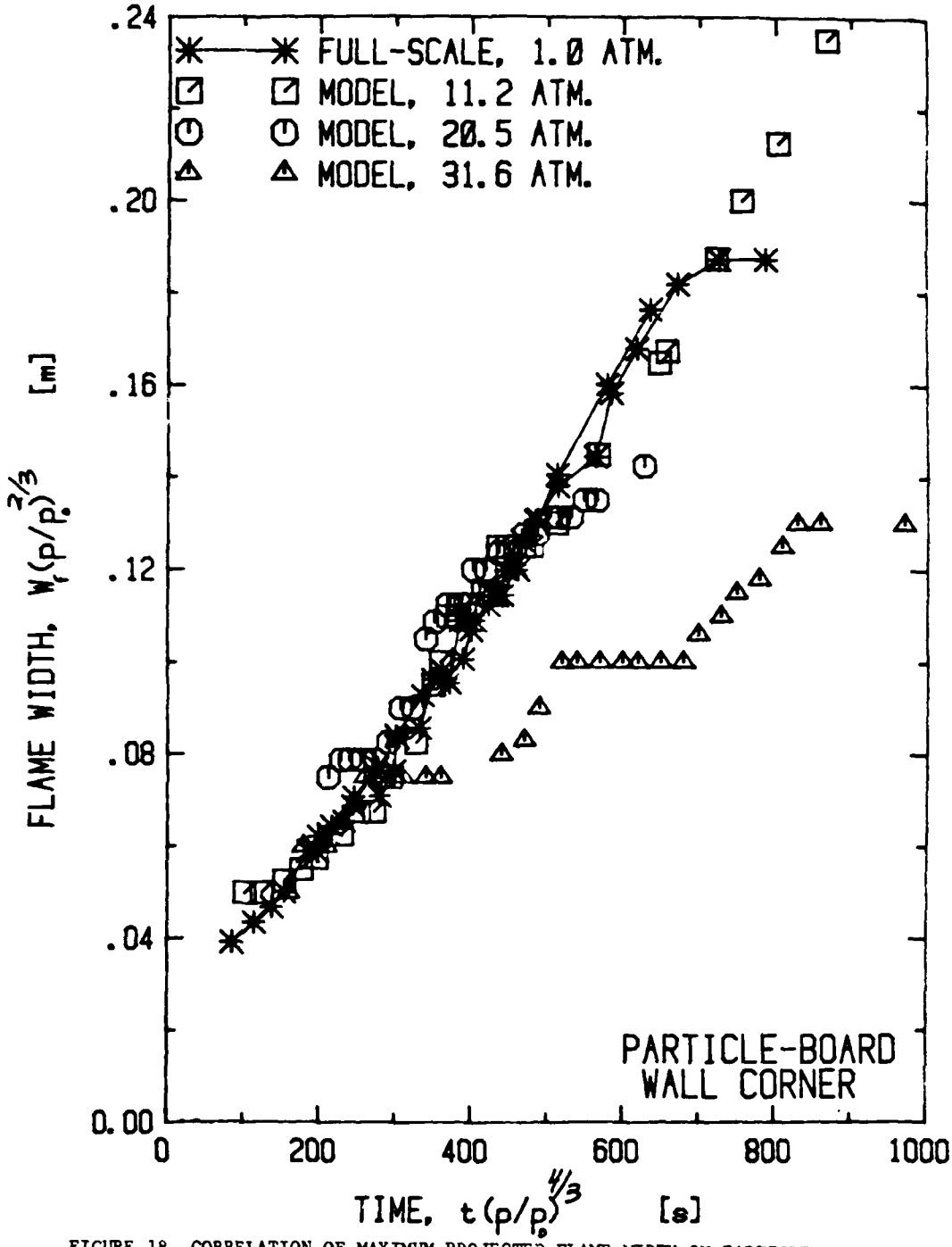

FIGURE 18 CORRELATION OF MAXIMUM PROJECTED FLAME WIDTH ON PARTICLE-BOARD WALL CORNERS

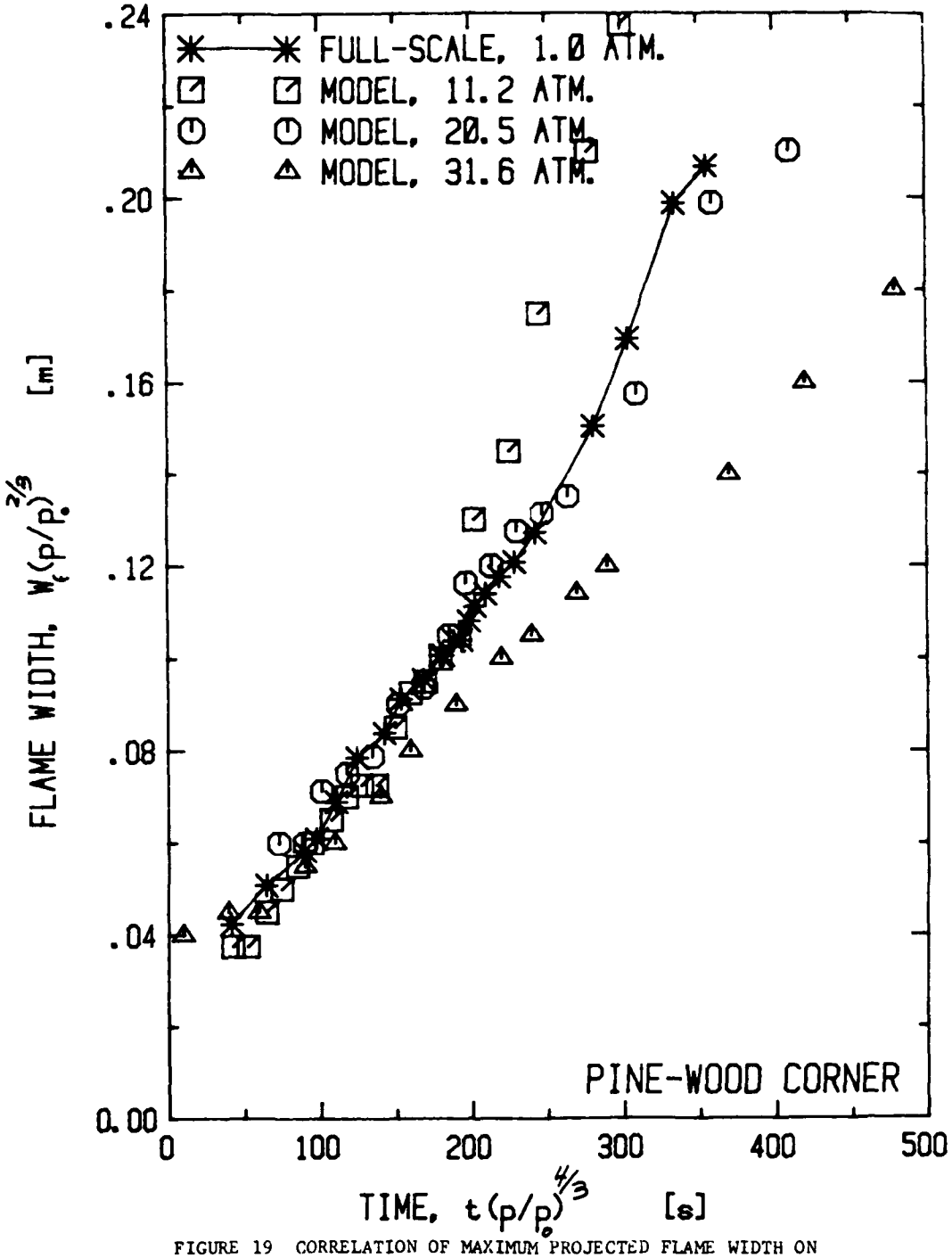

FIGURE 19 CORRELATION OF MAXIMUM PROJECTED FLAME WIDTH ON PINE-WOOD CORNERS

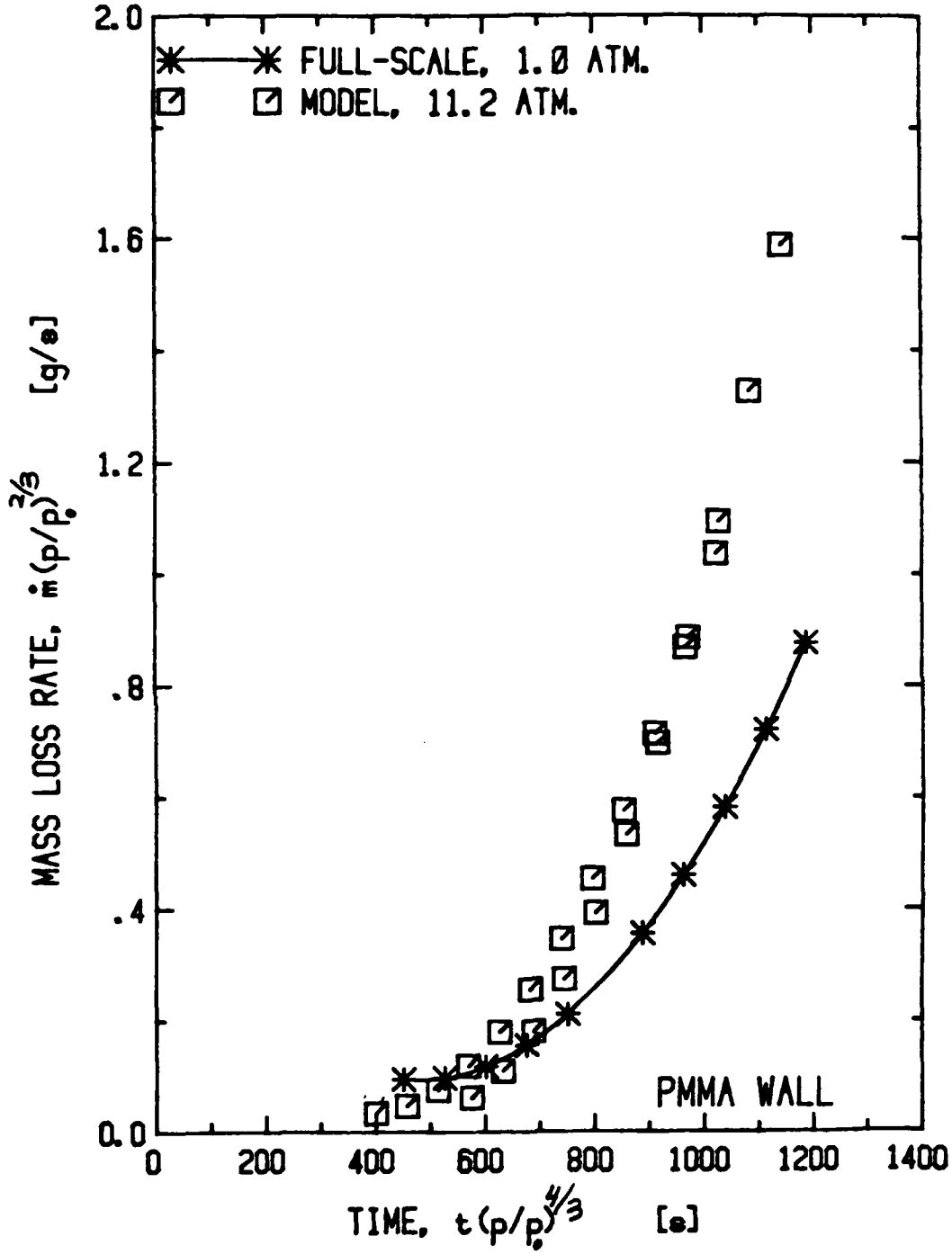

FIGURE 20 CORRELATION OF MASS LOSS RATE FOR PMMA WALLS

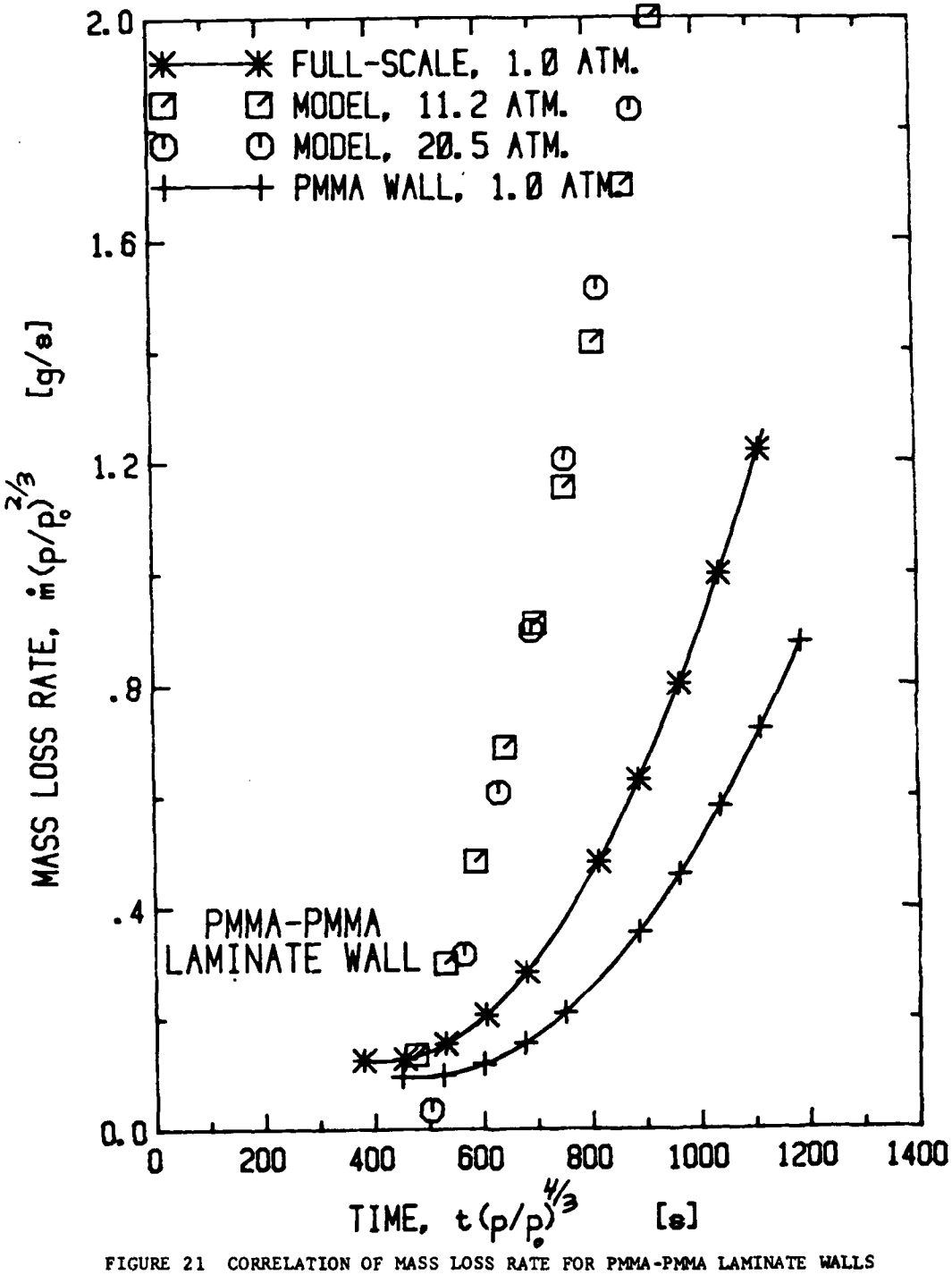

FIGURE 21 CORRELATION OF MASS LOSS RATE FOR PMMA-PMMA LAMINATE WALLS

laminate fuels (see Figures 3 and 15) lead to the higher scaled mass loss rates at elevated pressure for the laminate. Although the lack of data correlation at later test times is due to he fact that oversized model fuels are used, the early divergence of the model dat. flame dimensions (and hence mass loss rate) is difficult to explain.

Equally difficult to explain is the high scaled mass loss rate associated with the model PMMA-Inert laminate at 20.5 atm, as shown in Figure 22. The behavior of the model data at 11.2 atm and at 31.6 atm is quite reasonable since the model laminates are approaching the thermally thick condition of the uniform PMMA wall.

The mass loss rate correlations for both the PMMA and particle-board wall-corners, shown in Figures 23 and 24, reflect the flame spread modeling success for these configurations. However, such is not the case for the pine-wood fuel, as seen in Figure 25. It is apparent that the low mass loss rates at one-atmosphere must be due to flame extinction just after fire spread. Since char formation at elevated pressures does not lead to a similar extinction phenomenon, much higher, scaled burning rates are attained.

III
ANALYSIS

3.1 LAMINATED FUELS

3.1.1 BACKGROUND. Rigorous application of the pressure modeling technique would require that the dimensions of all layers of a laminated fuel should be decreased as the -2/3 power of absolute air pressure. This is usually not practical. However, many real materials (perhaps most) are composed of a thin face (or wearing) layer laminated to much thicker, "backing" layers. During fire spread on such materials, gasification may be confined to the face layer alone or regression through the face layer to a backing layer may occur. Involvement of more than one backing layer in gasification is unlikely during upward flame spread on vertical walls 2-3 m high at one atmosphere. In fact, the entire thermal wave could be confined to the thin face layer during upward spread at one atmosphere if an exposure fire imposed a sufficiently large external flux on the wall material.

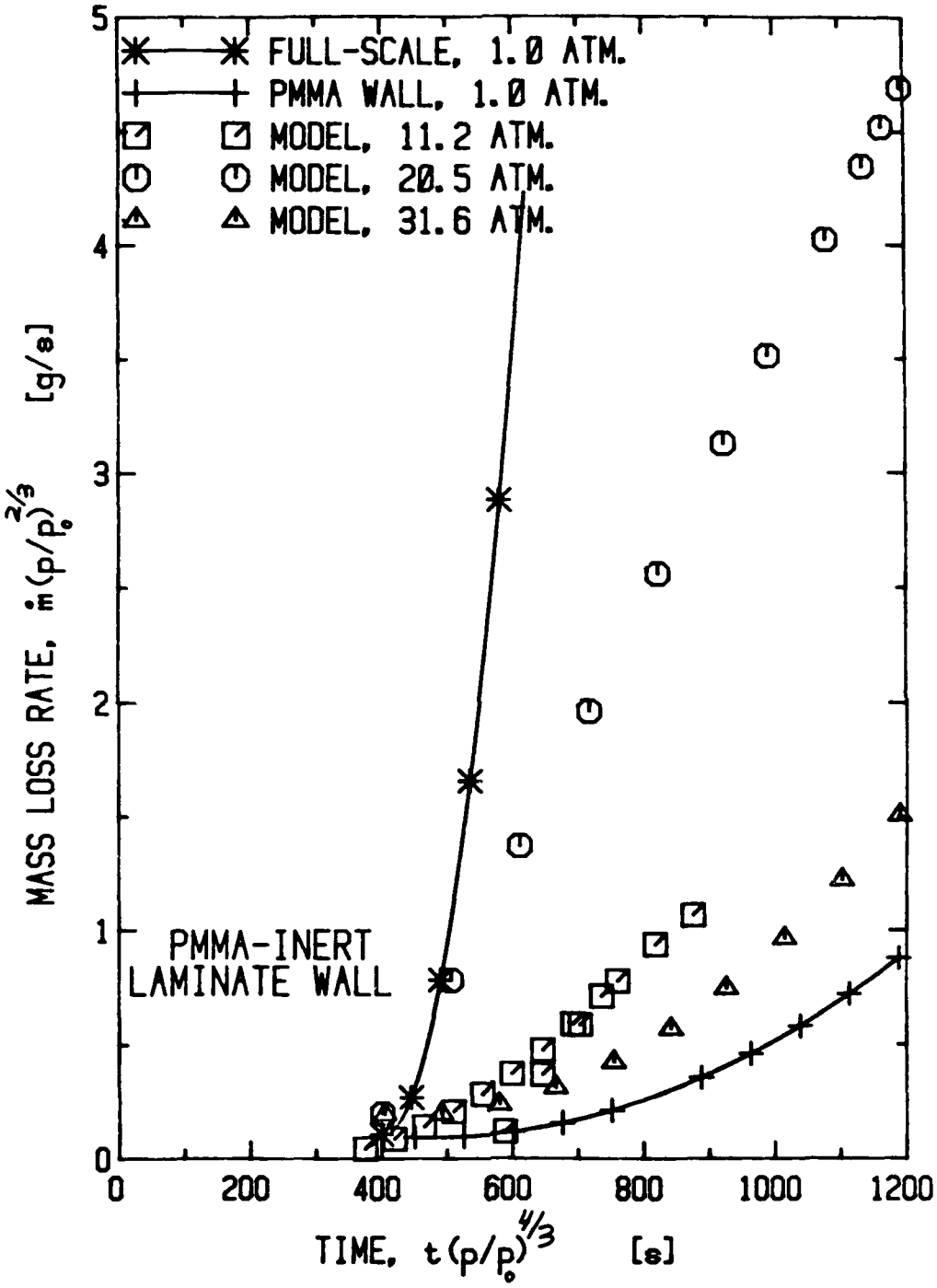

FIGURE 22 CORRELATION OF MASS LOSS RATE FOR PMMA-INERT LAMINATE WALLS

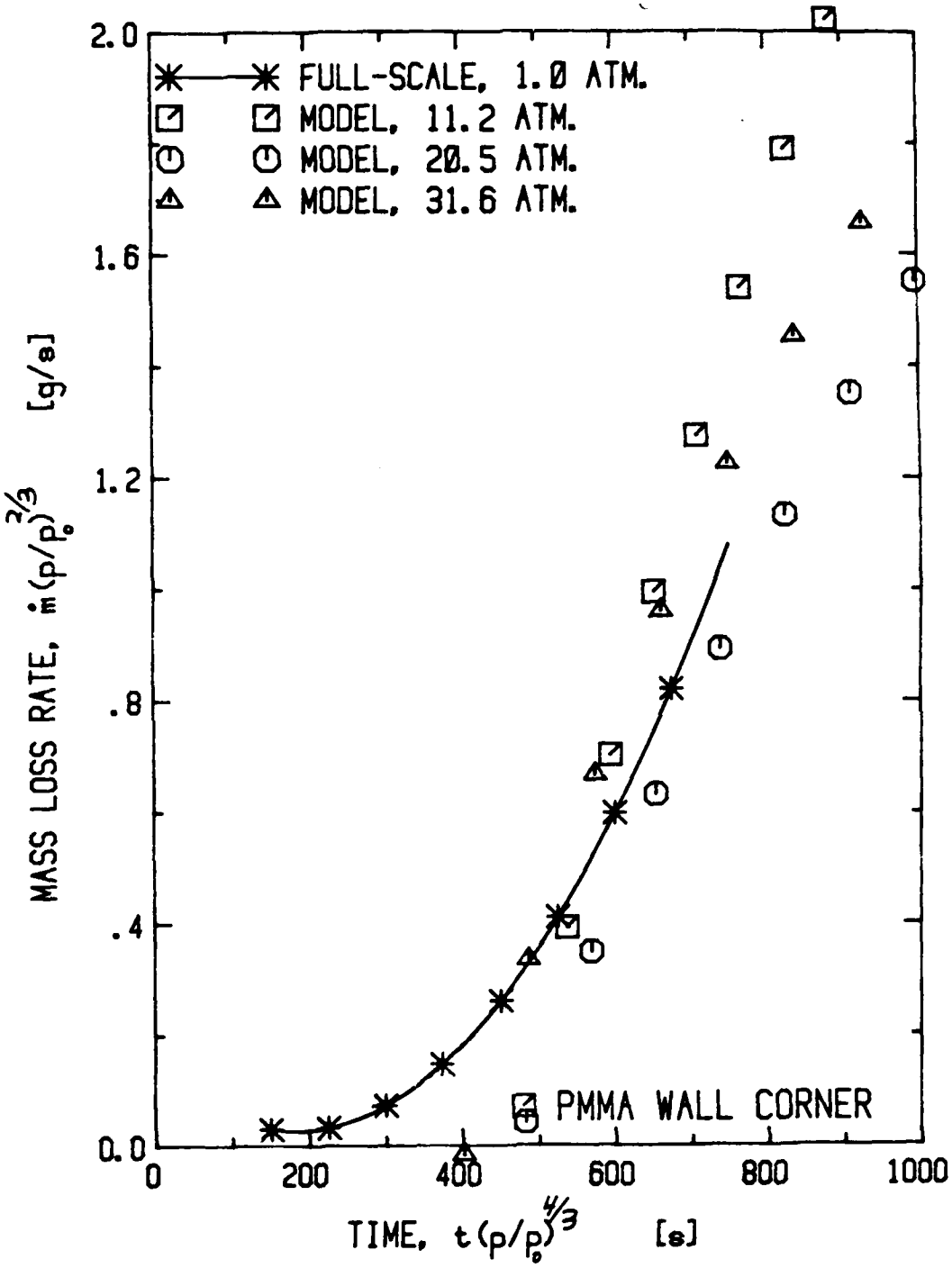

FIGURE 23 CORRELATION OF MASS LOSS RATE FOR PMMA WALL CORNERS

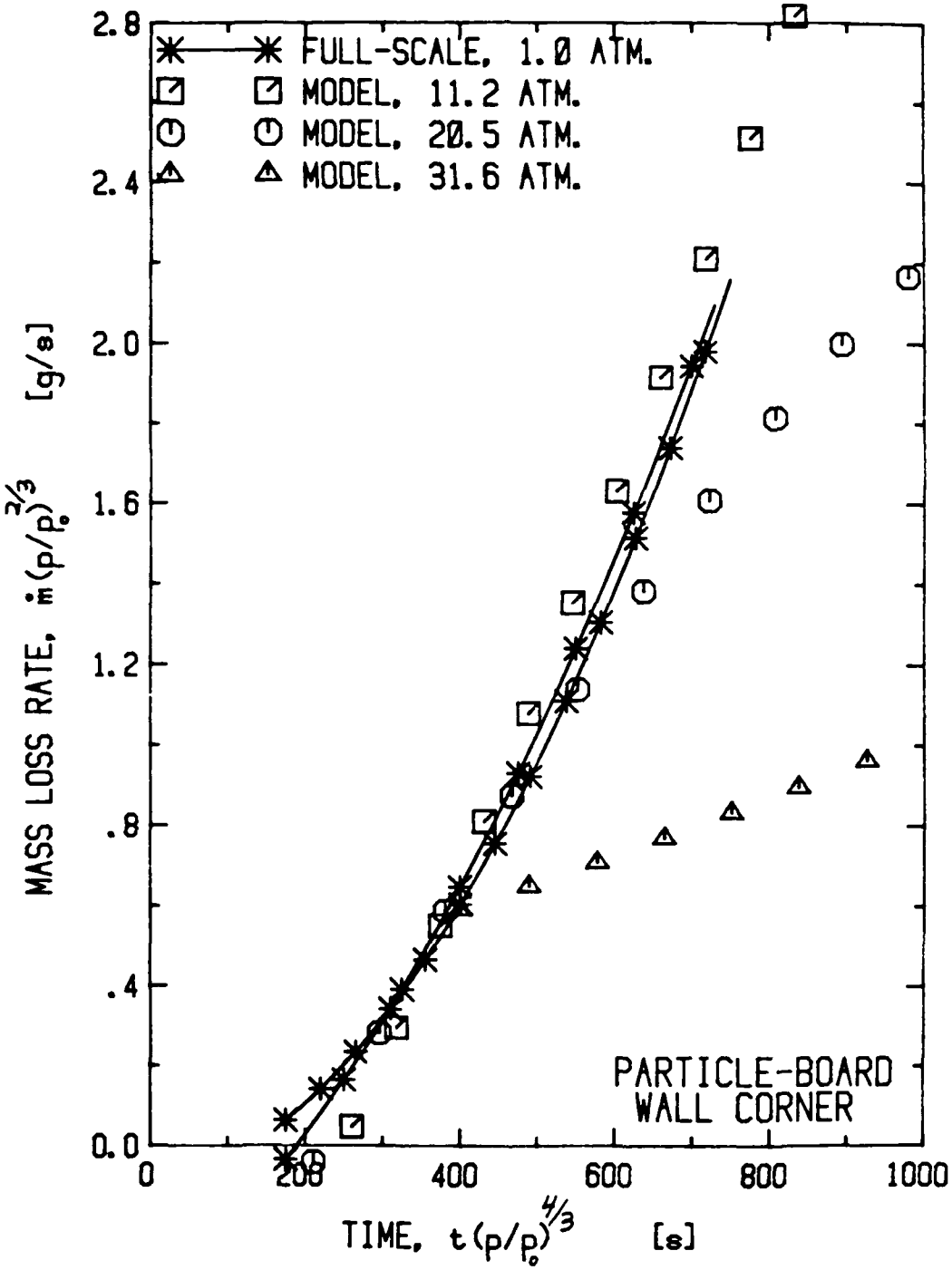

FIGURE 24 CORRELATION OF MASS LOSS RATE FOR PARTICLE-BOARD WALL CORNERS

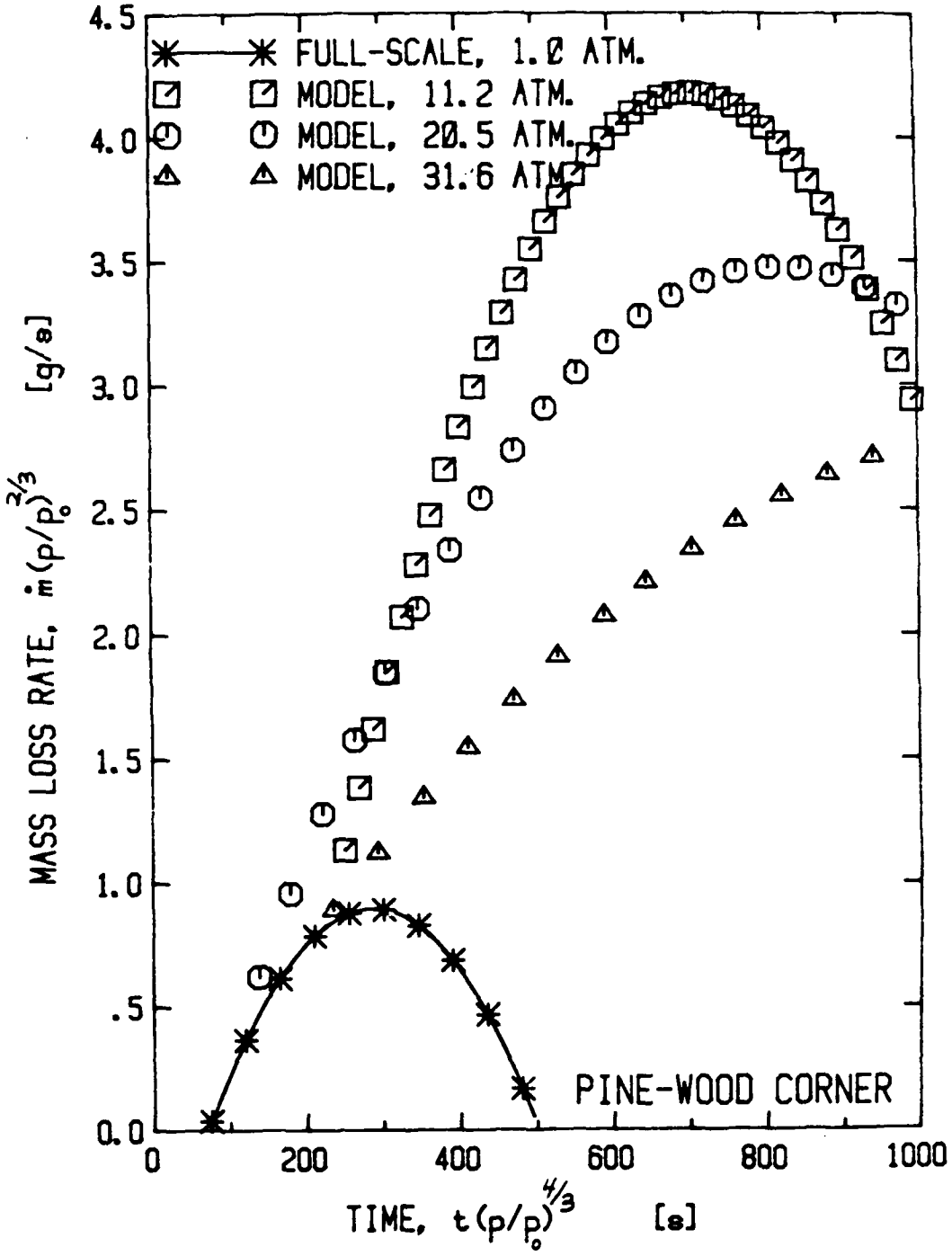

FIGURE 25 CORRELATION OF MASS LOSS RATE FOR PINE-WOOD WALL CORNERS

3.1.2 BEHAVIOR OF THERMAL WAVE DURING FIRE SPREAD. Assume fuel gasification is confined to the "face" layer of a laminated material. By definition the face layer would be thermally thick if the entire thermal wave were also confined to this layer during upward spread. Pressure modeling of such a "thermally thick" layer would require no modification of layer thickness.

A much more likely scenario is that the thermal wave extends into the backing layer during one atmosphere, upward spread. Since the thermal wave thickness[7] is of the order, α/V, where α is the thermal diffusivity ($\lambda/\rho c$) and V is the fuel regression rate, the increase in fuel regression rate as the 2/3 power of absolute air pressure should lead to a decrease in thermal wave thickness as $p^{-2/3}$. For sufficiently high air pressure, p, the entire thermal wave could be confined to the face layer of the model fuel if the face layer thickness were not reduced from the full-scale value. A face layer of PMMA about 2.7 mm thick, for example, would probably contain the entire thermal wave at 30 atmospheres during upward spread on a wall 0.25 m high (modeling a 2.5 m high full-scale wall).

The implications of this decrease in thermal wave coverage can be determined from a simplified one-dimensional analysis of flame spread rates. Assume that the thermal wave extends over a face layer (subscript "1") of thickness, d, and penetrates to a distance, δ , from the face layer into the backing layer (subscript "2"). Furthermore, assume that flame spread occurs when a net flame heat flux, $\dot{q}''$, raises the surface temperature of the face layer from ambient, T_∞ , up to the pyrolysis temperature, T_p during a time interval, Δt . If the temperature of the heated backing, is T^* at the face layer boundary and T_∞ a distance, δ , from the face layer when pyrolysis first occurs, then from energy conservation:

$$\dot{q}'' \Delta t = \rho_1 c_1 d \left(\frac{T_p + T^*}{2} - T_\infty\right) + \rho_2 c_2 \delta \left(T^* - T_\infty\right)/2 \qquad (1)$$

Because of thermal conduction across the face layer:

$$\dot{q}'' = \lambda_1 \left(T_p - T^*\right)/d \qquad (2)$$

Across the heated portion of the backing, thermal conduction gives:

$$\dot{q}'' = \lambda_2 (T^* - T_\infty)/\delta \tag{3}$$

From Eqs. (2) and (3):

$$T^* - T_\infty = T_p - T_\infty - \dot{q}'' d/\lambda_1 \tag{4}$$

$$\delta = \frac{\lambda_2}{\dot{q}''} [T_p - T_\infty - \dot{q}'' d/\lambda_1] \tag{5}$$

Substitution of Eqs. (4) and (5) into Eq. (1) yields an expression for the time interval, Δt , required to heat the fuel surface to the pyrolysis temperature:

$$\Delta t = \frac{\rho_1 c_1 d (T_p - T_\infty - \dot{q}'' d/2\lambda_1)}{\dot{q}''} + \frac{\rho_2 c_2 \lambda_2}{2\dot{q}''^2} [T_p - T_\infty - \dot{q}'' d/\lambda_1]^2 \tag{6}$$

The flame spread rate is inversely proportional to this heating time inverval. For upward fire spread, it is known[8] that V_p is also directly proportional to the current pyrolysis height, x_p. Thus,

$$V_p \propto x_p/\Delta t \tag{7}$$

When the fuel consists of a uniform, thermally thick material (no face layer), then d = 0 in Eq. (6). The spread velocity, from Eqs. (6) and (7), becomes:

$$V_p \propto 2 x_p \dot{q}''^2/\rho c \lambda (T_p - T_\infty)^2 \tag{8}$$

When the fuel consists of a thermally thin face layer alone, with no backing material, then $T_p = T^*$ in Equation 4 and $\rho_2 c_2 \lambda_2 = 0$ in Eq. (6). The spread velocity, from Eqs. (6) and (7), is then given by:

$$V_p \propto x_p \dot{q}''/\rho c d (T_p - T_\infty) \tag{9}$$

With a laminated fuel consisting of both a face layer and backing, flame spread velocity is derived from the complete expression in Eq. (6) as follows:

$$V_p \propto x_p / \left[\frac{\rho_1 c_1 d \, (T_p - T_\infty - \dot{q}'' \, d/2\lambda_1)}{\dot{q}''} + \frac{\rho_2 c_2 \lambda_2}{2\dot{q}''^2} (T_p - T_\infty - \dot{q}'' \, d/\lambda_1)^2 \right] \quad (10)$$

The preceding relations can be used to show qualitatively the relative magnitudes of flame spread rates for various types of materials. For instance, the PMMA fuel used for the laminated wall fires in the present study has a pyrolysis (or vaporization) temperature at one-atmosphere close to 636 K (see Ref. 19) and other thermal properties given in Table 1. With an assumed net heat flux to the PMMA of 10^4 W/m^2 (1 W/cm^2), the ratio of upward spread rate to the pyrolysis height, V_p/x_p, is 3.6 times greater for an isolated 1 mm thick layer (Eq. (9)) than for a thermally thick slab (Eq. (8)). Use of Eq. (10) shows that the same 1 mm PMMA layer backed by the inert ceramic material should support an upward spread rate nearly as large as the rate with the unbacked layer alone, or a V_p/x_p ratio 3.55 times greater than for the thermally thick slab.

An examination of Figures 4 and 10 allows the measured, full-scale upward spread rates on thermally thick PMMA and the PMMA-Inert laminate to be compared for the *same values of flame height*. For instance, at a flame height, x_f, of 0.6 m ($t = 700_s$ for the uniform slab, $t = 350_s$ for the laminate), the upward spread rate on the laminate is about 2.2 times greater than that on the uniform wall. Assuming that the 0.6 m flame height depends only on pyrolysis height for the PMMA fuel walls, the ratio, V_p/x_p, for the laminate should also be about 2.2 times larger than that for the uniform wall. Use of the simplified analysis with the actual PMMA face layer thickness, d, of 3 mm on the inert backing yields a ratio, V_p/x_p, which is about 1.5 times higher than the value corresponding to thermally thick PMMA. The analysis thus seems to give a good qualitative description of the dependence of spread rates on fuel thermal characteristics.

Solid phase thermal conduction and upward spread rate for laminated materials at elevated ambient pressures can also be studied with the preceding relations. From Eq. (5), it is seen that the depth, δ , of thermal wave penetration into the backing material decreases sharply as the net heat flux to the fuel increases with pressure (roughly as $p^{2/3}$). If the face layer thickness,

d, is reduced as $p^{-2/3}$, $\dot{q}''$ d will remain constant and then, from Eq. (5), δ will simply decrease as the required $p^{-2/3}$.

A constant face layer thickness, however, is shown by Eq. (5) to result in a δ of zero when $\dot{q}'' = \lambda_l (T_p - T_\infty)/d$. For a 3 mm thick face layer of PMMA, this condition is satisfied when $\dot{q}'' = 2.35 \times 10^4$ W m^2 (or 2.35 W/cm^2), at which point there would be no penetration of the thermal wave into the backing material. Such an increase in heat flux might occur at a pressure of only 3.6 atmospheres if the net flux at one-atmosphere is 10^4 W/m^2. At higher ambient pressures, the constant thickness face layer then becomes thermally thick with a spread rate given by Eq. (8) and V_p/x_p increasing as $\dot{q}''^2$, or $p^{4/3}$. For a face layer thickness varying as $p^{-2/3}$, it can be shown that the spread rate relation in Eq. (10) also yields a value of V_p/x_p increasing as $p^{4/3}$ and (as noted previously) always substantially greater than that given by Eq. (8) if the backing is the inert ceramic. Thus, lower scaled spread rate parameters, V_p/x_p, will be measured for the constant thickness model than for the full-scale laminate.

3.1.3 PRESSURE MODELING LAMINATED FUELS A simplified heat transfer analysis shows that scaled spread rates much lower than full-scale values would be predicted by pressure modeling if 1) the $\rho c \lambda$ of the constant thickness face layer of a laminate is much greater than that of the backing layer and 2) the face layer thickness is sufficiently small yet still contains most of the thermal wave at elevated pressures. Such a situation could probably be expected for most real composite materials since the face layer is usually quite thin and dense (for wear resistance) while the backing may be a low density foam or honeycomb.

This modeling behavior could be corrected by reducing the face layer thickness as $p^{-2/3}$. Such reductions may not always require fabrication of new laminated materials but possibly a machining operation (grinding or sanding) of the surface of the small-scale fuel.

Assume that gasification extends into the backing layer during upward fire spread at one atmosphere. In this case, accurate modeling would require a reduction (by machining) of surface layer thickness so that the model contains

the correct amount of surface layer fuel. Accurate machining would be difficult, however. Alternatively, two cases could be examined: model spread rates both with and without the entire, unmodified face layer can be obtained and the more hazardous result used to characterize the material.

3.2 CHARRING FUELS

The heat and mass transfer processes within a charring fuel can be modeled numerically to determine how pyrolysis reactions will influence pressure modeling success. Such calculations have been performed using the SPYVAP computer code[9] for transient, one-dimensional thermal conduction and pyrolysis with one-step Arrhenius kinetics. This numerical procedure is documented in detail in Appendix A, which is taken from Reference 9. Parameters for the numerical procedure are listed in Table III and computed results are given in Figures 26-33. An external radiant flux is assumed to have a constant value beginning at the start ($t = 0$) of the transient pyrolysis process to simulate the presence of a flame. Convective heat flux also is allowed due to an assumed, constant flame temperature of 1350 K. Unless noted otherwise, the optical depth (kL_m), material thickness and heat transfer coefficients are all scaled according to the pressure modeling scheme. Values of optical depth at one-atmosphere $(kL_m)_o$ are selected to yield a flame radiant (exposure) flux of either 20 or 40 kW/m^2 with a 1350 K flame temperature, as noted on each of Figures 26-33. At elevated pressures, the radiant exposure flux, $\dot{q}_r''$, is given by the following expression (see Reference 1):

$$\dot{q}_r'' = \sigma\ (1350\ K)^4\ [1 - \exp\ (-\ (\frac{p}{p_o})^{2/3}\ (kL_m)_o)]$$

where σ is the Stefan-Boltzmann constant.

As shown in Table III, the char-forming wood fuels are assumed to have specific heats and thermal conductivities which are functions of both the local, solid-phase temperature, T[K], and the relative amounts of char and virgin material at each instant. These relations and the remaining kinetics parameters were obtained from studies by Kung[10,11], from previous SPYVAP calculations performed by Tamanini[12] and from extrapolations of measurements reported in References 13-18.

TABLE III

PARAMETERS USED FOR PYROLYSIS CALCULATIONS

Wall Material & Scaled Thickness	Char to Fuel Density Ratio	Specific Heat [J/kg K] Fuel	Specific Heat [J/kg K] Char	Thermal Conductivity [W/mk] Fuel	Thermal Conductivity [W/mk] Char	Heat of Pyrolyis [J/kg]
Pine-Wood, 19 mm	0.2	420.4+2.616T	234.4+1.458T	$0.035+2.18\times10^{-4}T$	$0.021+1.31\times10^{-4}T$	-4.186×10^{4}
Particle-board, 19 mm	0.2	700.7+4.36T	234.4+1.458T	$0.044+2.75\times10^{-4}T$	$0.021+1.31\times10^{-4}T$	-4.186×10^{4}

Front surface boundary condition:

Gas Temperature = 1350K

Convective heat transfer coefficient = 12.5 W/m^2K

Emissivity = 0.95

Standard Kinetics Properties:

Pre-exponential Factor = 5.25×10^{7} [s^{-1}]

Activation Energy = 1.256×10^{8} [J/kg-mole]

Back surface boundary condition:

Gas Temperature = 298K

Convective heat transfer coefficient = 10 W/m^2K

Emissivity = 0.0

Low Activation Kinetics:

Pre-exponential Factor = 1.5×10^{3} [s^{-1}]

Activation Energy = 6.28×10^{7} [J/kg-mole]

3.2.1 FUEL MASS FLUX In Figures 26-29, computed values of fuel mass flux at the "front" face of the fuel (see Table III) are correlated for one-atmosphere and two elevated pressure conditions. Mass flux is corrected for pressure as shown in these figures because $\dot{m}''$ should increase as $p^{2/3}$ in the modeling scheme. As noted before, fuel thickness is generally reduced for the calculations as $p^{-2/3}$ from the full-scale values given in Table III. Although such a reduction in thickness is not made for the char-forming fuels in the actual elevated pressure experiments, the numerical solution technique requires the reduction in order to have an adequate number of grid points within the thermal wave.

Mass flux from a pinewood fuel, simulated with the parameters given in Table III, is shown in Figures 26-28 for an exposure radiant flux at one-atmosphere of 20 or 40 kW/m^2. Initially, there is a rapid rise in fuel mass flux to a peak value due to the radiant exposure. This fuel "pulse" is then followed by a decay period because of the increasing thickness of the char, which insulates the virgin fuel.

It appears that the higher, most widely accepted value[16] of Arrhenius activation energy for fuel pyrolysis yields the best pressure modeling of the pinewood fuel mass flux. Modeling errors also are reduced for the higher exposure flux. The actual radiant flux to the charring fuels in the corner configuration is likely to be close to this 40 kW/m^2 value due to radiant emission from the adjacent, high temperature fuel surfaces (see Figures 30-33). In any case, it is probable that adequate pressure modeling of fuel mass flux would lead to corresponding success in modeling the actual flame heat transfer, and hence the fire spread process.

In Figure 29, the calculated mass flux corresponding to a higher density, char-forming fuel, such as particle-board, is correlated. The predicted success of pressure modeling in this case is not as good as that for the lower density pinewood. This prediction seems to be sustained by the correlation of flame height measurements in Figures 6 and 7.

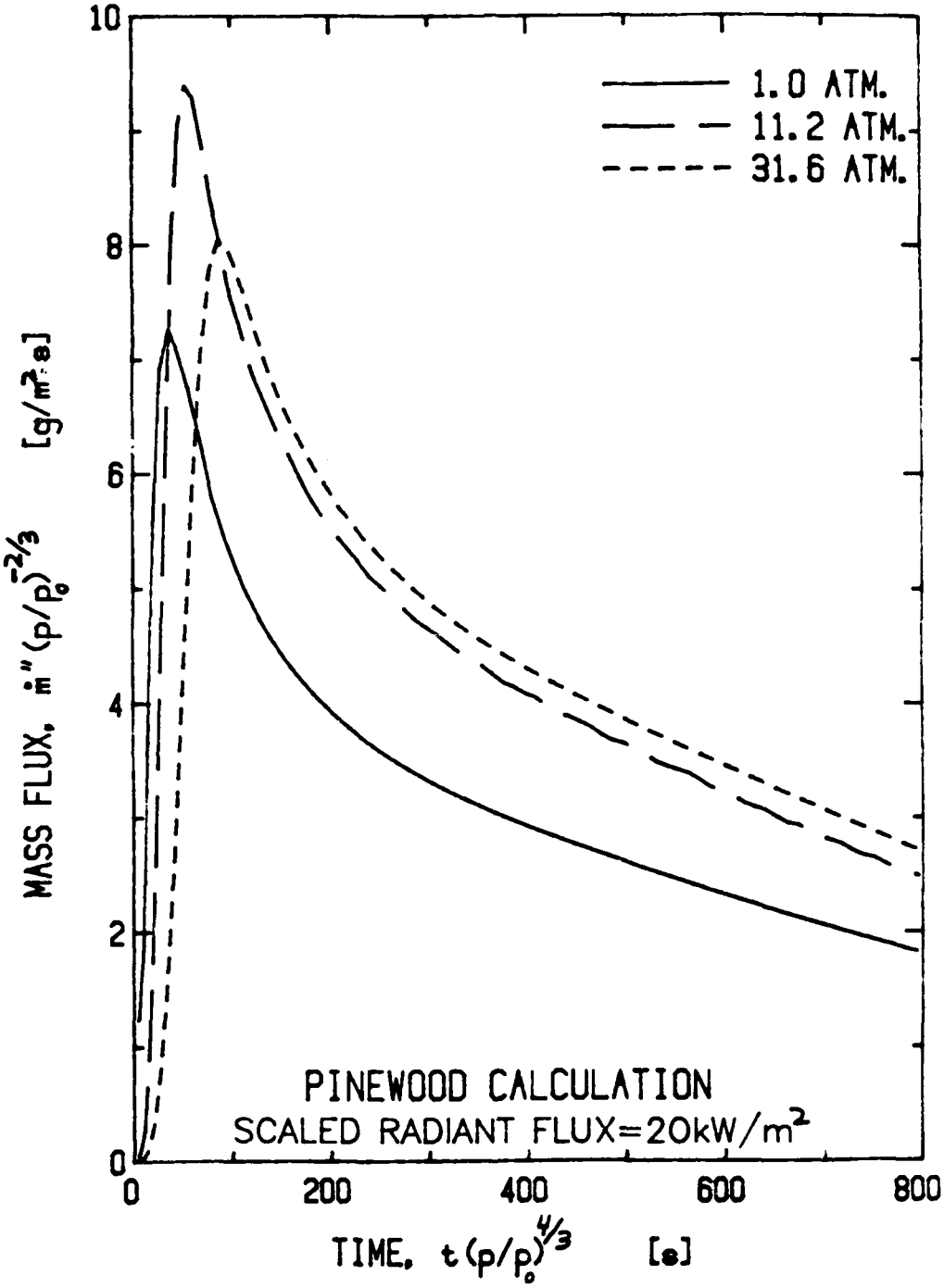

FIGURE 26 CALCULATION OF ONE-DIMENSIONAL PINE-WOOD PYROLYSIS: SCALED VAPOR MASS FLUX DUE TO 20 kW/m^2 SCALED HEAT FLUX WITH STANDARD THERMAL AND KINETICS PROPERTIES

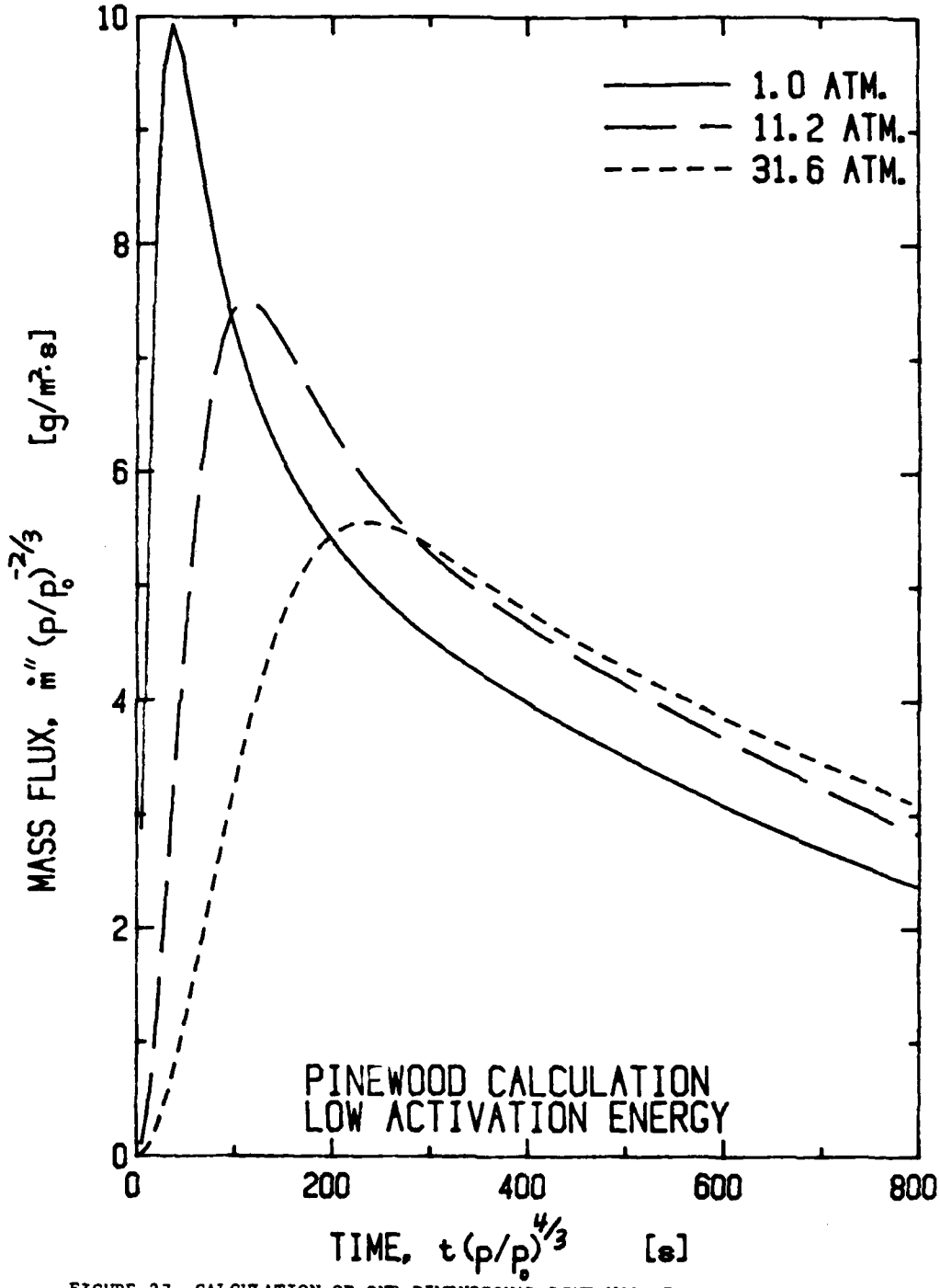

FIGURE 27 CALCULATION OF ONE-DIMENSIONAL PINE-WOOD PYROLYSIS: SCALED VAPOR MASS FLUX DUE TO 20 kW/m^2 SCALED HEAT FLUX WITH LOW ACTIVATION ENERGY IN PYROLYSIS KINETICS

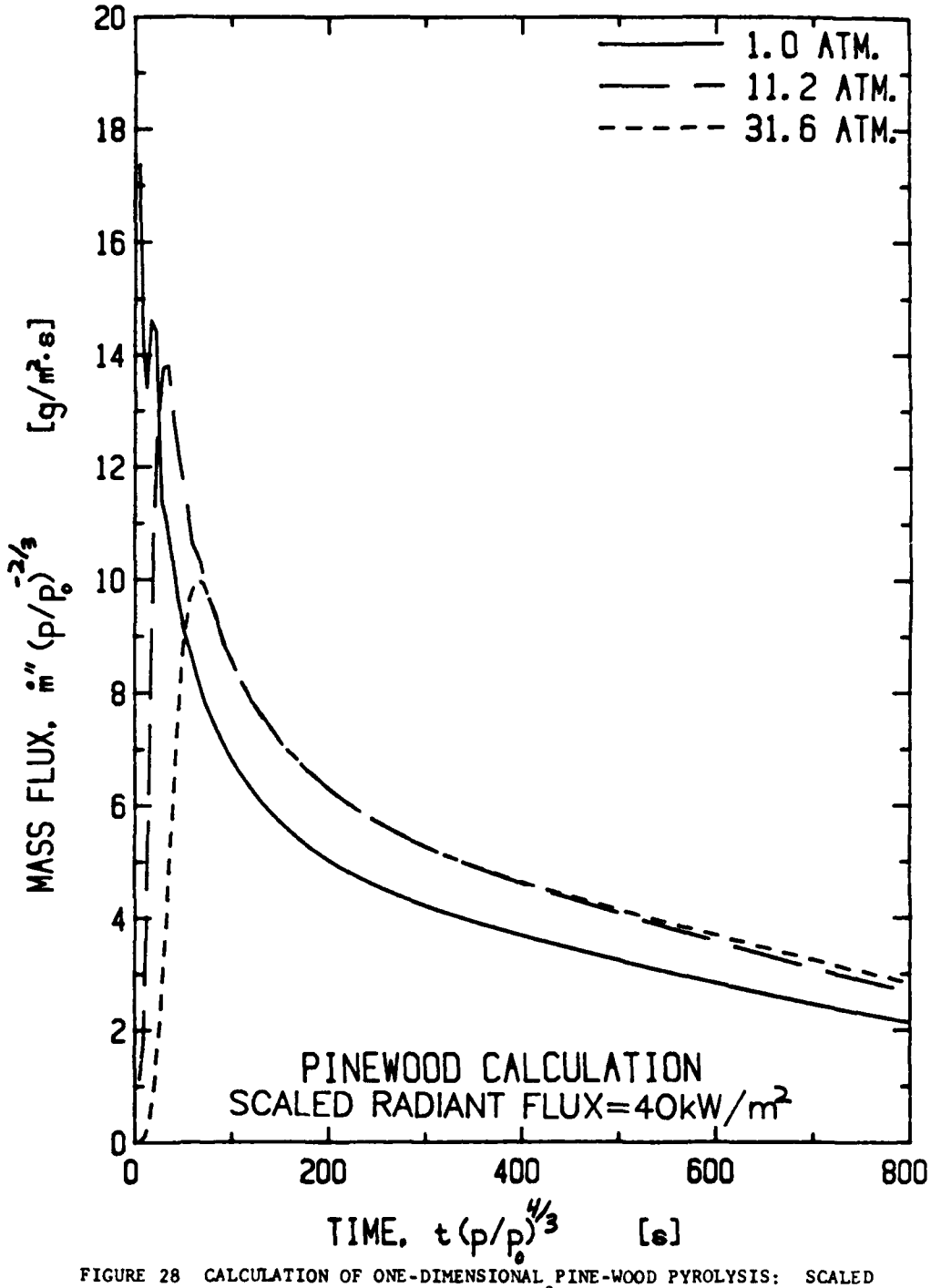

FIGURE 28 CALCULATION OF ONE-DIMENSIONAL PINE-WOOD PYROLYSIS: SCALED VAPOR MASS FLUX DUE TO 40 kW/m^2 SCALED HEAT FLUX WITH STANDARD THERMAL AND KINETICS PROPERTIES

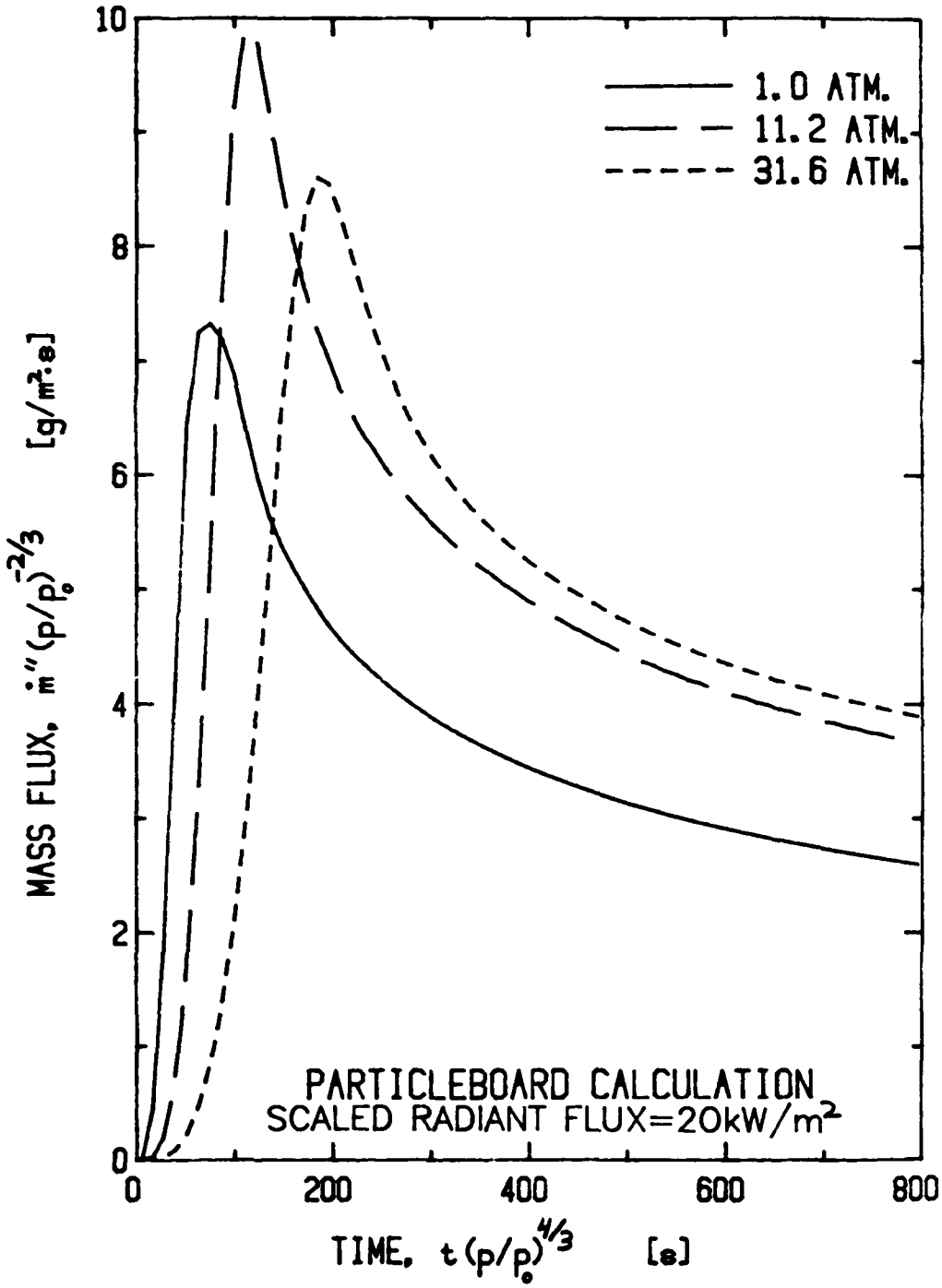

FIGURE 29 CALCULATION OF ONE-DIMENSIONAL PARTICLE-BOARD PYROLYSIS: SCALED VAPOR MASS FLUX DUE TO 20 kW/m^2 SCALED HEAT FLUX

As described in Section 2.2, the cellulosic fuels at one-atmosphere undergo a flame extinction process after fire spread proceeds some distance from the corner apex. Empirical studies with a vareity of materials have shown that such flame extinction occurs when fuel mass flux drops below the 2 to 4 $g/m^2.s$ range. The calculated mass flux at one-atmosphere is seen in Figures 26 and 29 to fall below the 3 $g/m^2.s$ level some 380 and 560 seconds after initial radiant exposure of pinewood and particle-board, respectively. Coincidentally, the measured rates of increase in flame height on pinewood and particle-board corners, shown in Figures 13 and 12 respectively, drop to zero at about these same times. Lateral flame spread on the full-scale fuels stops as a direct result of the extinction phenomenon at respective times after ignition of 360 and 690 seconds for pinewood and particle-board, as shown in Figures 19 and 18.

3.2.2 FUEL SURFACE TEMPERATURE The calculated temperature of the "front" face of the fuel during radiant exposure and fuel pyrolysis is shown in Figures 30-33. In all cases, the fuel surface temperature reaches a steady value within about 100 seconds after the start of radiant exposure. Predicted values of char surface temperature at one-atmosphere are about 800 K (900 K with a 40 kW/m^2 flux) for the cellulosic fuels.

At elevated pressures, the computed surface temperatures for the char-forming, cellulosic fuels are quite high, up to 1200 K at 31.6 atm. Surface temperature itself is thus not being pressure modeled (i.e. preserved), but the resultant enhancement of radiant heat loss from the surface does allow for pressure modeling of the net heat flux to the fuel. If both heat loss due to surface reradiation and heat gain due to flame heat flux increase roughly as required by the modeling scheme, then the net radiant heat flux and hence the fuel mass flux, should be modeled well (assuming convective heat transfer is relatively unimportant). The predicted heat loss due to surface emission is in fact seen to increase somewhat less than $p^{2/3}$ (a factor of 3.6 rather than 5) between one and 11.2 atm for pinewood and particle-board fuels. This may be the reason for the success in modeling flame growth on the cellulosic wall-corners.

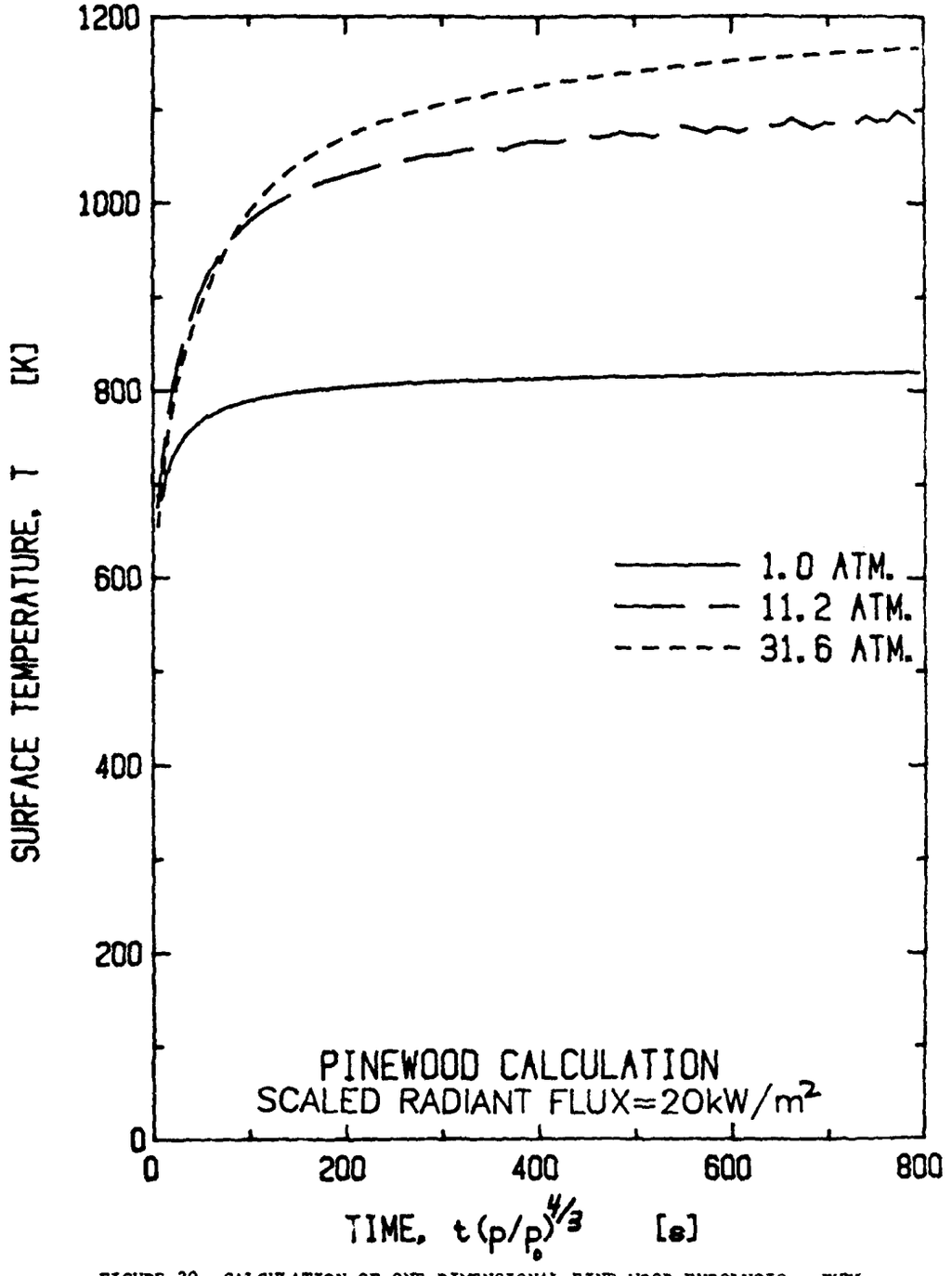

FIGURE 30 CALCULATION OF ONE-DIMENSIONAL PINE-WOOD PYROLYSIS: FUEL SURFACE TEMPERATURE DUE TO 20 kW/m^2 SCALED HEAT FLUX WITH STANDARD THERMAL AND KINETICS PROPERTIES

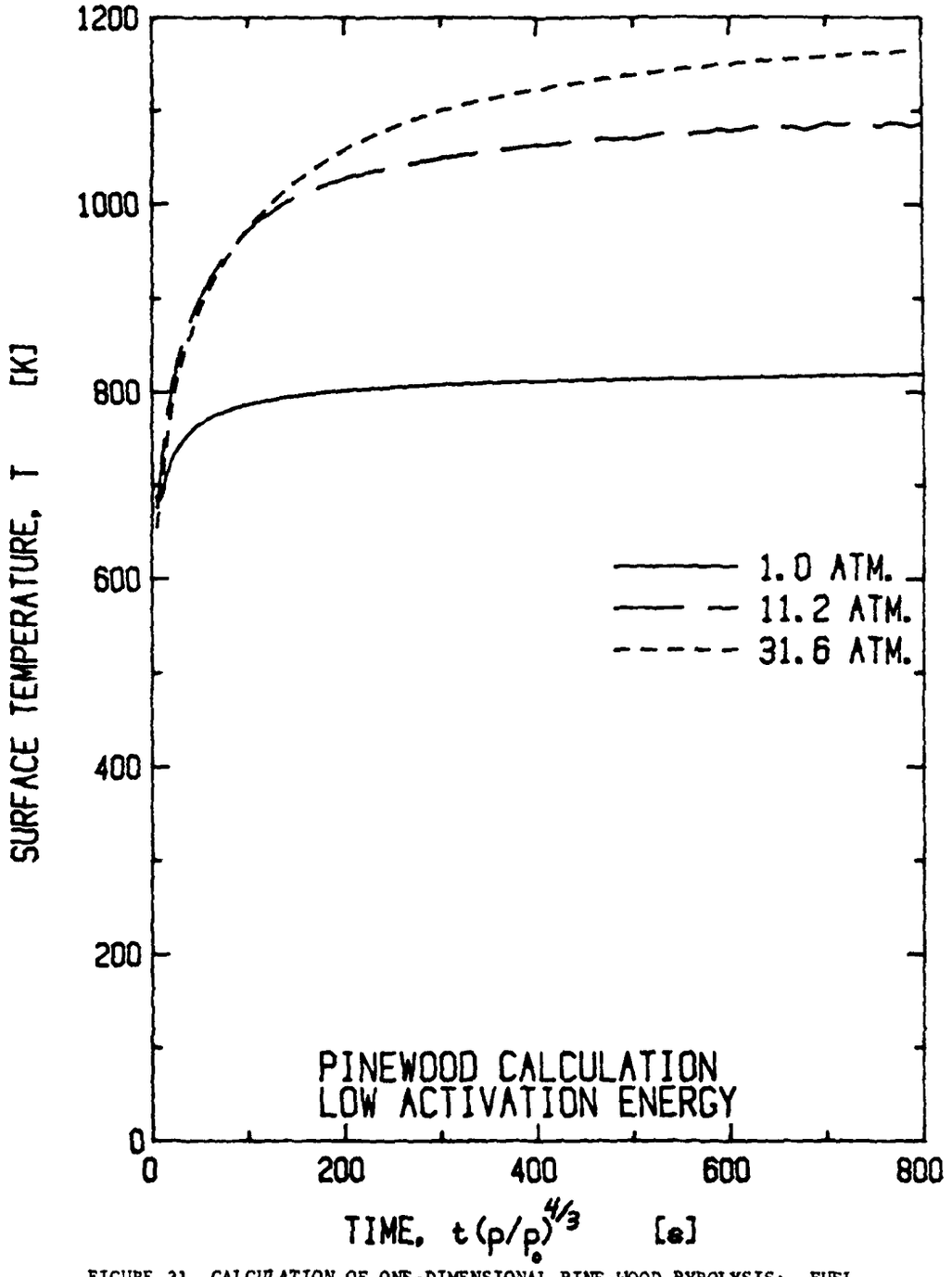

FIGURE 31 CALCULATION OF ONE-DIMENSIONAL PINE-WOOD PYROLYSIS: FUEL SURFACE TEMPERATURE DUE TO 20 kW/m^2 SCALED HEAT FLUX WITH LOW ACTIVATION ENERGY IN PYROLYSIS KINETICS

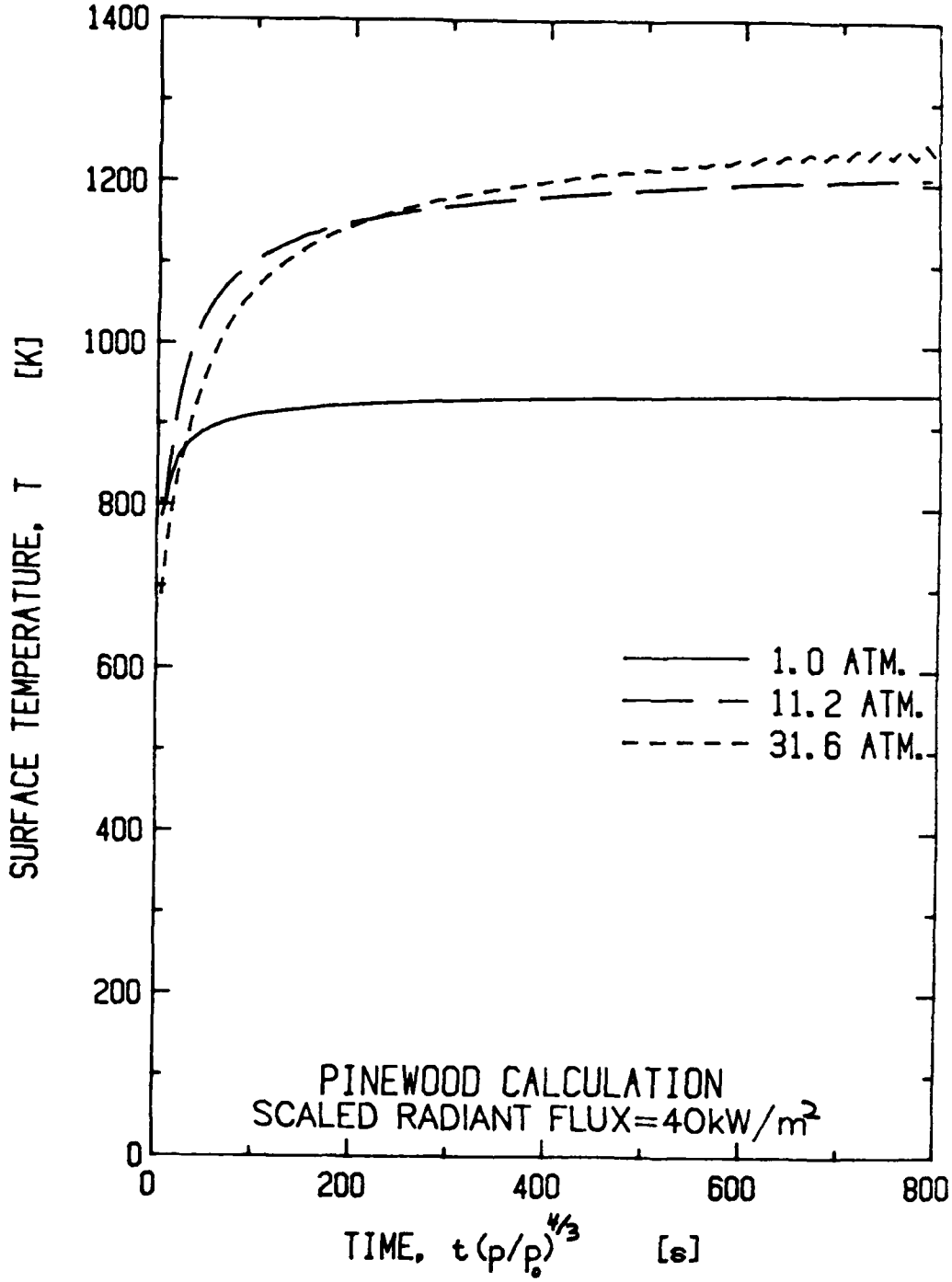

FIGURE 32 CALCULATION OF ONE-DIMENSIONAL PINE-WOOD PYROLYSIS: FUEL SURFACE TEMPERATURE DUE TO 40 kW/m^2 SCALED HEAT FLUX WITH STANDARD THERMAL AND KINETICS PROPERTIES

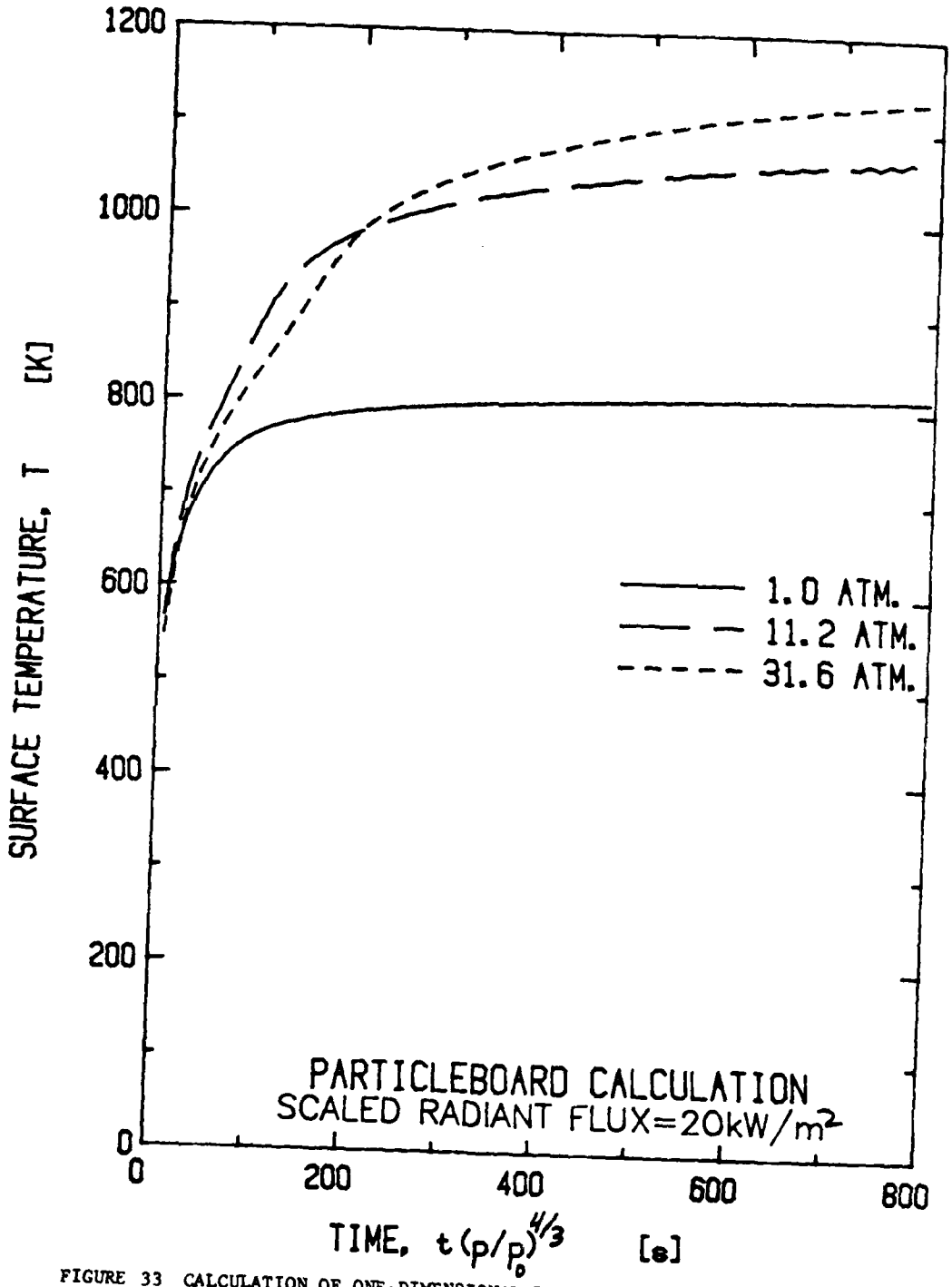

FIGURE 33 CALCULATION OF ONE-DIMENSIONAL PARTICLE-BOARD PYROLYSIS: FUEL SURFACE TEMPERATURE DUE TO 20 kW/m^2 SCALED HEAT FLUX

3.2.3 CHAR PRODUCTION Another important output of the numerical calculations is the predicted thickness of the char layer which develops at a given location after fuel pyrolysis is complete. When pine-wood fuel is simulated (high activation energy) with a 40 kW/m^2 exposure, this char layer grows to about 43% of the total fuel thickness after 800 seconds of radiant exposure at one-atmosphere. Corresponding char fractions of scaled fuel thickness at 11.2 and 31.6 atmospheres are 62% and 71% for the same scaled exposure times. It appears from these data and from results with a 20 kW/m^2 exposure that the scaled char thickness increases over the value at one-atmosphere by a factor of $(p/p_o)^{0.15}$ when the high activation energy kinetics is used. While any such pressure dependence represents a departure from the modeling scheme, the small increase in relative char thickness helps to reduce fuel mass flux, and thus enhances the effect of the calculated increase in fuel surface temperature at elevated pressure. Together, the insulating property of the excess char formation and the heat loss from a high temperature surface act to keep fuel mass flux increasing at close to the required 2/3 power of pressure.

It should be noted that use of the low activation energy kinetics leads to a calculated char fraction (of fuel thickness) which is nearly independent of pressure (about 33% at 20 kW/m^2).

IV
SUMMARY OF RESULTS

Measurements of time-resolved flame dimensions, upward spread rates and fuel mass loss rates for full-scale and model configurations burning at ambient and elevated air pressures, respectively, yield the following results:

1. Pressure modeling is sufficiently accurate for the prediction of fire growth from a point ignition on a uniform PMMA wall when both upward and lateral flame spread processes occur.

2. The behavior of the flame spread process at elevated air pressures for walls composed of a face layer of PMMA with a thick nonburning backing layer is not completely consistent with a simplified analysis of thermal conduction processes. When the backing layer is also PMMA, spread rates at elevated

pressures are much greater than expected, but spread rates are more consistent with heat transfer theory when the backing is a low density ceramic.

3. Pressure modeling of fire growth in a wall corner configuration is quite accurate for cellulosic, char-forming materials and for PMMA. The cellulosics at one atmosphere exhibit a flame extinction phenomenon after significant lateral flame spread that is not observed at elevated pressures.

4. Thermally thick, rigid, high density polyurethane foam in a corner configuration will not support significant flame spread at one-atmosphere but will at elevated pressures with a properly scaled, small PMMA ignition source. This behavior is perhaps due to excessive radiant heat loss from the char and the intumescent character of the char at one-atmosphere. Gas phase chemical kinetics, which may be the most important factor in the initiation of flame spread on the full-scale foam, is clearly not modeled.

5. A simplified analysis of thermal conduction in a laminated material is used to show how flame spread rates are affected by the thermal properties of the face layer and backing at both one-atmosphere and at elevated pressures.

6. A numerical technique is used to predict one-dimensional, transient fuel mass flux, fuel surface temperature and char thickness during material exposure to a prescribed radiant (and convective) heat flux. Calculated results show that reasonable pressure modeling of flame spread rates should be expected for the cellulosic fuels due to increases in surface temperature and char production for conditions simulating elevated air pressure. Predicted times for extinction of these fuels at one-atmosphere, due to char buildup, are in agreement with the observed times.

V
CONCLUSIONS

1. Pressure modeling of three-dimensional fire spread on uniform walls and wall corners has now been validated for PMMA and for wood fuels. It has not yet been established that the modeling technique is also valid for predicting fire growth on other charring fuels in corner configurations. Results from

this and previous studies have shown that in general, the complex process by which self-sustained fire spread is initiated is not pressure modeled. Such fire spread initiation occurs readily at elevated pressures because surface radiant heat loss and the action of gas phase chemical retardents cannot be modeled. With wood and PMMA fuels, fire spread rates on wall-ceiling corners should also be predictable by pressure modeling, based on previous work[20] with ceiling channel configurations.

2. It appears that much more experimental information is needed before pressure modeling can be used to predict fire growth on practical composite materials. At present the thickness of all components (including adhesives) within the thermal wave developed during fire spread must be modified according to the pressure modeling scheme. However, radiant exposure in real enclosure fires may well be sufficiently high (2-4 W/cm^2) to confine thermal wave penetration to a surface layer of fuel during fire spread. Pressure modeling of such a fire spread process would then be accurate without any modification of the laminated material.

3. Pressure modeling can serve as a scientific tool for studying fire growth on idealized charring and laminate fuels in a variety of configurations. In this way, the potential for fire growth as a function of fuel geometry can be determined. However, further study is needed to see if pressure modeling correctly predicts the relative hazard of different fuel compositions.

VI

REFERENCES

1. Alpert, R.L., "Pressure Modeling of Vertically Burning Aircraft Materials," U.S. Dept. of Transportation, Final Report No. FAA-RD-78-139, January 1979.
2. de Ris, J., Kanury, A.M., and Yuen, M.C., "Pressure Modeling of Fires," Fourteenth Symposium (International) on Combustion, The Combustion Institute, p. 1033, 1973.
3. Materials Bank Compendium of Fire Property Data, Edited by the Products Research Committee, February 1980.
4. Steward, F.R., "Prediction of the Height of Turbulent Buoyant Diffusion Flames," Combustion Science and Technology, 2, p. 203, 1970.
5. You, H.Z. and Faeth, G.M., "Ceiling Heat Transfer during Fire Plume and Fire Impingement," Fire and Materials, 3, No. 3, 1979.
6. Steward, F.R., "Linear Flame Heights for Various Fuels," Combustion and Flame, 8, p. 171, 1964.
7. Carslaw and Jaeger, Conduction Heat Transfer, Chapter 8, Second Edition, Oxford University Press, 1951.
8. Orloff, L., de Ris, J., and Markstein, G.H., "Upward Turbulent Fire Spread and Burning of Fuel Surfaces," Fifteenth Symposium (International) on Combustion, The Combustion Institute, p. 183, 1974.
9. "The Third Bedroom Fire Test of the Home Fire Project," Vol. III, Edited by A. T. Modak, Appendix A: "A Numerical Model for One-Dimensional Heat Conduction with Pyrolysis in a Slab of Finite Thickness" by F. Tamanini, Factory Mutual Research Corp. Technical Report No. 21011.7, RC-B-69, November 1976.
10. Kung, H.C., "A Mathematical Model of Wood Pyrolysis," Combustion and Flame, 18, p. 185-195, 1972.
11. Kung, H.C., "The Burning of Vertical Wooden Slabs," Fifteenth Symposium (International) on Combustion, The Combustion Institute, p. 243, 1974.
12. Tamanini, F., "The Application of Water Sprays to the Extinguishment of Crib Fires," Combustion Science and Technology, 14, 1976.

13. White, R.H., and Schaffer, E.L., "Finite Difference Thermal Analysis Applied to Charring Wood," Proceedings of the First International Conference on Numerical Methods in Thermal Problems, Edited by R.W. Lewis and K. Morgan, MIT, p 871, 1979.

14. Quintiere, J., Harkleroad, M., and Walton, W., "Measurement of Material Flame Spread Properties," U.S. National Bureau of Standards, NBSIR 82-2557, August 1982.

15. Holve, D.J. and Kanury, A.M., "A Numerical Study of the Response of Building Components to Heating in a Fire," Journal of Heat Transfer, 104, p. 344, May 1982.

16. Phillips, A.M. and Becker, H.A., "Pyrolysis and Burning of Single Sticks of Pine in a Uniform Field of Temperature, Gas Composition and Velocity," Combustion and Flame, 46, p. 221, 1982.

17. Atreya, Arvind, "Burning of Wood," Harvard University Report, 1982.

18. White, James, Weyerhauser Technical Center, Longview, WA, Personal Communication.

19. Orloff, L., Modak, A.T., and Alpert, R.L., "Burning of Large-Scale Vertical Surfaces," Sixteenth Symposium (International) on Combustion, The Combustion Institute, 1976.

20. Alpert, R.L., Mathews, M.K., and Modak, A.T., "Modeling of Ceiling Fire Spread and Thermal Radiation," Federal Aviation Administration, Report No. DOT/FAA/CT-81/70, October 1981.

APPENDIX A

A NUMERICAL MODEL FOR ONE-DIMENSIONAL HEAT CONDUCTION WITH PYROLYSIS IN A SLAB OF FINITE THICKNESS

F. Tamanini

Factory Mutual Research Corporation

A.1 INTRODUCTION

The purpose of this appendix is to document a procedure for computing the profiles of temperature, density and mass flux, as well as the surface energy fluxes associated with them, in a slab of finite thickness undergoing pyrolysis. No new physics is introduced to make the model more realistic than similar models developed by other researchers. In particular, the fundamental equations are those proposed by Kung[1] and later used by this writer[2]; with respect to those versions of the model, however, the current procedure offers greater flexibility and a few additional options.

The features of the model are:

1) Heat conduction is calculated by allowing for variable thermal properties. The thermal conductivity (k) and the specific heat (c_p) are assumed to be linear functions of the local temperature.

2) Pyrolysis follows a first order Arrhenius reaction: the thermal decomposition transforms active material into constant, pre-assigned fractions of char and volatiles. Before pyrolysis is completed the solid matrix consists of a mixture of char and unpyrolyzed active material, whose thermal properties are obtained by linear interpolation of the property values pertaining to the two components.

---

[1] Kung, H.C., "A Mathematical Model of Wood Pyrolysis," Combustion and Flame, 18, 185-195 (1972)

[2] Tamanini, F., "A Study of the Extinguishment of Vertical Wood Slabs in Self-sustained Burning by Water Spray Application," Combustion Science and Technology, 14, 1,2,3, p. 1 (1976) and "Everything You Always Wanted To Know From a Thermocouple (in a fire test), But Were Afraid To Ask," Society of Fire Protection Engineers, Technology Report 75-2, (1975)

3) Thermal decomposition contributes to the local energy balance through a volume generation of heat. The heat of pyrolysis associated with that process is assumed to be constant at a reference temperature.

4) Accumulation of volatiles within the solid matrix is neglected. All the gaseous products of the decomposition process are assumed to escape toward either or both surfaces as they are generated.

5) Convective heat transfer between the volatiles and the solid matrix is taken into account by postulating perfect thermal contact.

6) Boundary conditions at the two bounding surfaces can be specified in terms of temperature or heat flux. If the temperature is prescribed, the model yields the heat flux and vice versa. To allow for a situation often encountered in practice, the model can also use as a boundary condition a temperature-time history at a location inside the slab.

The computer program illustrated here consists of a MAIN program and two subroutines: SPYVAP (Slab Pyrolysis with Variable Properties) and OUTPUT. The following sections concentrate on the description of subroutine SPYVAP, which contains the main machinery of the model. Subroutine OUTPUT calculates secondary quantities of interest, such as heat flux components, mean slab density, etc., but its main function is to do just what its name implies. The version of MAIN reported here is the one used to perform the calculations discussed in Section V of this report. The function of MAIN is to supervise the calls of the two subroutines as well as to initialize the array containing the temperature/heat flux profiles used as boundary conditions and effect input/output of the initial conditions. Users of the procedure should not need to modify SPYVAP but will have to rewrite MAIN to adapt it to their particular application. Changes in OUTPUT may also be necessary to satisfy personal aesthetic requirements or special output needs.

A.2 MODEL EQUATIONS AND BOUNDARY CONDITIONS

The model finds solutions to the problem of unsteady heat conduction in one dimension. The governing equation, with the appropriate terms to account for convective heat transfer between the solid and the volatiles and for energy release in the pyrolysis process, reads:

$$\frac{\partial(\rho_s h_s)}{\partial t} = \frac{\partial}{\partial x}\left(k_s \frac{\partial T}{\partial x}\right) + \frac{\partial}{\partial x}(M_g h_g) - Q\frac{\partial \rho_s}{\partial t} \qquad (1)$$

where: t time,

x distance from the front surface,

ρ density,

k thermal conductivity,

h enthalpy,

M_g mass flux of volatiles (positive in the negative-x direction),

Q heat of pyrolysis (positive when reaction is exothermic).

The subscripts s and g refer to the solid matrix and the volatiles (pyrolysis gases) respectively. The enthalpy, h, is defined as:

$$h = \int_{T_o}^{T} c_p(T)\, dT \qquad (2)$$

where:

$$c_p(T) = c_p^o + c_p^* (T - T_o) \quad . \qquad (2')$$

The mass flux of pyrolysis gases, M_g, is calculated from:

$$\frac{\partial M_g}{\partial x} = \frac{\partial \rho_s}{\partial t} \qquad (3)$$

As for determining the direction of the migration of the pyrolysis gases, the model offers two options:

1) The volatiles flow in the direction of decreasing densities of the solid matrix.

2) The outflow of volatiles is laminar and there is no net pressure difference between the two faces of the slab.

Since in laminar flow the pressure drop is proportional to the flow mean velocity, the following condition is used to implement the latter of the two options:

$$\int_0^{\ell} M_g(x)\, dx = 0 \tag{4}$$

where ℓ is the thickness of the slab. To arrive at eq (4) changes in the density of the volatiles, as well as changes in the porosity of the solid matrix, have been neglected.

After a certain amount of pyrolysis has occurred, part of the solid matrix is char, the rest is as yet unpyrolyzed active material. It is assumed that the density of the active material (ρ_a) and that of the solid matrix (ρ_s) are linearly related:

$$\rho_s(t,x) = \left(1 - \frac{\rho_f}{\rho_i}\right)\cdot\rho_a\ (t,x) + \rho_f \tag{5}$$

where ρ_i and ρ_f are the initial and final densities respectively.

The density of the char can be calculated from values for ρ_a and ρ_s as :

$$\rho_c(t,x) = \rho_s(t,x) - \rho_a(t,x) \tag{6}$$

At the beginning $\rho_a = \rho_s = \rho_i$ and $\rho_c = 0$; after complete pyrolysis $\rho_c = \rho_s = \rho_f$ and $\rho_a = 0$.

The rate of pyrolysis is determined by using a first-order Arrhenius reaction:

$$\frac{\partial \rho_a}{\partial t} = -\, a_p\, \rho_a \exp\,(-\, E/RT) \tag{7}$$

where a_p is the pre-exponential factor, E is the activation energy and R the gas constant.

Possible recondensation within the solid is not taken into account. It should be noted that eq (7) is written by some authors with $\rho_s - \rho_f$ instead of ρ_a in the right hand side. Since the two quantities are proportional to each other (cf eq (5)), the difference is conceptually not too important. However, the adoption of ρ_a instead of $\rho_s - \rho_f$ amounts to introducing the factor $(1 - \rho_f/\rho_i)$ which must be taken into account before some of the values for a_p available in the literature can be used in the model.

The contributions from the char and the active material to the energy content of the solid is expressed as:

$$\rho_s h_s = \rho_a h_a + \rho_c h_c \tag{8}$$

Equation (8) can be used to obtain an expression for the mean specific heat of the solid (c_{ps}) as a function of those of the active material (c_{pa}) and the char (c_{pc}) and the local density (ρ_s) :

$$c_{ps} = \frac{\rho_a}{\rho_s} c_{pa} + \frac{\rho_c}{\rho_s} c_{pc} \tag{8'}$$

where ρ_a and ρ_c can be written as functions of ρ_s using eq (5).

For the thermal conductivity k_s, a linear variation with density is assumed between the value of the active material (k_a) and that of the char (k_c) :

$$k_s = \frac{\rho_a}{\rho_i} k_a + \frac{\rho_c}{\rho_f} k_c \tag{9}$$

Again, with the aid of eq (5) ρ_s can be substituted in the above relationship to ρ_a and ρ_c. Furthermore, k_a and k_c are treated as linear functions of temperature:

$$k = k^o + k^* (T - T_o) \tag{9'}$$

By substituting eq (8) in eq (1) and rearranging terms, one obtains:

$$(\rho_a c_{pa} + \rho_c c_{pc}) \frac{\partial T}{\partial t} = \frac{\partial}{\partial x}\left(k_s \frac{\partial T}{\partial x}\right) + \frac{\partial}{\partial x}(M_g h_g) - \frac{\partial \rho_s}{\partial t} \cdot \{Q + (h_a - h_c\ \rho_f/\rho_i)/(1-\rho_f/\rho_i)\} \tag{10}$$

This, rather than that of eq (1), is the form of the energy conservation equation which is actually solved by the model. The convective term was not expanded in order to keep the finite-difference scheme conservative.

The two components of the convective term are:

$$M_g \frac{\partial h_g}{\partial x} \qquad \text{and} \qquad h_g \frac{\partial M_g}{\partial x} = h_g \frac{\partial \rho_s}{\partial t}$$

The first represents a volumetric source or sink of energy for the solid, due to the fact that the specific enthalpy of the gas mass flow M_g is changing. The second component identifies the existence of a net energy loss from the solid equal to the sensible energy of the gases produced in the pyrolysis reaction. When this latter component is combined with the last term in eq (10), the factor multiplying $\partial\rho_s/\partial t$ becomes:

$$Q^* = Q + (h_a - h_c \cdot \rho_f/\rho_i)/(1 - \rho_f/\rho_i) - h_g \tag{11}$$

Kung, in his paper[1] (see footnote to first page of this Appendix), illustrates the relevance of this temperature-dependent heat of pyrolysis, Q^*. His derivation is repeated here for two reasons:

1) Values for the heat of pyrolysis quoted in the literature are often values for Q^* and not for the constant heat of pyrolysis Q at reference temperature T_o (at $T=T_o$, $h_a = h_c = h_g = 0$), used here. As a consequence, proper care should be taken in adopting values for the heat of pyrolysis recommended by other authors (the problem has also been discussed by this writer elsewhere[2]).

2) Users of subroutine SPYVAP may be tempted to delete from the model the volatiles - solid heat exchange by setting $c_{pg} = 0$. They should realize,

however, that this would have the net effect of also changing the energetics of the pyrolysis reaction through the disappearance of h_g from eq (9). In the current version of SPYVAP it is not possible to eliminate the first component of the convective term without, at the same time, canceling the second.

The general form of the boundary condition at the front surface of the slab is:

$$- k_s \frac{\partial T}{\partial x}\bigg|_{x=0} = \dot{q}''_{r,1} + h_1^* \cdot \left(T_{\infty,1} - T_{s,1}\right) - \varepsilon_1 \sigma T_{s,1}^4 \qquad (12)$$

where $\dot{q}''_r$ net radiative flux received by surface,

h^* convective heat transfer coefficient,

T_∞ temperature of the gases in front of the surface,

T_s surface temperature,

ε surface emissivity,

σ Stefan-Boltzmann constant ($= 5.669 \cdot 10^{-8}$ $W/m^2 \cdot K^4$)

The suffix 1 indicates that the quantities refer to the front surface. Since the model assumes a sign convention for the heat fluxes, according to which the heat flux is positive when entering the slab, the analogue of eq (12) for the back surface (suffix 2) requires a + instead of a - in front of the conduction term on the left hand side. The quantities h^* and ε are given constant values which may include 0.

The net radiative flux received by the surface is the quantity to be assigned the prescribed time-dependent values of heat flux, when the problem requires a surface flux boundary condition. When the surface temperature T_s is prescribed, the model computes the heat flux implied by the surface temperature variation and, therefore, $\dot{q}''_r$ replaces T_s as an output of the calculation. The possibility of assigning different values to the constants h and ε at both surfaces adds to the flexibility of the model. As an example, the case of convective heating with the front surface exposed to an environment at temperature $T_{\infty,1}$ is handled by setting $\varepsilon_1 = \dot{q}''_{r,1} = 0$ and by assigni. to h_1^* the value of the convective heat transfer coefficient.

A.3 FINITE DIFFERENCES FORM OF THE EQUATIONS

The slab is divided in N slices of constant thickness $\Delta x = \ell/N$. As a result, values of the dependent variables (T, ρ_s, M_g) are calculated at N+1 equally spaced grid points. It is conventionally assumed that grid point 1 lies on the front surface, grid point N+1 on the back surface. In the interior of the slab energy conservation is enforced for a slice bounded by planes half way between successive pairs of grid points. The temperature and density are assumed to be constant across the slice and equal to the values associated with the grid point at the center of the slice. Near the two surfaces an energy balance is imposed for the half slice extending from the surface to $\Delta x/2$ below it. The surface values of T and ρ_s are taken to characterize the whole half slice.

The finite differences formula is obtained by integrating eq (10) across a slice and by using the Crank-Nicolson method to express the different derivatives.

At an interior point i ($1 < i < N + 1$), conservation of energy in the step from time t^j to $j^{j+1} = t^j + \Delta t$ is written as:

$$(\rho_a c_{pa} + \rho_c c_{pc})_i^{j+\frac{1}{2}} \frac{\Delta x}{\Delta t} (T_i^{j+1} - T_i^j) = \left[k_{s,i+\frac{1}{2}}^{j+\frac{1}{2}} \left(T_{i+1}^{j+\frac{1}{2}} - T_i^{j+\frac{1}{2}} \right) + \right.$$

$$\left. k_{s,i-\frac{1}{2}}^{j+\frac{1}{2}} \left(T_{i-1}^{j+\frac{1}{2}} - T_i^{j+\frac{1}{2}} \right) \right] \Big/ \Delta x + M_{g,i+\frac{1}{2}}^{j+\frac{1}{2}} h_{g,i+\frac{1}{2}}^{j+\frac{1}{2}} - M_{g,i-\frac{1}{2}}^{j+\frac{1}{2}} h_{g,i-\frac{1}{2}}^{j+\frac{1}{2}} - \tag{13}$$

$$- \Delta x \left(\frac{\partial \rho_s}{\partial t} \right)_i^{j+\frac{1}{2}} \left[Q + (h_a - h_c \cdot \rho_f/\rho_i)/(1 - \rho_f/\rho_i) \right]_i^{j+\frac{1}{2}}$$

where:

$$\left(\frac{\partial \rho_s}{\partial t} \right)_i^{j+\frac{1}{2}} = - a_p \frac{\rho_{s,i}^{j+\frac{1}{2}} - \rho_f}{1 - \rho_f/\rho_i} \exp \left(- E/RT_i^{j+\frac{1}{2}} \right) \tag{14}$$

$$M_{g,i-\frac{1}{2}}^{j+\frac{1}{2}} = M_{g,i+\frac{1}{2}}^{j+\frac{1}{2}} - \left(\frac{\partial \rho_s}{\partial t}\right)_i^{j+\frac{1}{2}} \cdot \Delta x \tag{15}$$

and the mean enthalpies are calculated from eqs (2) and (2').

Following a commonly used convention, subscripts refer to grid point location, superscripts to time step. Fractional subscripts indicate location of the cell boundary, i.e., mid-point between adjacent grid points. Similarly, fractional superscripts ($j+\frac{1}{2}$) indicate average between present (j) and new or updated values (j+1).

With these rules in mind, eq (13) can be written as:

$$(-B_{i-1} + C_{i-1})\, T_{i-1}^{j+1} + (A_i + B_i + B_{i-1} - C_i + C_{i-1})\, T_i^{j+1} + (-B_i - C_i)\, T_{i+1}^{j+1} =$$

$$= (B_{i-1} - C_{i-1})\, T_{i-1}^{j} + (A_i - B_i - B_{i-1} + C_i - C_{i-1})\, T_i^{j} + \tag{16}$$

$$+ (B_i + C_i)\, T_{i+1}^{j} + 4\, T_o\, (-C_i + C_{i-1}) + D_i$$

where

$$A_i = (\rho_a c_{pa} + \rho_c c_{pc})_i^{j+\frac{1}{2}}\, \Delta x/\Delta t \tag{17}$$

$$B_i = k_{s,i+\frac{1}{2}}^{j+\frac{1}{2}} \,/\, (2 \cdot \Delta x) \tag{18}$$

$$C_i = \frac{1}{4} M_{g,i+\frac{1}{2}}^{j+\frac{1}{2}} \cdot \left(c_{pg}^{o} + \frac{1}{2} c_{pg}^{*} \left(T_{i+\frac{1}{2}}^{j+\frac{1}{2}} - T_o\right)\right) \tag{19}$$

$$D_i = -\,\Delta x \left(\frac{\partial \rho_s}{\partial t}\right)_i^{j+\frac{1}{2}} \cdot \left(Q + (h_a - h_c\, \rho_f/\rho_i)/(1 - \rho_f/\rho_i)\right)_i^{j+\frac{1}{2}} \tag{20}$$

The form of eq (16) can be further simplified by writing:

$$m_i\, T_{i-1}^{j+1} + u_i\, T_i^{j+1} + f_i\, T_{i+1}^{j+1} = b_i \tag{21}$$

where the constants m_i, u_i, f_i and b_i represent the three coefficients in brackets in the LHS and the whole term in the RHS of eq (16) respectively.

At a point on the surface (i=1 or i=N+1), the analogue of eq (13) can be obtained by enforcing conservation of energy for the half slice extending from the surface to $\Delta x/2$ below it. In the case of the front surface the energy balance becomes:

$$\frac{1}{2}\left(\rho_a c_{pa} + \rho_c c_{pc}\right)_1^{j+\frac{1}{2}} \frac{\Delta x}{\Delta t}\left(T_1^{j+i} - T_1^{j}\right) = k_{s,1.5}^{j+\frac{1}{2}}\left(T_2^{j+\frac{1}{2}} - T_1^{j+\frac{1}{2}}\right)\Big/\Delta x +$$

$$+ M_{g,1.5}^{j+\frac{1}{2}} h_{g,1.5}^{j+\frac{1}{2}} - M_{g,1}^{j+\frac{1}{2}} h_{g,1}^{j+\frac{1}{2}} - \frac{1}{2}\Delta x \left(\frac{\partial \rho_s}{\partial t}\right)_1^{j+\frac{1}{2}} \cdot \left[Q + (h_a - h_c \rho_f/\rho_i)/(1-\rho_f/\rho_i)\right]_1^{j+\frac{1}{2}} +$$

$$+ \dot{q}''_{r,1} + h_i^* \left(T_{\infty,1} - T_1^{j+\frac{1}{2}}\right) - \varepsilon_1 \sigma \left(T_1^{j+\frac{1}{2}}\right)^3 \cdot T_1^{j+\frac{1}{2}} \qquad (13')$$

where:

$$M_{g,1}^{j+\frac{1}{2}} = M_{g,1.5}^{j+\frac{1}{2}} - \left(\frac{\partial \rho_s}{\partial t}\right)_1^{j+\frac{1}{2}} \Delta x/2 \qquad (15')$$

The analogue of eq (16) now is :

$$\left(\frac{1}{2} A_1 + B_1 + B_o - C_1 + C_o\right) T_1^{j+1} + \left(- B_1 - C_1\right) T_2^{j+1} =$$

$$= \left(\frac{1}{2} A_1 - B_1 - B_o + C_1 - C_o\right) T_1^{j} + \left(B_1 + C_1\right) T_2^{j} + \qquad (16')$$

$$+ 4\, T_o \left(- C_1 + \frac{1}{2} C_o\right) + \frac{1}{2} D_1 + h_1^* T_{\infty,1} + \dot{q}''_{r,1}$$

where:

$$B_o = \frac{1}{2} h_1^* + \frac{1}{2} \varepsilon_1 \sigma \left(T_1^{j+\frac{1}{2}}\right)^3 \tag{18'}$$

$$C_o = \frac{1}{2} M_{g,1}^{j+\frac{1}{2}} \cdot \left(c_{pg}^o + \frac{1}{2} c_{pg}^* \left(T_1^{j+\frac{1}{2}} - T_o\right) \right) \tag{19'}$$

Finally:

$$u_1 T_1^{j+1} + f_1 T_2^{j+1} = b_1 + \dot{q}''_{r,1} \tag{21'}$$

The conservation of energy at the back surface is written in a similar way, leading to:

$$(-B_N + C_N) T_N^{j+1} + \left(\frac{1}{2} A_{N+1} + B_{N+1} + B_N - C_{N+1} + C_N\right) T_{N+1}^{j+1} =$$

$$= (B_N - C_N) T_N^{j} + \left(\frac{1}{2} A_{N+1} - B_{N+1} - B_N + C_{N+1} - C_N\right) T_{N+1}^{j} + \tag{16''}$$

$$+ 4 T_o \left(C_N - \frac{1}{2} C_{N+1}\right) + \frac{1}{2} D_{N+1} + h_2^* T_{\infty,2} + \dot{q}''_{r,2}$$

where:

$$B_{N+1} = \frac{1}{2} h_2^* + \frac{1}{2} \varepsilon_2 \sigma \left(T_{N+1}^{j+\frac{1}{2}}\right)^3 \tag{18''}$$

$$C_{N+1} = \frac{1}{2} M_{g,N+1}^{j+\frac{1}{2}} \cdot \left(c_{pg}^o + \frac{1}{2} c_{pg}^* \left(T_{N+1}^{j+\frac{1}{2}} - T_o\right) \right) \tag{19''}$$

Finally:

$$m_{N+1} T_N^{j+1} + u_{N+1} T_{N+1}^{j+1} = b_{N+1} + \dot{q}''_{r,2} \tag{21''}$$

Equations (21'), (21") and eq (21) for i=2,N form a system of N+1 equations in N+1 unknowns. The unknown quantities are: T_i^{j+1} for i=2,N and T_1^{j+1}, T_{N+1}^{j+1} (when surface boundary condition is on flux) or $\dot{q}''_{r,1}$, $\dot{q}''_{r,2}$ (when surface boundary condition is on temperature). The solution of the system of equations is found by using an algorithm for the inversion of tridiagonal matrices.

The switch from a surface boundary condition where $\dot{q}''_r$ is prescribed to a surface temperature condition (where T_1^{j+1} or T_{N+1}^{j+1} is prescribed) is accomplished by interchanging the positions of $\dot{q}''_{r,1}$ (or $\dot{q}''_{r,2}$) and T_1^{j+1} (or T_{N+1}^{j+1})in the set of equations. For example, when the heat flux $\dot{q}''_{r,1}$ is prescribed at the front surface, the first two equations of the system read:

$$u_1 T_1^{j+1} + f_1 T_2^{j+1} = b_1 + \dot{q}''_{r,1} \tag{22}$$

$$m_2 T_1^{j+1} + u_2 T_2^{j+1} + f_2 T_3^{j+1} = b_2 \tag{23}$$

In the above equations, all the unknown equatities appear to the left, all those that are known to the right of the equal sign. If the problem prescribes a surface temperature history, then T_1^{j+1} is known and $\dot{q}''_{r,1}$ is the quantity to be determined. The positioning of known and unknown variables on separate sides of the equal sign can then be enforced by interchanging $u_1 T_1^{j+1}$ and $\dot{q}''_{r,1}$ in eq (22) and by replacing eq (23) with the sum of itself and eq (22). Upon reordering of the terms in the second equation, the alternate set finally is:

$$-\dot{q}''_{r,1} + f_1 T_2^{j+1} = b_1 - u_1 T_1^{j+1} \tag{22'}$$

$$-\dot{q}''_{r,1} + (f_1 + u_2) T_2^{j+1} + f_2 T_3^{j+1} = b_1 + b_2 - (u_1 + m_2) T_1^{j+1} \tag{23'}$$

In a similar way, the last two equations of the system can be modified to allow for a surface temperature condition at the back surface.

As mentioned earlier, the model offers the option of prescribing the boundary condition below the surface, rather than at the surface. This is done through a two-step iterative procedure, which selects the surface temperature value that satisfies the prescribed "below the surface" temperature history. The procedure and the provisions to delay instabilities are further illustrated in the section describing the details of subroutine SPYVAP. However, the potential user should be aware of the fact that those provisions may not be sufficient in situations where the temperature condition is prescribed at a location too far from the surface. A more precise definition of what depth is too far will require preliminary numerical experimentation on the part of the user for the particular case to which the model is being applied.

A.4 COMPUTER PROGRAM

A.4.1 MAIN Program

The MAIN program, whose listing is given in one of the following sections, was designed for a particular application, in which some of the input data were entered through cards while others were read from a disk file. Clearly, different users will have different requirements and they will need to modify MAIN accordingly. Despite its lack of generality, this part of the program is reported here to illustrate what variables require to be initialized. Understanding the current version of MAIN and the format of the output (subroutine OUTPUT) is all that is required in order to use the computer model.

A list of the FORTRAN variables used in subroutime SPYVAP is given in the next section. For convenience, those which must be initialized in MAIN are also reported here.

a) Grid Geometry

DX slab thickness, ℓ[m]

N number of slices (number of grid points = N + 1)

b) Thermal Properties and Pyrolysis

CPA, CPC, CPG specific heats of active material, char and volatiles, c^o_{pa}, c^o_{pc}, c^o_{pg} [joules/Kg•C] (eq 2')

CPAS, CPCS, CPGS temperature coefficients of specific heats, c^*_{pa}, c^*_{pc}, c^*_{pg} [joules/Kg•C^2] (eq 2')

DARCY parameter for control of migration of volatiles (= 1. for condition of eq (4); ≠ 1. for flow in the direction of decreasing density)

PF pre-exponential factor, a_p [s^{-1}] (eq 7)

QPØ heat of pyrolysis at reference temperature (T_o), Q [joules/Kg] (eq 1)

RHOF fraction of initial density at completion of pyrolysis, ρ_f/ρ_i [-] (eq 5)

RHOW initial density, ρ_i [Kg/m^3]

TCA, TCC	thermal conductivities of active material and char, k_a^o, k_c^o [W/m °C] (eq 9')
TCAS, TCCS	temperature coefficients of thermal conductivities, k_a^*, k_c^* [W/m °C^2] (eq 9')
TRNEG	activation energy, E [joules/Kg-mole] (eq 7)
TØK	initial temperature (also reference temperature), T_o [°K]

c) Boundary Conditions

(J = 1/2 or 1/2 in the variable name indicates quantity referring to the front/back surface)

EPS1, EPS2	surface emissivities, ε_1, ε_2 (eq 12)
H1, H2	convective heat transfer coefficients, h_1^*, h_2^* [W/m^2°C] (eq 12)
KBC(J)	index for type of boundary condition (= 1, temperature B.C.; = 2 heat flux B.C.)
TBC(J,I)	boundary condition values, T or $\dot{q}_r''$ [°K or W/m^2]
TIMEBC (I)	times corresponding to B.C. values, t[s]
TINF1, TINF2	temperature of gases in front of slab surface, $T_{\infty,1}$, $T_{\infty,2}$ [°K] (eq 12)
XBC (J)	distance below surface at which temperature B.C. is prescribed, [m]

d) Control of Step Size and Accuracy

DTIMAX	maximum time step [s]
DTIMIN	minimum time step [s]
DTSTEP	desired mean temperature variation per integration step [°K]
ISTEP	step number
ITERID	desired maximum number of iterations per integration step
ITERMX	absolute maximum number of iterations per integration step
LASTEP	maximum total number of steps
ERRMX	maximum error between temperatures from successive iterations
RELAX	relaxation of temperature values from successive iterations (= 0, no relaxation; = 1, maximum effect)

SLIMIT — maximum increase of rate of change of boundary condition value; expressed as a fraction of the rate at previous step (when SLIMIT > 0) or assuming |SLIMIT|*DTSTEP as limit on mean temperature variation due to correction (when SLIMIT < 0); operates when temperature beneath the surface is prescribed .

TMLAST — time limit for performance of integration (limit on physical time and not on computer time), [s]

e) Output Control

NPROF — number of integration steps between outputs of profile variables

NSTAT — number of integration steps between outputs of station variables

As a general rule variables are entered in their dimensional form, with dimensions in S.I. units (Kg, m, s and derived units). Temperatures are in degrees Kelvin (°K). The variable ISTEP must be initialized to 0 by MAIN. Note that the pyrolysis option can be deleted from the model by assigning 0 to the pre-exponential factor a_p (PF). In that case the thermal properties of the solid are equal to those of the active material (c_{pa}, k_a) at all times.

In the version of MAIN presented here a large part of the program is occupied by a set of instructions which perform the operation of reading from a disk file the boundary values for temperature or heat flux at the two surfaces and the times corresponding to these values. As a result, arrays TBC(J,I) and TIMEBC(I) are initialized; the operation is controlled by the values of the parameters CHF, CHB, DBCMN and TMX. The reader does not need to worry about this section since he/she will have to rewrite it in any case.

The second function performed by MAIN is to print the initial conditions and a table of the boundary values. The only reminder here is that the different quantities are printed in S.I. units. Finally, a small section is dedicated to the supervision of the calls of subroutines SPYVAP and OUTPUT. The number of integration steps to be performed before returning to MAIN (IOUT) is the only variable required by SPYVAP in the arguments list. Similarly, subroutine OUTPUT requires the argument IPRINT to be initialized to 1 for output of station variables, to 2 for output of profiles. When IPRINT = 0 no output takes place. Note that the value of IPRINT is determined using the auxiliary real variables ANSTAT and ANPROF.

Execution terminates when any of the following three conditions is verified:

1) current time equals TMLAST,

2) total number of integration steps equals LASTEP, or

3) termination code IFIN is returned from SPYVAP at a value $\neq 0$.

Which one of these conditions terminated execution of the program can be determined from the last line of the printed output.

A.4.2 Subroutine SPYVAP

The only variable passed to this subroutine through the argument list is IOUT, which is the number of steps to be performed before returning control to MAIN. All the other transfers are implicitly accomplished by using the common area SPYCOM for storage. Subroutine SPYVAP is organized in 8 chapters, the first 3 of which are executed only when ISTEP=0, usually corresponding to the first call of the subroutine. The different chapters are now described in detail.

Chapter 0

The number of the last step to be completed before returning to MAIN (ISTEPR) is evaluated. Control is then transferred to the beginning of chapter 1 if ISTEP is equal to 0, otherwise execution proceeds from the beginning of chapter 3.

Chapter 1

Current time (TIME) is initialized with the time at which the first boundary values are available and the time step is set equal to DTIMIN. The thickness of the slice, Δx, is substituted for the slab thickness, ℓ, in DX. The variable IBC(J), with J=1 for front and J=2 for back surface, represents the grid point immediately to the left of the location where a temperature boundary condition is prescribed. IBC(J)=0 when the condition is at the surface. The distance between the interior boundary point and the grid point immediately to its left, expressed as a fraction of Δx, is stored in XBC(J). A minimum temperature (TL) is determined below which the pyrolysis calculation is not performed: such temperature is the temperature at which 1 percent of the pyrolyzable material would be gasified for a pyrolysis duration equal to the heat diffusion time associated with the slab.

Finally all specific heats are normalized with respect to c^o_{pa}, which is stored in CPW, and all thermal conductivities with respect to k^o_a, which is stored in TCW.

Chapter 2

Temperatures in arrays T(I) and TP(I) are set equal to the initial temperature T_o (TØK). The value 1 is put in array RHO(I), which contains local densities normalized with respect to the initial density, ρ_s/ρ_i. Other arrays and auxiliary variables are also initialized in this chapter.

Another quantity defined here is the initial time rate of increase of the variable to be used for the surface boundary condition: this quantity is stored in array SLOPE (J) (J=1, front; J-2, back surface). SLOPE(J) is used in the case in which a temperature-time history at distance x_{BC} below the surface is specified for the boundary condition. As indicated by Carlslaw and Jaeger ("Conduction of Heat in Solids", Oxford University Press, p. 388, 1959), the temperature increase $T - T_o$ at a distance x from the surface caused by a linear increase of surface temperature from T_o to T_s in time Δt is given by:

$$T - T_o = (T_s - T_o)\ (1+2y^2)\ \mathrm{erfc}\ (y) \tag{24}$$

where:

$$y = \frac{x}{2\sqrt{\alpha \cdot \Delta t}} \tag{25}$$

and α is the thermal diffusivity of the material. The above fact is recognized in the program and eq (24) is used by determining α from the thermal properties of the active material at reference temperature and by setting Δt equal to DTIMAX.

Chapter 3

This chapter is concerned with determining the boundary values to be used in the integration step to be performed. This is done by interpolating linearly the values contained in array TBC(J,I). Note that temperature boundary values are calculated at the new time t^{j+1} (= $t^j + \Delta t$), while heat flux boundary values are evaluated at the mean between current and new time $t^{j+\frac{1}{2}}$ (= $t^j + \frac{1}{2}\Delta t$).

When a temperature condition is prescribed not at the surface but below it, it is necessary to determine the appropriate value for the surface temperature. Such value is calculated through a two-step iterative procedure. A first approximation to the value of the surface temperature is found by assuming a time rate of increase equal to that of the previous step. Then the temperature profile in the slab is calculated by solving the energy equation and the value at the depth, where the temperature is prescribed, is compared with the boundary value.

On the basis of this comparison a second approximation to the surface temperature is found. In doing so, the scaling factor implied by eq (24) is properly taken into account, by introducing approximate expressions for the error function. A new temperature profile is found and a third, final value for the surface temperature is calculated by linear interpolation between the first two surface temperatures and the corresponding temperatures at the prescribed depth.

In general, the procedure will work smoothly for as long as the value of the quantity y (eq (25)) is not too large. A limit on the per-step variation of the rate of change of the surface temperature is imposed through the variable SLIMIT (SLIMIT = 1 allows a maximum variation of 100 percent on SLOPE (J) when $y \cong 0$). However, in some cases a considerable amount of numerical experimentation with different values of the control parameters may be necessary to avoid the onset of oscillations in the values of the surface temperature.

Chapter 4

After the appropriate set of boundary conditions has been found, this chapter becomes the top of the iteration loop. First, density changes, DRHO(I), are calculated from eq (14) and the mean densities during the time step $\rho_{s,i}^{j+\frac{1}{2}}/\rho_i$ are stored in array RHOA(I). Then, the updated distribution of the flux of volatiles is calculated from eq (15): when DARCY = 1. the condition of eq (4) is implemented; otherwise the volatiles are assumed to flow in the direction of decreasing densities. Mean values of thermal conductivity, $k_{s,i}^{j+\frac{1}{2}}$, and specific heat, $c_{ps,i}^{j+\frac{1}{2}}$, are calculated from eqs (9) and (8') respectively.

The convective term and the energy source due to pyrolysis are then evaluated. By the end of this chapter, the quantities A_i, B_i, C_i and D_i defined in eqs (17)-(20) have all been assigned their respective values. Because of the order in which the different operations are performed by the program, the instructions, whose execution is superfluous when some of the options of the procedure are not in use, are simply bypassed with a consequent saving in execution time.

Chapter 5

All the operations relating to the tridiagonal matrix are performed here. the coefficients m_i, u_i, f_i and b_i in eqs (21), (21') and (21") are evaluated first; when the boundary condition is on the temperature of the surface, the values of some of the coefficients are modified as implied, for example, by eqs (22') and (23') in the case of the front surface. The tridiagonal matrix is then inverted using the algorithm discussed by Forsythe and Moler ("Computer Solution of Linear Algebraic System," Prentice-Hall, p. 118) and the solution values are stored in BT(I). Taking again the front surface as an example, it is realized that when the boundary condition is on the surface temperature, BT(1) contains $\dot{q}''_{r,1}$ and not T_1^{j+1} and, therefore, the appropriate switch is made so that BT(I) contains the temperatures T_i^{j+1}.

Chapter 6

This part of the subroutine performs the following operations:

1) update of TP(I) array containing the temperatures T_i^{j+1} at the new time and check of the difference with respect to the result of the previous iteration, with decision on whether to perform another iteration or accept the calculated profile as sufficiently accurate;
2) evaluation of new step size to be used in the next step and determination of extrapolated values for temperatures T_i^{j+1} and dimensionless density increments for the next step;
3) evaluation of total energy that has entered the slab through the front (Q1DT) and the back surface (Q2DT).

A few additional comments will illustrate the operations carried out in the chapter. When the accuracy requirement is not met, the option is available to relax the temperature profile using the profile from the previous iteration. The maximum weight assigned to the temperatures from the previous iteration is equal to the value of the variable RELAX. The value of such weight is decreased automatically as the residual error approaches the maximum allowed (ERRMX). A series of controls are available to optimize the step size. First of all, whenever the number of required iterations reaches ITERMX, the step size is halved, a message is printed and the calculation is restarted from the current time. Upon successful completion of a step, the value of the step size (DTIME) for the following integration is evaluated by insuring that the average of the absolute temperature variation in the slab remains close to DTSTEP. DTIME is decreased if the integration just completed required a number of iterations greater than ITERID. Finally, execution stops when the value calculated for DTIME is lower than DTIMIN.

Chapter 7

The step number counter (ISTEP) is updated and a decision is made whether to return control to MAIN or go to the beginning of chapter 3 for another integration. Return to MAIN can be caused by any of the following conditions:

1) current time is greater than or equal to TMLAST,
2) step counter shows that a number of steps equal to LASTEP has been completed,
3) a return code other than 0 is in IFIN, or
4) the number of steps (IOUT) required for the current call of the subroutine has been completed.

A.4.3 Subroutine OUTPUT

This subroutine is dedicated to the output of station variables and profiles with the frequency implied by the values of NSTAT and NPROF in MAIN. Profiles are printed only when the parameter IPRINT is greater than 1; in addition, the density and mass flux values (at the grid points) are printed only when pyrolysis is taking place as evidenced by a value of RHOBAR less than 1.

Note that the quantities appearing in the output are all associated with the mean time $t^{j+\frac{1}{2}} = t^j + \frac{1}{2}\Delta t$ (TIMEAV) : the arrays printed for the temperature and density profiles are TBAR(I) and RHOA(I) respectively.

The only exception is in the additional output referring to the boundary temperature match : this is active when a temperature boundary condition is prescribed below the surface instead of at the surface. The temperatures shown are the value that the boundary temperature should have at time $t^{j+1} = t^j + \Delta t$ and that implied at the same time by the computed profile (T(I)). The difference between the two values gives an indication of how closely the temperature boundary condition is being enforced by the model.

The three components (see eq (12)) of the net surface heat flux are reported among the station variables. They are:

1) radiative flux $\dot{q}''_{r_*}$, (QRAD1, QRAD2),
2) convective flux $h^*(T_\infty - T_s)$, (QCONV1, QCONV2),
3) surface reradiation $\varepsilon\sigma T_s^4$, (RERAD1, RERAD2).

The integrals for the two surfaces of the net fluxes are given in Q1DT and Q2DT. The quantities MG1 and MG2 are the blowing rates at the two surfaces, positive when out. As a reminder, all dimensional quantities are shown in S.I. units. More specifically:

times in s
mass fluxes in Kg/m^2s
energy fluxes in W/m^2
temperatures in °K.

A.5 LISTING OF VARIABLES IN SUBROUTINE SPYVAP

The meaning of the FORTRAN variables which appear in the subroutine SPYVAP is given in the following list. In order to facilitate the understanding of the subroutine the explanation of the different variables is accompanied by a cross reference listing, which indicates the numbers of the statements where the individual variables are used. As a general rule, the index I is used to indicate grid points (1, NP1 range), while J distinguishes between front (J=1) and back surface (J=2).

A(I) coefficient A_i defined in eq (17)

B(I) coefficient B_i defined in eq (18)

BC(J) value of boundary condition (on temperature or heat flux)

BCTR1(J), BCTR2(J) temperature calculated from the first and second iteration when temperature is prescribed at a given distance below the surface

BETA actual amount of relaxation of temperature profiles

BETAM1 1. - BETA

BT(I) coefficient b_i appearing in eqs (21), (21') and (21")

C(I) coefficient C_i defined in eq (19)

CHG maximum absolute temperature change per step

CPA, CPC, CPG specific heats at reference temperature for active material, char, volatile products, c^o_{pa}, c^o_{pc}, c^o_{pg}

CPW = CPA reference specific heat

CPAS, CPCS, CPGS temperature coefficients of specific heats, c^*_{pa}, c^*_{pc}, c^*_{pg} (see eq (2'))

CPGD4 = .25*CPG

C1 $C_o/2$ (see eq (19'))

C2 $C_{N+1}/2$ (see eq (19"))

D(I) coefficient D_i defined in eq (20)

DARCY parameter for type of volatiles migration: when =1 condition of eq (4) is satisfied, otherwise migration follows the direction of decreasing densities of the solid

AD-A130 070 PRESSURE MODELING OF CHAR-FORMING AND LAMINATED MATERIALS(U) FACTORY MUTUAL RESEARCH CORP NORWOOD MASS R L ALPERT JUN 83 OGON3-BU DOT/FAA/CT-83/24 2/2

UNCLASSIFIED DTFA03-81-C-00043 F/G 11/4 NL

END
DATE
FILMED
8 83
DTIC

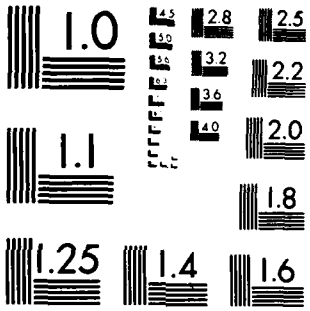

MICROCOPY RESOLUTION TEST CHART
NATIONAL BUREAU OF STANDARDS-1963-A

DRHO(I)	dimensionless density change, $(\rho_i^{j+1} - \rho_i^j)/\rho_i$
DQ1DT, DQ2DT	increments of energy stored in the slab through front and back surface
DTIMAX, DTIMIN	maximum and minimum time step size
DTIME	size of time step
DTSTEP	desired mean temperature variation per step
DX	spacing between grid points Δx (initially slab thickness).
EPS1, EPS2	product of Stefan-Boltzmann constant with emissivity at front and back surface (initially emissivity)
ERR	error between temperature profiles from successive iterations
ERRMX	maximum accepted value for ERR/CHG or ERR (in °K), whichever is smaller
F(I)	coefficient f_i, appearing in eqs (21), (21') and (21")
FACT	scale factor used for determining temperature values at the surface when temperature is prescribed inside the slab
HFLUX1, HFLUX2	radiative heat transfer, $\dot{q}_r''$, at front and back surface (positive when going in)
H1, H2	convective heat transfer coefficient, h^*, for front and back surface
I	grid point index
IBC(J)	first grid point to the left of location where temperature boundary condition is imposed (= Ø for surface boundary condition)
ICPL	= N+2 - I
IER	grid point of maximum temperature error between successive iterations
IFIN	termination label (= Ø for normal run)
IOUT	number of steps to be completed by subroutine before returning to MAIN
ISTEP	current step number
ISTEPR	last step to be completed by subroutine before returning to MAIN
ISURF(J)	= 1 for J=1, = N+1 for J=2

ITER	number of completed iterations
ITERID	desired number of iterations per step
ITERMX	maximum number of iterations per step
J	index indicating front (J=1) or back surface (J=2)
K	index referring to current boundary values in TBC (J,K) and TIMEBC(K) arrays
KBC(J)	= 1, temperature boundary condition; = 2, heat flux boundary condition
LASTEP	maximum number of integration steps
M(I)	coefficient m_i, appearing in eqs (21), (21') and (21")
MG(I)	mass flux of volatiles, M_g (see eq (15))
MG1, MG2	mass fluxes of volatiles at front and back surface (positive when out of the slab, cf eq (15')
N	number of slices in slab
NP1	number of grid points (= N+1)
PF	pre-exponential factor, a_p
QP	last term in brackets in eq (10)
QPØ	heat of pyrolysis at reference temperature, Q
Q1DT, Q2DT	energy stored in slab through front and back surface
RCDX	= RHOW*CPW*DX
RDEN	factor used in determination of coefficient for relaxation of temperature profiles
RELAX	maximum value of coefficient for relaxation of temperature profiles
RHO(I)	dimensionless density at current step, ρ_i^j/ρ_i
RHOA(I)	dimensionless mean density $(\rho_i^{j+1}+\rho_i^j)/2\rho_i$
RHOF	dimensionless final density ρ_f/ρ_i
RHOFM1	= 1. - RHOF
RHOW	initial density, ρ_i

SLIMIT	maximum variation of the rate of change of boundary values when boundary condition is prescribed on temperature inside the slab
SLOPE(J)	rate of change of boundary values at current time step
T(I)	temperature at current time, T_i^j
TBAR(I)	mean temperature, $(T_i^{j+1} + T_i^j)/2$
TBC(J,K)	boundary values for temperature or heat flux
TCA, TCC	thermal conductivities of active material and char at the reference temperature, k_a^o, k_c^o
TCAS, TCCS	temperature coefficients of thermal conductivities, k_a^*, k_c^* (see eq (9'))
TCW	reference thermal conductivity
TCWDHX	= .5*TCW/DX
THDIFF	= TCW/RHOW/CPW reference thermal diffusivity
TIME	current time, t^j
TIMEAV	mean time, $t^{j+\frac{1}{2}} = t^j + \Delta t/2$
TIMEBC(K)	times associate with boundary values in TBC(J,K)
TIMEDT	new time, $t^{j+1} = t^j + \Delta t$
TINF1, TINF2	temperature of the environments facing the front and back surface of the slab
TL	minimum pyrolysis temperature
TP(I)	new temperatures, T_i^{j+1}
TRNEG	initially activation energy E, then set to - E/R
TSLCR(J)	new rate of change of boundary values
TSTR1(J), TSTR2(J)	surface temperature values from first and second iteration
TMLAST	maximum time
TØK	reference and initial temperature
U(I)	coefficient u_i, appearing in eqs (21), (21') and (21")
XBC(J)	initially distance from the surface of the boundary location at which temperature is prescribed, then distance of same location from the first grid point to the left expressed as fraction of Δx

XD	dimensionless distance, y (see eq (25))
XDEPTH(J)	initial values of XBC(J)
YD(J)	attenuation coefficient for in-depth temperature change (see eq (24))

A.6 FORTRAN LISTING

A.6.1 MAIN Program

```
SN 0002          COMMON/SPYCOM/BC(2),CPA,CPC,CPG,CPAS,CPCS,CPGS,DARCY,DTIMAX,
                1        DTIME,DTIMIN,DTSTEP,DX,EPS1,EPS2,ERRMX,HFLUX1,HFLUX2,
                2        H1,H2,IBC(2),IFIN,ISTEP,ITER,ITERID,ITERMX,KBC(2),
                3        LASTEP,MG(44),MG1,MG2,N,NP1,PF,QPO,Q1DT,Q2DT,RELAX,
                4        RHO(44),RHOA(44),RHOF,RHOW,SLIMIT,T(44),TBAR(44),
                5        TBC(2,150),TCA,TCC,TCAS,TCCS,TIME,TIMEAV,TIMEBC(150),
                6        TINF1,TINF2,TMLAST,TRNEG,TOK,XBC(2)
SN 0003          REAL MG,MG1,MG2
SN 0004          INTEGER DIAV1,DIAV2,DIAV3
SN 0005          DEFINE FILE 8(13000,80,L,IAV)
           C-------- INITIALIZATION OF CONSTANTS ------------------------------
           C-------- THERMAL PROPERTIES
SN 0006      110 CONTINUE
SN 0007          READ(5,100,END=320) CPA,CPC,CPG,CPAS,CPCS,CPGS
SN 0008          READ(5,100) TCA,TCC,TCAS,TCCS,RHOW
           C-------- PYROLYSIS CONSTANTS AND SLAB THICKNESS
SN 0009          READ(5,100) DX,RHOF,PF,TRNEG,QPO,TOK,DARCY
           C-------- PARAMETERS FOR BOUNDARY CONDITIONS AND GRID
SN 0010          READ(5,105) KBC(1),KBC(2),N,LASTEP,NSTAT,NPROF,ITERMX,ITERID
SN 0011          ISTEP=0
SN 0012          READ(5,100) H1,H2,TINF1,TINF2,EPS1,EPS2,XBC(1),XBC(2)
SN 0013          READ(5,100) DTIMAX,DTIMIN,DTSTEP,TMLAST,ERRMX,RELAX,SLIMIT
SN 0014      100 FORMAT(8F10.3)
SN 0015      105 FORMAT(8I10)
SN 0016          ANSTAT=NSTAT
SN 0017          ANPROF=NPROF
           C-------- INPUT OF BOUNDARY CONDITIONS ------------------------------
SN 0018          READ(5,100) CHF,CHB,DBCMN,TMX
SN 0019          CH1=CHF
SN 0020          CH2=CHB
SN 0021          IF(CHF.LT.CHB) GO TO 115
SN 0023          CH1=CHB
SN 0024          CH2=CHF
SN 0025      115 CONTINUE
SN 0026          J=3
SN 0027          IF(CHF.EQ.1000.) J=1
SN 0029          IF(CHB.EQ.1000.) J=2
SN 0031          IAV=1681
SN 0032          DIAV1=INT((CH1-1.)/10.)
SN 0033          I1=INT(CH1)-10*DIAV1
SN 0034          DIAV2=-1
SN 0035          I2=1
SN 0036          IF(CH2.EQ.1000.) GO TO 120
SN 0038          DIAV2=INT((CH2-1.)/10.)
SN 0039          I2=INT(CH2)-10*DIAV2
SN 0040          DIAV2=DIAV2-DIAV1-1
SN 0041      120 CONTINUE
SN 0042          DIAV3=18-DIAV1-DIAV2
SN 0043          I=1
SN 0044      125 CONTINUE
SN 0045          READ(8'IAV,130) MIN,SEC
SN 0046      130 FORMAT(6X,I2,2X,F5.2,65X)
```

```
SN 0047          TIMEBC(I)=60.*FLOAT(MIN)+SEC
SN 0048          IAV=IAV+DIAV1
SN 0049          READ(8'IAV,135) (T(IR),IR=1,10)
SN 0050      135 FORMAT(10F8.3)
SN 0051          TBC(1,I)=T(I1)
SN 0052          IF(DIAV2.EQ.-1) GO TO 140
SN 0054          IAV=IAV+DIAV2
SN 0055          READ(8'IAV,135) (T(IR),IR=1,10)
SN 0056      140 CONTINUE
SN 0057          IAV=IAV+DIAV3
SN 0058          FIND(8'IAV)
SN 0059          TBC(2,I)=T(I2)
SN 0060          IF(CHF.LT.CHB) GO TO 145
SN 0062          TBC(2,I)=TBC(1,I)
SN 0063          TBC(1,I)=T(I2)
SN 0064      145 CONTINUE
SN 0065          IF(J.EQ.3) GO TO 150
SN 0067          TBC(J,I)=0.
SN 0068          IF(KBC(J).EQ.1) TBC(J,I)=TOK-273.
SN 0070      150 CONTINUE
SN 0071          IF(I.EQ.1) GO TO 155
SN 0073          IF(TIMEBC(I).GT.TMLAST) GO TO 160
SN 0075          IF(TIMEBC(I).GE.TIMEBC(I-1)+TMX) GO TO 155
SN 0077          IF(ABS(TBC(1,I)-TBC(1,I-1)).LT.DBCMN) GO TO 125
SN 0079      155 CONTINUE
SN 0080          IF(I.EQ.150) GO TO 160
SN 0082          I=I+1
SN 0083          GO TO 125
SN 0084      160 CONTINUE
SN 0085          IR=I
SN 0086          IF(IR.EQ.150.AND.TMLAST.GT.TIMEBC(150)) TMLAST=TIMEBC(150)
SN 0088          IF(KBC(1).EQ.2.AND.KBC(2).EQ.2) GO TO 170
SN 0090          DO 165 J=1,2
SN 0091          DO 165 I=1,IR
SN 0092          IF(KBC(J).EQ.1) TBC(J,I)=TBC(J,I)+273.
SN 0094      165 CONTINUE
SN 0095      170 CONTINUE
           C
           C-------- OUTPUT OF INITIAL CONDITIONS ------------------------------
SN 0096          WRITE(6,210) N,DX,TOK,RHOW,RHOF,PF,TRNEG,QPO,DARCY
SN 0097      210 FORMAT('1GEOMETRY, INITIAL CONDITIONS AND PYROLYSIS:'/' N=',
                1  I3,2X,'ST=',1PE10.3,2X,'TOK=',E10.3,2X,'RHOW=',E10.3,2X,
                2  'RHOF=',E10.3,2X,'PF=',E10.3,2X,'TRNEG=',E10.3,2X,'QPO=',
                3  E10.3/' DARCY=',OPF3.0)
SN 0098          WRITE(6,220) CPA,CPAS,CPC,CPCS,CPG,CPGS,TCA,TCAS,TCC,TCCS
SN 0099      220 FORMAT('OTHERMAL PROPERTIES:'/' SPECIFIC HEATS:',18X,'CPA=',
                1                                1PE10.3,2X,'CPAS=',
                2  E10.3,2X,'CPC=',E10.3,2X,'CPCS=',E10.3,2X,'CPG=',E10.3,2X,
                3  'CPGS=',E10.3/' THERMAL CONDUCTIVITIES:',13X,'TCA=',E10.3,2X,
                4  'TCAS=',E10.3,2X,'TCC=',E10.3,2X,'TCCS=',E10.3)
SN 0100          WRITE(6,230) KBC(1),XBC(1),TINF1,H1,EPS1,KBC(2),XBC(2),TINF2,
                1    H2,EPS2
SN 0101      230 FORMAT('OBOUNDARY CONDITIONS:'/22X,'KBC',8X,'XBC',11X,'TINF',
                1  12X,'H',13X,'EPS'/' FRONT SURFACE:',I10,1P4E15.3/' BACK SURFA
                2' ,I11,4E15.3)
SN 0102          WRITE(6,250) (TIMEBC(I),I=1,IR)
SN 0103      250 FORMAT('OTIME',4X,1P11E11.3/(9X,11E11.3))
```

```
SN 0104          WRITE(6,260) CHF,(TBC(1,I),I=1,IR)
SN 0105      260 FORMAT('OCH# ',F4.0,1P11E11.3/' FRONT BC',11E11.3/(9X,11E11.3))
SN 0106          WRITE(6,270) CHB,(TBC(2,I),I=1,IR)
SN 0107      270 FORMAT('OCH# ',F4.0,1P11E11.3/' BACK BC ',11E11.3/(9X,11E11.3))
SN 0108          WRITE(6,240) DTIMAX,DTIMIN,DTSTEP,ERRMX,SLIMIT,RELAX,ITERMX,ITER
SN 0109      240 FORMAT('OSTEP CONTROL PARAMETERS:'/' DTIMAX=',1PE9.2,2X,
                1  'DTIMIN=',E9.2,2X,'DTSTEP=',E9.2,2X,'ERRMX=',E9.2,2X,
                3  'SLIMIT=',E9.2,2X,
                2  'RELAX=',E9.2,2X,'ITERMX=',0PI3,2X,'ITERID=',I3/'1')
            C
            C-------- CALL OF SUBROUTINE SPYVAP ----------------------------------
SN 0110      310 CONTINUE
SN 0111          IOUT=(ISTEP/NSTAT+1)*NSTAT
SN 0112          IOUT=MIN0(IOUT,(ISTEP/NPROF+1)*NPROF)
SN 0113          IOUT=IOUT-ISTEP
SN 0114          CALL SPYVAP(IOUT)
            C-------- CHECK FOR OUTPUT ----------------------------------------
SN 0115          IPRINT=0
SN 0116          IF(FLOAT(ISTEP/NSTAT).EQ.FLOAT(ISTEP)/ANSTAT) IPRINT=1
SN 0118          IF(FLOAT(ISTEP/NPROF).EQ.FLOAT(ISTEP)/ANPROF) IPRINT=2
SN 0120          IF(IFIN.NE.0.OR.TIME.GE.TMLAST.OR.ISTEP.EQ.LASTEP) IPRINT=2
SN 0122          IF(IPRINT.GT.0) CALL OUTPUT(IPRINT)
SN 0124          IF(IFIN.EQ.0.AND.TIME.LT.TMLAST.AND.ISTEP.NE.LASTEP) GO TO 310
SN 0126          WRITE(6,200) ISTEP,LASTEP,TIME,TMLAST,IFIN
SN 0127      200 FORMAT(///' ** TERMINATED WITH ISTEP=',I5,' LASTEP=',I5,
                1    ' TIME=',1PE11.3,' TMLAST=',E11.3,' IFIN=',I3)
SN 0128          GO TO 110
SN 0129      320 STOP
SN 0130          END
```

A.6.2 Subroutine SPYVAP

```
SN 0002          SUBROUTINE SPYVAP(IOUT)
            C******* F.TAMANINI, FACTORY MUTUAL RESEARCH CORP., MARCH 1976 ********
            C*
            C*   THIS SUBROUTINE COMPUTES TEMPERATURE AND DENSITY PROFILES FOR
            C*   ONEDIMENSIONAL UNSTEADY HEAT CONDUCTION IN A SOLID SLAB OF
            C*   FINITE THICKNESS UNDERGOING PYROLYSIS.
            C*
            C*   TWO TYPES OF SURFACE BOUNDARY CONDITIONS CAN BE HANDLED:
            C*      1) PRESCRIBED TEMPERATURE AT (OR NEAR) THE SURFACE
            C*      1) PRESCRIBED SURFACE HEAT FLUX (NOT INCLUDING CONVECTIVE
            C*         HEAT TRANSFER OR SURFACE RERADIATION)
            C*
            C*   THE RATE OF PYROLYSIS IS GIVEN BY A FIRST ORDER ARRHENIUS REACTIO
            C*
            C*   PYROLYSIS GASES DIFFUSING THROUGH THE SOLID ARE ASSUMED TO BE
            C*   IN PERFECT THERMAL CONTACT WITH THE SOLID AND TO BE MOVING IN
            C*   THE DIRECTION OF DECREASING SOLID DENSITIES OR TO MIGRATE
            C*   TOWARD BOTH FREE SURFACES IN SUCH A WAY THAT THE NET PRESSURE
            C*   DROP ACROSS THE SLAB IS ZERO.
            C*
            C*   SPECIFIC HEATS (ACTIVE SOLID, CHAR AND PYROLYSIS GASES) AND
            C*   THERMAL CONDUCTIVITIES (ACTIVE SOLID AND CHAR) ARE TREATED AS
            C*   LINEAR FUNCTIONS OF LOCAL TEMPERATURE.
            C*
            C*   S.I. UNITS ARE USED THROUGHOUT (KG,M,SEC)
            C*
            C*********************************************************************
SN 0003          COMMON/SPYCOM/BC(2),CPA,CPC,CPG,CPAS,CPCS,CPGS,DARCY,DTIMAX,
                1        DTIME,DTIMIN,DTSTEP,DX,EPS1,EPS2,ERRMX,HFLUX1,HFLUX2,
                2        H1,H2,IBC(2),IFIN,ISTEP,ITER,ITERID,ITERMX,KBC(2),
                3        LASTEP,MG(44),MG1,MG2,N,NP1,PF,QPD,Q1DT,Q2DT,RELAX,
                4        RHO(44),RHOA(44),RHOF,RHOW,SLIMIT,T(44),TBAR(44),
                5        TBC(2,150),TCA,TCC,TCAS,TCCS,TIME,TIMEAV,TIMEBC(150),
                6        TINF1,TINF2,TMLAST,TRNEG,TOK,XBC(2)
SN 0004          DIMENSION  A(44),B(44),BCTR1(2),BCTR2(2),BT(44),C(44),D(44),
                1           DRHO(44),F(44),ISURF(2),M(44),SLOPE(2),TP(44),TSLCR(2
                2           TSTR1(2),TSTR2(2),U(44),XDEPTH(2),YD(2)
SN 0005          REAL M,MG,MG1,MG2
            C
            CHAPTER 0 0 0 0 0 0 --- PRELIMINARIES --- 0 0 0 0 0 0 0 0 0 0 0 0 0 0 0
            C
SN 0006          ISTEPR=ISTEP+IOUT
SN 0007          IF(ISTEP.GT.0) GO TO 310
            C
            CHAPTER 1 1 1 ---GEOMETRY, CONTROL INDEXES AND THERMODYNAMIC VARIABLE
            C
SN 0009          K=1
SN 0010          IF(N.LT.44) GO TO 125
SN 0012          WRITE(6,130) N
SN 0013      130 FORMAT('1DIMENSION OF ARRAYS IS INSUFFICIENT TO HANDLE ',
                1     I3,' GRID POINTS')
SN 0014          IFIN=1
```

```
SN 0015          RETURN
SN 0016      125 CONTINUE
SN 0017          NP1=N+1
SN 0018          RDEN=ALOG(1./ERRMX)
SN 0019          DTIME=DTIMIN
SN 0020          TIME=TIMEBC(1)
SN 0021          DX=DX/FLOAT(N)
            C
            C--------- INDEXES FOR CONTROL OF SURFACE B.C. (J=1,FRONT; =2,BACK) ---
            C          KBC(J)=1, TEMPERATURE B.C.; =2, HEAT FLUX B.C.
            C          IBC(J): FIRST GRID POINT LEFT OF WHERE TEMP.B.C. IS IMPOSED
            C          IBC(J)=0  FOR SURFACE TEMP.B.C.
            C
SN 0022          DO 110 J=1,2
SN 0023          XDEPTH(J)=XBC(J)
SN 0024          IF(KBC(J).EQ.2) GO TO 105
SN 0026          IF(XBC(J).EQ.0.) GO TO 106
SN 0028          XBC(J)=XBC(J)/DX
SN 0029          IBC(J)=1+INT(XBC(J))
SN 0030          XBC(J)=XBC(J)-AINT(XBC(J))
SN 0031          IF(J.EQ.1) GO TO 110
SN 0033          IBC(J)=NP1-IBC(J)
SN 0034          XBC(J)=1.-XBC(J)
SN 0035          GO TO 110
SN 0036      105 XBC(J)=0.
SN 0037      106 IBC(J)=0
SN 0038      110 CONTINUE
            C--------- MINIMUM PYROLYSIS TEMPERATURE ----------------------------
SN 0039          CPW=CPA
SN 0040          TCW=TCA
SN 0041          RHOFM1=1.-RHOF
SN 0042          TL=1.E30
SN 0043          IF(PF.EQ.0.) GO TO 115
SN 0045          TRNEG=-TRNEG/8314.
SN 0046          PF=PF/RHOFM1
SN 0047          TL=-TRNEG/(ALOG(100.*PF*CPW*RHOW/TCW)+2.*ALOG(DX*FLOAT(N)))
SN 0048          WRITE(6,120) TL
SN 0049      120 FORMAT('0***'/' PYROLYSIS CALCULATION IS NOT PERFORMED FOR TEMPE
            1TURES LESS THAN',F8.2,'  DEGK'/75X,'***'//)
SN 0050      115 CONTINUE
            C
            C--------- SPECIFIC HEATS AND THERMAL CONDUCTIVITIES ----------------
SN 0051          THDIFF=TCW/RHOW/CPW
SN 0052          RCDX=RHOW*CPW*DX
SN 0053          CPA=CPA/CPW
SN 0054          CPAS=CPAS/CPW
SN 0055          CPC=CPC/CPW
SN 0056          CPCS=CPCS/CPW
SN 0057          TCWDHX=.5*TCW/DX
SN 0058          TCA=TCA/TCW
SN 0059          TCAS=TCAS/TCW
SN 0060          TCC=TCC/TCW
SN 0061          TCCS=TCCS/TCW
SN 0062          CPGD4=.25*CPG
SN 0063          IF(CPGS*CPG.NE.0.) CPGS=.5*CPGS/CPG
SN 0065          EPS1=EPS1*5.669E-8
SN 0066          EPS2=EPS2*5.669E-8
```

```
                C
                CHAPTER 2 2 2 -- INITIALIZATION OF ARRAYS AND OTHER VARIABLES --- 2 2 2
SN 0067               IFIN=0
SN 0068               DO 210 J=1,2
SN 0069               TSLCR(J)=1.
SN 0070               SLOPE(J)=.01
SN 0071               IF(TBC(J,1).NE.TBC(J,2)) SLOPE(J)=(TBC(J,2)-TBC(J,1))/
                     1                         (TIMEBC(2)-TIMEBC(1))
SN 0073               IF(XBC(J).EQ.0.) GO TO 210
SN 0075               XD=.5*XDEPTH(J)/SQRT(THDIFF*DTIMAX)
SN 0076               IF(XD.GT.10.) XD=10.
SN 0078               SLOPE(J)=SLOPE(J)/(1.+2.*XD*XD)/ERFC(XD)
SN 0079           210 CONTINUE
SN 0080               ISURF(1)=1
SN 0081               ISURF(2)=NP1
SN 0082               Q1DT=0.
SN 0083               Q2DT=0.
SN 0084               DQ1DT=0.
SN 0085               DQ2DT=0.
SN 0086               MG1=0.
SN 0087               MG2=0.
SN 0088               C1=0.
SN 0089               C2=0.
SN 0090               DO 220 I=1,NP1
SN 0091               T(I)=TOK
SN 0092               TP(I)=TOK
SN 0093               RHO(I)=1.
SN 0094               RHOA(I)=1.
SN 0095               DRHO(I)=0.
SN 0096               MG(I)=0.
SN 0097               C(I)=0.
SN 0098               D(I)=0.
SN 0099           220 CONTINUE
                CHAPTER 3 3 3 3 3 3 ---EVALUATION OF BOUNDARY VALUES--- 3 3 3 3 3 3 3
                C--------- LINEAR INTERPOLATION OF BOUNDARY CONDITIONS ---------------
SN 0100           310 CONTINUE
SN 0101               TIMEAV=TIME+.5*DTIME
SN 0102               TIMEDT=TIME+DTIME
SN 0103               IF(TIMEAV.LE.TIMEBC(K+1)) GO TO 311
SN 0105               K=K+1
SN 0106               GO TO 310
SN 0107           311 CONTINUE
SN 0108               DO 315 J=1,2
SN 0109               BC(J)=TIMEDT
SN 0110               IF(KBC(J).EQ.2) BC(J)=TIMEAV
SN 0112               BC(J)=(BC(J)-TIMEBC(K))/(TIMEBC(K+1)-TIMEBC(K))
SN 0113           315 BC(J)=TBC(J,K)+BC(J)*(TBC(J,K+1)-TBC(J,K))
SN 0114               IF (KBC(1).EQ.1) TP(1) = BC(1)
SN 0115               IF (KBC(2).EQ.1) TP(NP1)  = BC(2)
SN 0116               HFLUX1=BC(1)
SN 0117               HFLUX2=BC(2)
SN 0118               ITER=0
                C
                C--------- CALCULATES SURFACE TEMPERATURES (FRONT, J=1; BACK, J=2)
                C          WHEN TEMPERATURE NEAR (AND NOT AT) THE SURFACE IS GIVEN
                C          AS BOUNDARY CONDITION
SN 0119           325 CONTINUE
```

```
SN 0120          IF(IBC(1).EQ.0.AND.IBC(2).EQ.0) GO TO 320
SN 0122          DO 350 J=1,2
SN 0123          IF(IBC(J).EQ.0) GO TO 350
SN 0125          IF(ITER.GT.0) GO TO 330
SN 0127          TSTR1(J)=T(ISURF(J))+SLOPE(J)*DTIME
SN 0128          TP(ISURF(J))=TSTR1(J)
SN 0129          GO TO 350
SN 0130      330 IF(ITER.GT.1) GO TO 340
           C
           C---- FIRST ITERATION
SN 0132          BCTR1(J)=TP(IBC(J))+XBC(J)*(TP(IBC(J)+1)-TP(IBC(J)))
SN 0133          XD=XDEPTH(J)*.5/SQRT(THDIFF*DTIME)
SN 0134          IF(XD.GT.10.) XD=10.
SN 0136          IF(XD.LE.1.5) FACT=1.-.6402*XD
SN 0138          IF(XD.GT.1.5) FACT=.5642*EXP(-XD*XD)/XD
SN 0140          FACT=(1.+2.*XD*XD)*FACT
SN 0141          YD(J)=FACT
SN 0142          IF(FACT.LT..01) FACT=.01
SN 0144          IF(ISTEP.EQ.0) BCTR1(J)=BC(J)
SN 0146          IF(BCTR1(J).NE.BC(J)) TSLCR(J)=SLOPE(J)+(BC(J)-BCTR1(J
                1                                          /DTIME/FACT
SN 0148          IF(BCTR1(J).EQ.BC(J)) TSLCR(J)=1.1*SLOPE(J)
SN 0150          IF(SLIMIT.GT.0.) GO TO 331
SN 0152          YD(J)=-SLIMIT*DTSTEP*DX*FLOAT(N)*.5/SQRT(THDIFF*DTIME)
SN 0153          IF(TSLCR(J)/SLOPE(J).LT.1.) YD(J)=10.*YD(J)
SN 0155          FACT=ABS(TSLCR(J)-SLOPE(J))*DTIME/YD(J)
SN 0156          IF(FACT.GT.1.) TSLCR(J)=SLOPE(J)+(TSLCR(J)-SLOPE(J))/FACT
SN 0158          GO TO 332
SN 0159      331 CONTINUE
SN 0160          YD(J)=SLIMIT/(1.-.1*ALOG(YD(J)))
SN 0161          FACT=TSLCR(J)/SLOPE(J)
SN 0162          IF(FACT.LT.0..AND.-FACT.GT.YD(J)) TSLCR(J)=-YD(J)*SLOPE(J)
SN 0164          IF(FACT.GE.0..AND.ABS(FACT-1.).GT.YD(J))
                1        TSLCR(J)=SLOPE(J)*(1.+SIGN(YD(J),FACT-1.))
SN 0166      332 CONTINUE
SN 0167          TSTR2(J)=T(ISURF(J))+TSLCR(J)*DTIME
SN 0168          TP(ISURF(J))=TSTR2(J)
SN 0169          GO TO 350
           C
           C---- SECOND ITERATION
SN 0170      340 BCTR2(J)=TP(IBC(J))+XBC(J)*(TP(IBC(J)+1)-TP(IBC(J)))
SN 0171          IF(BCTR2(J).NE.BCTR1(J)) TP(ISURF(J))=TSTR2(J)+(TSTR1(J)-TSTR2(
                1      *(BC(J)-BCTR2(J))/(BCTR1(J)-BCTR2(J))
SN 0173          TSLCR(J)=(TP(ISURF(J))-T(ISURF(J)))/DTIME
SN 0174          IF(SLIMIT.GT.0.) GO TO 341
SN 0176          FACT=ABS(TSLCR(J)-SLOPE(J))*DTIME/YD(J)
SN 0177          IF(FACT.GT.1.) TSLCR(J)=SLOPE(J)+(TSLCR(J)-SLOPE(J))/FACT
SN 0179          GO TO 342
SN 0180      341 CONTINUE
SN 0181          FACT=TSLCR(J)/SLOPE(J)
SN 0182          IF(FACT.LT.0..AND.-FACT.GT.YD(J)) TSLCR(J)=-YD(J)*SLOPE(J)
SN 0184          IF(FACT.GE.0..AND.ABS(FACT-1.).GT.YD(J))
                1        TSLCR(J)=SLOPE(J)*(1.+SIGN(YD(J),FACT-1.))
SN 0186      342 CONTINUE
SN 0187          IF(ISTEP.GT.0) SLOPE(J)=TSLCR(J)
SN 0189          IF(SLOPE(J).EQ.0.) SLOPE(J)=.01
SN 0191          IF(ABS(SLOPE(J)).LT..01) SLOPE(J)=SIGN(.01,SLOPE(J))
```

```
SN 0193          TP(ISURF(J))=T(ISURF(J))+SLOPE(J)*DTIME
SN 0194      350 CONTINUE
SN 0195      320 CONTINUE
           CHAPTER 4 4 4 4 4 4 4 4 ----BEGINNING OF LOOP ---- 4 4 4 4 4 4 4 4 4 4
           C--------- COMPUTES DENSITY INCREMENTS ------------------------------
SN 0196      400 CONTINUE
SN 0197          DO 410 I=1,NP1
SN 0198          IF(ITER.EQ.0) RHOA(I)=RHO(I)+.5*DRHO(I)
SN 0200          TBAR(I)=.5*(TP(I)+T(I))
SN 0201          DRHO(I)=0.
SN 0202          IF(TBAR(I).LE.TL) GO TO 405
SN 0204          IF(RHO(I).EQ.RHOF) GO TO 405
SN 0206          DRHO(I)=DTIME*PF*(RHOF-RHOA(I))*EXP(TRNEG/TBAR(I))
SN 0207          IF(RHO(I)+DRHO(I).LT.RHOF) DRHO(I)=RHOF-RHO(I)
SN 0209      405 RHOA(I)=RHO(I)+.5*DRHO(I)
SN 0210      410 CONTINUE
           C
           C---------COMPUTES NEW DISTRIBUTION OF GASEOUS FLUX, ASSUMING THAT
           C          FLUX IS IN THE DIRECTION OF DECREASING DENSITY (DARCY.NE.1.)
           C          OR THAT IT FOLLOWS DARCY'S LAW (DARCY.EQ.1.)
SN 0211          IF(RHOA(1).EQ.1..AND.RHOA(NP1).EQ.1.) GO TO 435
SN 0213          J=NP1
SN 0214          MG(NP1)=0.
SN 0215          MG2=0.
SN 0216          DO 420 I=2,NP1
SN 0217          ICPL=NP1+1-I
SN 0218          MG(ICPL)=MG(ICPL+1)-DRHO(ICPL+1)*DX*RHOW/DTIME
SN 0219          IF(ICPL.EQ.N) MG(ICPL)=.5*MG(ICPL)
SN 0221          IF(RHO(ICPL).GT.RHOA(J)) J=ICPL
SN 0223      420 CONTINUE
SN 0224          MG1=MG(1)-DRHO(1)*.5*DX*RHOW/DTIME
SN 0225          IF(DARCY.NE.1.) GO TO 415
SN 0227          MG2=.25*(MG1-MG(1)-MG(N)+MG(NP1))
SN 0228          DO 416 I=1,N
SN 0229      416 MG2=MG2+MG(I)
SN 0230          MG2=MG2/FLOAT(N)
SN 0231          GO TO 417
SN 0232      415 CONTINUE
SN 0233          IF(J.EQ.NP1) GO TO 435
SN 0235          IF(J.NE.1) MG2=.5*(MG(J)+MG(J-1))
SN 0237          IF(J.EQ.1) MG2=MG1
SN 0239      417 CONTINUE
SN 0240          DO 430 I=1,NP1
SN 0241      430 MG(I)=MG(I)-MG2
SN 0242          MG1=MG1-MG2
SN 0243          MG2=-MG(NP1)
SN 0244      435 CONTINUE
           C
           C--------- COMPUTES AVERAGE VALUES OF SPECIFIC HEAT ----------------
SN 0245          DO 440 I=1,NP1
SN 0246          A(I)=RCDX/DTIME
SN 0247          IF(RHOA(I).EQ.1..AND.CPAS.EQ.0.) GO TO 440
SN 0249          CORR=CPA+CPAS*(TBAR(I)-TOK)
SN 0250          IF(RHOA(I).EQ.1.) GO TO 441
SN 0252          CORR=((RHOA(I)-RHOF)*CORR+RHOF*(1.-RHOA(I))*(CPC+CPCS*
                1          (TBAR(I)-TOK)))/RHOFM1
SN 0253      441 A(I)=CORR*A(I)
```

```
SN 0254        440 CONTINUE
SN 0255            A(1)=.5*A(1)
SN 0256            A(NP1)=.5*A(NP1)
               C
               C--------- COMPUTES AVERAGE VALUES OF THERMAL CONDUCTIVITY ------------
SN 0257            DO 445 I=1,NP1
SN 0258            B(I)=TCWDHX
SN 0259            IF(RHOA(I).EQ.1..AND.TCAS.EQ.0.) GO TO 445
SN 0261            CORR=TCA+TCAS*(TBAR(I)-TOK)
SN 0262            IF(RHOA(I).EQ.1.) GO TO 446
SN 0264            CORR=((RHOA(I)-RHOF)*CORR+(1.-RHOA(I))*(TCC+TCCS*(TBAR(I)-
                  1            TOK)))/RHOFM1
SN 0265        446 B(I)=CORR*B(I)
SN 0266        445 CONTINUE
SN 0267            DO 450 I=1,N
SN 0268            B(I)=.5*(B(I)+B(I+1))
SN 0269        450 CONTINUE
               C
               C--------- COMPUTES COEFFICIENT OF CONVECTIVE TERM -------------------
SN 0270            IF(MG1.EQ.0..AND.MG2.EQ.0.) GO TO 460
SN 0272            DO 455 I=1,N
SN 0273            C(I)=MG(I)*CPGD4
SN 0274            IF(CPGS.EQ.0.) GO TO 455
SN 0276            C(I)=C(I)*(1.+((TBAR(I)+TBAR(I+1))*.5-TOK)*CPGS)
SN 0277        455 CONTINUE
SN 0278            C1=MG1*CPGD4*(1.+(TBAR(1)-TOK)*CPGS)
SN 0279            C2=-MG2*CPGD4*(1.+(TBAR(NP1)-TOK)*CPGS)
SN 0280        460 CONTINUE
               C
               C--------- COMPUTES ENERGY SOURCE DUE TO PYROLYSIS IN THE SOLID ------
SN 0281            IF(PF.EQ.0.) GO TO 470
SN 0283            DO 465 I=1,NP1
SN 0284            D(I)=0.
SN 0285            IF(DRHO(I).EQ.0.) GO TO 465
SN 0287            QP=TBAR(I)-TOK
SN 0288            QP=QP*(CPA+.5*CPAS*QP-RHOF*(CPC+.5*CPCS*QP))
SN 0289            QP=QPO+CPW*QP/RHOFM1
SN 0290            D(I)=-QP*DRHO(I)*DX*RHOW/DTIME
SN 0291        465 CONTINUE
SN 0292            D(1)=.5*D(1)
SN 0293            D(NP1)=.5*D(NP1)
SN 0294        470 CONTINUE
               CHAPTER 5 5 5 5 5 5 ---TRIDIAGONAL MATRIX OPERATIONS--- 5 5 5 5 5 5 5
               C
               C--------- COMPUTES COEFFICIENTS: M,U,F AND BT ----------------------
SN 0295            DO 510 I=1,N
SN 0296            F(I)=-B(I)-C(I)
SN 0297        510 CONTINUE
SN 0298            U(1)=B(1)-C(1)+2.*C1+.5*(H1+EPS1*TBAR(1)**3)
SN 0299            DO 515 I=2,N
SN 0300            U(I)=B(I)+B(I-1)-C(I)+C(I-1)
SN 0301        515 CONTINUE
SN 0302            U(NP1)=B(N)+C(N)-2.*C2+.5*(H2+EPS2*TBAR(NP1)**3)
SN 0303            DO 520 I=2,NP1
SN 0304            M(I)=C(I-1)-B(I-1)
SN 0305        520 CONTINUE
SN 0306            BT(1)=(A(1)-U(1))*T(1)-F(1)*T(2)+4.*TOK*(C1-C(1))+D(1)+H1*TINF1
```

```
SN 0307          DO 525 I=2,N
SN 0308          BT(I)=-M(I)*T(I-1)+(A(I)-U(I))*T(I)-F(I)*T(I+1)+
                1                4.*TOK*(C(I-1)-C(I))+D(I)
SN 0309      525 CONTINUE
SN 0310          BT(NP1)=-M(NP1)*T(N)+(A(NP1)-U(NP1))*T(NP1)+4.*TOK*(C(N)-C2)+
                1                D(NP1)+H2*TINF2
SN 0311          DO 530 I=1,NP1
SN 0312          U(I)=U(I)+A(I)
SN 0313      530 CONTINUE
             C
             C--------- MAKES APPROPRIATE CHANGES IN COEFFICIENTS WHEN A SURFACE
             C           TEMPERATURE BOUNDARY CONDITION IS GIVEN
             C
             C---- FRONT SURFACE
SN 0314          IF(KBC(1).EQ.1) GO TO 540
SN 0316          BT(1)=BT(1)+BC(1)
SN 0317          GO TO 545
SN 0318      540 CONTINUE
SN 0319          BT(1)=BT(1)-U(1)*TP(1)
SN 0320          BT(2)=BT(2)-M(2)*TP(1)+BT(1)
SN 0321          U(2)=U(2)+F(1)
SN 0322          U(1)=-1.
SN 0323          M(2)=-1.
SN 0324      545 CONTINUE
             C
             C---- BACK SURFACE
SN 0325          IF(KBC(2).EQ.1) GO TO 550
SN 0327          BT(NP1)=BT(NP1)+BC(2)
SN 0328          GO TO 555
SN 0329      550 CONTINUE
SN 0330          BT(NP1)=BT(NP1)-U(NP1)*TP(NP1)
SN 0331          BT(N)=BT(N)-F(N)*TP(NP1)+BT(NP1)
SN 0332          U(N)=U(N)+M(NP1)
SN 0333          U(NP1)=-1.
SN 0334          F(N)=-1.
SN 0335      555 CONTINUE
             C
             C--------- SOLVES THE TRIDIAGONAL MATRIX AND PUTS NEW TEMPERATURES
             C           IN ARRAY BT(I)
SN 0336          DO 560 I=2,NP1
SN 0337          M(I)=M(I)/U(I-1)
SN 0338      560 U(I)=U(I)-M(I)*F(I-1)
SN 0339          DO 565 I=2,NP1
SN 0340      565 BT(I)=BT(I)-M(I)*BT(I-1)
SN 0341          BT(NP1)=BT(NP1)/U(NP1)
SN 0342          DO 570 I=1,N
SN 0343          J=NP1-I
SN 0344      570 BT(J)=(BT(J)-F(J)*BT(J+1))/U(J)
             C
             C--------- MAKES APPROPRIATE CHANGES IN SURFACE VARIABLES WHEN
             C           SURFACE BOUNDARY CONDITION IS ON TEMPERATURE
SN 0345          IF(KBC(1).EQ.2) GO TO 585
SN 0347          HFLUX1=BT(1)
SN 0348          BT(1)=TP(1)
SN 0349      585 CONTINUE
SN 0350          IF(KBC(2).EQ.2) GO TO 590
SN 0352          HFLUX2=BT(NP1)
```

```
SN 0353          BT(NP1)=TP(NP1)
SN 0354      590 CONTINUE
           C
           CHAPTER 6 6 6 ---CONTROL OF NUMBER OF ITERATIONS AND STEP SIZE--- 6 6 (
           C
           C--------- CHECKS FOR MAXIMUM ERROR BETWEEN SUCCESSIVE ITERATIONS
           C           AND UPDATES TP(I) ARRAY
SN 0355          ERR=0.
SN 0356          CHG=0.
SN 0357          DO 610 I=1,NP1
SN 0358          IF(I.EQ.1.OR.I.EQ.NP1) GO TO 607
SN 0360          IF(ABS(BT(I)-TP(I)).LT.ERR) GO TO 607
SN 0362          ERR=ABS(BT(I)-TP(I))
SN 0363          IER=I
SN 0364      607 CONTINUE
SN 0365          BETAM1=TP(I)
SN 0366          TP(I)=BT(I)
SN 0367          BT(I)=BETAM1
SN 0368          CHG=AMAX1(CHG,ABS(TP(I)-T(I)))
SN 0369      610 CONTINUE
SN 0370          ITER=ITER+1
           C
           C--------- DOES 3 PRELIMINARY ITERATIONS WHEN B.C. IS NOT AT THE SURFA
SN 0371          IF (IBC(1).EQ.0.AND.IBC(2).EQ.0) GO TO 605
SN 0373          IF(ITER.LT.3) GO TO 325
SN 0375      605 CONTINUE
           C
           C--------- CHECKS FOR REQUIRED ACCURACY (ERRMX) ----------------------
SN 0376          IF(ISTEP.EQ.0) GO TO 615
SN 0378           IF (PF + CPAS + TCAS + EPS1 + EPS2 .EQ. 0.
                 1  .AND. IBC(1) + IBC(2).EQ. 0) GO TO  615
SN 0380          IF(ERR.LT.ERRMX.OR.ERR.LT.ERRMX*CHG) GO TO 615
SN 0382          IF(ITER.EQ.ITERMX) GO TO 625
           C
           C--------- RELAXATION OF ESTIMATED TEMPERATURE PROFILE ---------------
SN 0384          IF(RELAX.EQ.0.) GO TO 400
SN 0386          BETA=ERR/ERRMX
SN 0387          IF(CHG.GT.1.) BETA=BETA/CHG
SN 0389          BETA=AMIN1(1.,ALOG(BETA)/RDEN)
SN 0390          BETA=RELAX*BETA
SN 0391          BETAM1=1.-BETA
SN 0392          DO 640 I=1,NP1
SN 0393          TP(I)=BETA*BT(I)+BETAM1*TP(I)
SN 0394      640 CONTINUE
SN 0395          GO TO 400
           C
           C--------- TIME STEP IS HALVED WHEN TOO MANY (ITERMX) ITERATIONS ARE
           C           REQUIRED.  EXECUTION STOPS WHEN DTIME IS LESS THAN DTIMIN
SN 0396      625 CONTINUE
SN 0397          ERR=ERR/CHG
SN 0398          WRITE(6,611) ITER,ISTEP,IER,ERR
SN 0399      611 FORMAT(' *** MORE THAN',I3,' ITERATIONS REQUIRED AT ISTEP=',I4,
                1 ' / TEMP. RELATIVE ERROR AT I=',I3,' WAS ',1PE11.4)
SN 0400          DTIME=.5*DTIME
SN 0401          IF(DTIME.GT.DTIMIN) GO TO 310
SN 0403          IFIN=2
SN 0404          GO TO 630
```

```
SN 0405       615 CONTINUE
            C--------- COMPUTES TOTAL ENERGY WHICH ENTERED THE SLAB THROUGH
            C           FRONT (Q1DT) AND BACK (Q2DT) SURFACE
SN 0406           Q1DT=Q1DT+DQ1DT
SN 0407           Q2DT=Q2DT+DQ2DT
SN 0408           TBAR(1)=.5*(TP(1)+T(1))
SN 0409           TBAR(NP1)=.5*(TP(NP1)+T(NP1))
SN 0410           DQ1DT=HFLUX1+H1*(TINF1-TBAR(1))-EPS1*TBAR(1)**4
                 1                -4.*C1*(TBAR(1)-TOK)
SN 0411           DQ2DT=HFLUX2+H2*(TINF2-TBAR(NP1))-EPS2*TBAR(NP1)**4
                 1               +4.*C2*(TBAR(NP1)-TOK)
SN 0412           DQ1DT=.5*DTIME*DQ1DT
SN 0413           DQ2DT=.5*DTIME*DQ2DT
SN 0414           Q1DT=Q1DT+DQ1DT
SN 0415           Q2DT=Q2DT+DQ2DT
            C
            C--------- UPDATES TIME AND DENSITY. CALCULATES NEW STEP SIZE AND
            C           MAGNITUDE OF TP(I) AND DRHO(I) AT NEXT STEP
SN 0416           TIME=TIMEDT
SN 0417           CHG=0.
SN 0418           DO 645 I=2,N
SN 0419           ERR=ABS(TP(I)-T(I))
SN 0420           CHG=CHG+ERR
SN 0421       645 CONTINUE
SN 0422           CHG=CHG/FLOAT(N-1)
SN 0423           ERR=DTSTEP/CHG
SN 0424           IF(ERR.GT.1.) ERR=1./ERR
SN 0426           ERR=1.-ERR
SN 0427           IF(ITER.GT.ITERID) ERR=ERR*FLOAT(ITERID)/FLOAT(ITER)
SN 0429           DTIME=AMIN1(DTIMAX,DTIME*(DTSTEP/CHG)**ERR)
SN 0430           IF(ITER.LE.ITERID) GO TO 635
SN 0432           DTIME=DTIME*SQRT(FLOAT(ITERID)/FLOAT(ITER))
SN 0433       635 CONTINUE
SN 0434           IF(DTIME.GT.DTIMIN) GO TO 630
SN 0436           IFIN=3
SN 0437       630 CONTINUE
SN 0438           IF(TIME+DTIME.GT.TMLAST) DTIME=TMLAST-TIME
SN 0440           CHG=DTIME/2./(TIME-TIMEAV)
SN 0441           DO 620 I=1,NP1          IF (ISTEP.EQ.0) CHG = 0.
SN 0442           TBAR(I)=.5*(TP(I)+T(I))
SN 0443           ERR=T(I)
SN 0444           T(I)=TP(I)
SN 0445           TP(I)=T(I)+CHG*(T(I)-ERR)
SN 0446           RHO(I)=RHO(I)+DRHO(I)
SN 0447           DRHO(I)=CHG*DRHO(I)
SN 0448           IF(DRHO(I)+RHO(I).LT.RHOF) DRHO(I)=RHOF-RHO(I)
SN 0450       620 CONTINUE
            C
            CHAPTER 7 7 7 7 7 7 --- END OF LOOP --- 7 7 7 7 7 7 7 7 7 7 7 7 7 7 7 7
            C
            C--------- CHECKS WHETHER TO RETURN TO MAIN FOR OUTPUT -------------
SN 0451           ISTEP=ISTEP+1
SN 0452           IF(TIME.GE.TMLAST.OR.ISTEP.EQ.LASTEP) RETURN
SN 0454           IF(ISTEP.EQ.ISTEPR) RETURN
SN 0456           IF(IFIN.NE.0) RETURN
SN 0458           GO TO 310
SN 0459           END
```

A.6.3 Subroutine OUTPUT

```
SN 0002          SUBROUTINE OUTPUT(IPRINT)
SN 0003          COMMON/SPYCOM/BC(2),CPA,CPC,CPG,CPAS,CPCS,CPGS,DARCY,DTIMAX,
                1       DTIME,DTIMIN,DTSTEP,DX,EPS1,EPS2,ERRMX,HFLUX1,HFLUX2,
                2       H1,H2,IBC(2),IFIN,ISTEP,ITER,ITERID,ITERMX,KBC(2),
                3       LASTEP,MG(44),MG1,MG2,N,NP1,PF,QPO,Q1DT,Q2DT,RELAX,
                4       RHO(44),RHOA(44),RHOF,RHOW,SLIMIT,T(44),TBAR(44),
                5       TBC(2,150),TCA,TCC,TCAS,TCCS,TIME,TIMEAV,TIMEBC(150),
                6       TINF1,TINF2,TMLAST,TRNEG,TOK,XBC(2)
SN 0004          REAL MG,MG1,MG2
SN 0005          REAL*8 LAB(3)/4HTEMP,7HDENSITY,8HMASSFLUX/
            C-------- COMPUTES FRACTION OF INITIAL WEIGHT
SN 0006          RHOBAR=1.
SN 0007          IF(RHOA(1).EQ.1..AND.RHOA(NP1).EQ.1.) GO TO 20
SN 0009          RHOBAR=.5*RHOA(1)
SN 0010          DO 21 I=2,N
SN 0011          RHOBAR=RHOBAR+RHOA(I)
SN 0012       21 CONTINUE
SN 0013          RHOBAR=RHOBAR+.5*RHOA(NP1)
SN 0014          RHOBAR=RHOBAR/FLOAT(N)
SN 0015       20 CONTINUE
            C-------- COMPUTES HEAT FLUXES
SN 0016          QCONV1=H1*(TINF1-TBAR(1))
SN 0017          RERAD1=EPS1*TBAR(1)**4
SN 0018          QCONV2=H2*(TINF2-TBAR(NP1))
SN 0019          RERAD2=EPS2*TBAR(NP1)**4
            C-------- PRINTOUT OF STATION VARIABLES
SN 0020          WRITE(6,102) ISTEP,KBC(1),KBC(2),ITER,DTIME
SN 0021      102 FORMAT(//' ISTEP=',I5,' KBC(1)=',I2,' KBC(2)=',I2,' ITER=',I2,
                1   ' DTIME=',1PE10.3)
SN 0022          WRITE(6,103) MG1,MG2,RHOBAR
SN 0023      103 FORMAT(' MG1=',1PE10.3,' MG2=',E10.3,' RHOBAR=',0PF8.5)
SN 0024          WRITE(6,104) TIMEAV,HFLUX1,QCONV1,RERAD1,Q1DT,
                1  HFLUX2,QCONV2,RERAD2,Q2DT
SN 0025      104 FORMAT(' TIMEAV=',F8.2,' QRAD1=',1PE10.3,' QCONV1=',E10.3,
                1  ' RERAD1=',E10.3,' Q1DT=',E10.3/16X,' QRAD2=',E10.3,
                2  ' QCONV2=',E10.3,' RERAD2=',E10.3,' Q2DT=',F10.3)
            C-------- PRINTOUT OF BOUNDARY CONDITION MATCH
SN 0026          IF(XBC(1).EQ.0.) GO TO 23
SN 0028          TBCC=T(IBC(1))+XBC(1)*(T(IBC(1)+1)-T(IBC(1)))
SN 0029          WRITE(6,105) BC(1),TBCC
SN 0030      105 FORMAT(' FRONT B.C.:',26X,F8.3,7X,F8.3)
SN 0031          WRITE(6,106)
SN 0032      106 FORMAT('+',15X,'TEMPERATURE SHOULD BE:',12X,'IS:')
SN 0033       23 CONTINUE
SN 0034          IF(XBC(2).EQ.0.) GO TO 24
SN 0036          TBCC=T(IBC(2))+XBC(2)*(T(IBC(2)+1)-T(IBC(2)))
SN 0037          WRITE(6,107) BC(2),TBCC
SN 0038      107 FORMAT(' REAR B.C.:',27X,F8.3,7X,F8.3)
SN 0039          IF(XBC(1).EQ.0.) WRITE(6,106)
SN 0041       24 CONTINUE
SN 0042          IF(IPRINT.EQ.1) RETURN
            C-------- PRINTOUT OF ARRAYS
```

```
SN 0044          WRITE(6,100) LAB(1),(TBAR(I),I=1,NP1)
SN 0045      100 FORMAT(' ---PROFILES---'/1H ,A8,11F11.3/(9X,11F11.3))
SN 0046          IF(RHOBAR.EQ.1.) RETURN
SN 0048          WRITE(6,101) LAB(2),(RHOA(I),I=1,NP1)
SN 0049      101 FORMAT(1H ,A8,11F11.5/(9X,11F11.5))
SN 0050          DO 30 I=2,N
SN 0051          J=NP1+1-I
SN 0052          MG(J)=.5*(MG(J)+MG(J-1))
SN 0053       30 CONTINUE
SN 0054          MG(1)=MG1
SN 0055          WRITE(6,108) LAB(3),(MG(I),I=1,NP1)
SN 0056      108 FORMAT(1H ,A8,1P11E11.3/(9X,11E11.3))
SN 0057          RETURN
SN 0058          END
```

ATE

LMED

8